



**University of
Zurich^{UZH}**

The influence of digital elevation model data on debris flow runout modelling

GEO 511 Master's Thesis

Author

Stefan Wehrli
12-918-447

Supervised by

Brian McCardell (brian.mcardell@wsl.ch)
Ilmar Hurkxkens (hurkxkens@arch.ethz.ch)
Prof. Dr. Christian Huggel

Faculty representative

Prof. Dr. Christian Huggel

16.08.2019
Department of Geography, University of Zurich



**University of
Zurich^{UZH}**

The influence of digital elevation model data on debris flow runout modelling

Master Thesis GEO 511

Author:

Stefan Wehri

12-918-447

Supervised by:

Dr. Brian McArdell, WSL (brian.mcardell@wsl.ch)

Ilmar Hurkxkens, ETH Zürich (hurkxkens@arch.ethz.ch)

Supervisor and Faculty Member:

Prof. Dr. Christian Huggel (christian.huggel@geo.uzh.ch)

August 16, 2019

Department of Geography, University of Zurich

Abstract

Fast-moving flows of mud and rock are among the most numerous and dangerous types of landslides in the world. It is of great public and private interest to define and investigate hazardous areas where future debris flows are expected to occur. The behaviour of debris flows is characterised through processes of entrainment and deposition. Numerical modelling should allow to understand these dynamics from initiation to deposition. The RAMMS debris flow modelling software is applied in this thesis to show potential flow paths, runout distances and expected values for flow depth and velocity. These simulated patterns vary depending on the grid resolution of the digital elevation model (DEM); This is the focus of this thesis.

Debris flow modelling results are sensitive to DEM resolution. However, often only a few DEMs are available. In Switzerland, torrent channels are usually underrepresented in the publicly available DEMs. This has been proven by a comparison of cross-sectional areas at selected transects. Cross-sections could be recorded with dGPS measurements. The profiles were read out at the same transects from different DEMs. The computation of the cross-sectional areas allowed the comparison to be made. Five torrents with different channel widths were chosen as study areas. It was found that the spatial resolution of the DEM should not exceed one tenth of the channel width in order to ensure an appropriate representation of the channel's capacity.

Debris flow runout simulations have been made to investigate the influence of DEM resolution on the modelling results. High-resolution DEMs of the study areas as well as artificially generated surfaces were used. These have been resampled to other resolutions by using the nearest neighbour technique. As a result, various DEMs of the same surface having different grid sizes were available as input DEMs for RAMMS software package. By keeping all parameters constant, except for the input DEM, variations in the simulation results became visible. An increase in the affected area could be observed when using a coarser DEM grid size. A remarkable effect was detected in the channels. Unrealistic pools were formed at relatively coarse grid sizes. These natural artefacts significantly influence debris flow modelling results. A computer experiment has shown that the resolution of a DEM should be at least a quarter of the channel width in order to avoid their appearance.

The results of this study help to understand the influence of DEM resolution on debris flow runout modelling better. Furthermore, it underlines the need for high-resolution DEMs, especially when the torrent channel is narrow. A first try on a new time- and cost-effective solution to improve the channel representation within existing DEMs seems promising.

Contents

Abstract	I
Contents	III
List of figures	VI
List of tables	VIII
Abbreviations	IX
1 Introduction	1
1.1 Motivation	1
1.2 Background of research	3
1.3 Objectives	4
1.4 Thesis Structure.....	5
2 Background	7
2.1 Debris flow triggering mechanisms and morphology	7
2.2 Climate impact on debris flow activity	8
2.3 Debris flow processes	8
2.3.1 Entrainment.....	9
2.3.2 Deposition.....	9
2.3.3 Parameters	9
2.4 Elevation models	11
2.4.1 Production	11
2.4.2 Resampling.....	12
2.5 RAMMS.....	13
2.5.1 General	14
2.5.2 Input information.....	15
2.5.3 Output.....	16
2.5.4 Alternative models.....	17
2.6 Hazard mapping.....	17
3 Study areas	19
3.1 Illgraben	21
3.2 Cases in Graubünden	22
4 Data	25

4.1	Geodata	25
4.2	Artificial height models	26
4.3	Field data	26
5	Methods.....	27
5.1	Digital elevation models.....	27
5.1.1	Field work.....	27
5.1.2	Cross-section visualisation	28
5.1.3	Channel capacity	28
5.1.4	Evaluation.....	29
5.2	Debris flow runout modelling.....	30
5.2.1	Preparation of the input DEMs.....	30
5.2.2	Modelling in RAMMS.....	32
5.2.3	Visualisation of runout zones	33
5.3	Sensitivity of the model to DEMs	34
5.3.1	Affected area.....	34
5.3.2	Channel deformation	34
6	Results	35
6.1	Digital elevation models.....	35
6.2	Debris flow runout modelling.....	40
6.2.1	Artificial cases.....	40
6.2.2	Real world cases	42
6.3	Sensitivity of the model to DEMs	47
6.3.1	Affected area.....	47
6.3.2	Channel deformation	49
7	Discussion	51
7.1	Digital elevation models.....	51
7.1.1	DEM type.....	51
7.1.2	Temporal changes in channel geometry	52
7.1.3	Cross-sectional area calculation	52
7.2	Debris flow runout modelling.....	53
7.2.1	Input topography.....	53
7.2.2	Scenario definition.....	53
7.2.3	RAMMS.....	53
7.3	Sensitivity of the model to DEMs	55
7.3.1	Sensitivity analysis	55
7.3.2	Outlook: A possible solution.....	56
8	Conclusion	59
9	Literature	61

10 Appendix.....	67
10.1 Digital elevation models.....	67
10.2 Debris flow runout modelling.....	71
10.3 Sensitivity of the model to DEMs	73
Acknowledgements.....	75
Personal Declaration	76

List of figures

Figure 1: Glyssibach debris flow in Brienz in summer 2005 (Swiss Air Force, 2005).....	1
Figure 2: Resulting maximum flow height of a simulation based on a 2 m grid (RAMMS interface).....	2
Figure 3: Resulting maximum flow height of a simulation based on a 25 m grid (RAMMS interface).....	2
Figure 4: Relevance of debris flow modelling (own graphic representation, Images: map.apps.ch (21.02.2019), RAMMS interface, hmq-umwelt.ch (21.02.2019)).....	3
Figure 5: Three entities of the methods, results and discussion chapter.	5
Figure 6: A typical watershed (adapted from Ancey, 2001).....	7
Figure 7: Schematic of a granular front debris flow (Pierson, 1986).....	8
Figure 8: Schematic view of levees near channel bends. (right) Seen from top. (left) In cross section. (adapted from Johnson and Rodine, 1984).....	9
Figure 9: Difference between DSM (blueish) and DTM (greenish).	11
Figure 10: The process from the original DEM to the simulation DEM by using bilinear interpolation resampling technique (elevation values are displayed threefold vertically exaggerated).....	12
Figure 11: The process from the original DEM to the simulation DEM by using nearest neighbour resampling technique followed by bilinear interpolation.	13
Figure 12: Visualisation of the simulation DEM.....	13
Figure 13: RAMMS project workflow (adapted from Christen et al., 2012).....	14
Figure 14: Block model by Voellmy and Salm (inspired by Oggier, 2011)	15
Figure 15: Diagram of hazard levels as a function of probability and intensity (e.g. BAFU, 2016).	17
Figure 16: Locations of the study areas (swisstopo, 2018).	19
Figure 17: Study areas and approximate alluvial fans outlines in red (created with Google Earth).	20
Figure 18: Illgraben debris fan with the village of Susten and confluence with Rhone River in foreground and the catchment in the background (F. Dufour, WSL). The area enclosed by the dashed line shows the active part of the catchment (Badoux et al., 2009).	21
Figure 19: Typical view of the Illgraben debris flow channel. No vegetation can form inside the channel due to strong erosion.	21
Figure 20: Arrival of the debris-flow front upstream of check dam 29 during the July 28, 2006 event (C. Gwerder, WSL). (Badoux <i>et al.</i> , 2009)	21
Figure 21: Situation when looking down from the fan apex at the Fraschmardin torrent. The location of the actual channel is marked in blueish colour, while the protection dam is coloured in a yellowish colour.	22
Figure 22: Fraschmardin torrent with its typical trapezoidal shape within the forest.....	22
Figure 23: Fraschmardin torrent with its typical trapezoidal shape along the forest.....	22
Figure 24: Val Mela torrent partly filled with snow just before it crosses the road.	23
Figure 25: Val Mela torrent channel filled with avalanche snow.	23
Figure 26: The Forbesch torrent channel partly filled with snow (in front). The hamlet TGA is located just on the side of the debris fan (in background).	23
Figure 27: Elevation data (own graphic representation, Images: geodata4edu.ch (26.02.2019), Rhino-CAD interface (26.02.2019), Brian McArdell (22.01.2019).	25
Figure 28: Cross-section measurement at Illgraben (Photo: Brian McArdell).....	27
Figure 29: Leica GPS1200	28
Figure 30: Antenna of Leica GPS1200	28

Figure 31: Visualisation of a calculated cross-sectional area (blue area in figure). The orange line illustrates the cross-section. The numbers correspond to the description given in the text.	29
Figure 32: Components which have been used to create the various synthetic surfaces (Grasshopper interface). The red dashed lines indicate links of components that need to be established in order to specify the desired channel path.	31
Figure 33: Representation of a synthetic surface with a sinus channel in the 3D-view (Rhino interface).	32
Figure 34: Representation of a channel cross-section in Val Mela depending on different data origins.	35
Figure 35: Cross-sectional areas [m ²] of the channel cross-sections based on the same data as Figure 34.	35
Figure 36: Selection of cross-section representations at Illgraben (map: swisstopo 2018)	36
Figure 37: Selection of cross-section representations at Franschmardin (map: swisstopo 2018)	37
Figure 38: Calculated cross-sectional areas for all field sites where measurements were taken (field sites not separately labelled) based on the different DEMs as a percentage of the dGPS-based cross-sectional area (sorted ascending). The absolute calculated cross-sectional area based on the dGPS data is in the top row. The corresponding width and depth of this transect are in the bottom rows.	38
Figure 39: Percentage of the dGPS based cross-sectional areas against the channel width according to dGPS data. The regression lines are primarily used to show trends rather than a linear correlation.	39
Figure 40: Maximum flow height [m] of a simulated debris flow as a function of the spatial resolution (on top of each simulation result) on a surface with a channel in a sinus course.	40
Figure 41: Maximum velocity [m/s] of a simulated debris flow as a function of the spatial resolution (on top of each simulation) on a surface with a channel in a sinus course.	41
Figure 42: Shaded reliefs of a surface with a random channel course as a function of the spatial resolution and the corresponding results for the maximum flow height [m] of a simulated debris flow on these surfaces.	41
Figure 43: Maximum flow height [m] for an extreme event simulation in the Franschmardin torrent as a function of the spatial resolution [m].	42
Figure 44: Maximum velocity [m/s] for an extreme event simulation in the Forbesch torrent as a function of the spatial resolution [m].	43
Figure 45: Flow height [m] above 1 m for a simulation with the borderline scenario at a specific timestep in the Illgraben torrent as a function of the spatial resolution [m].	44
Figure 46: Maximum flow height [m] for a simulation with the borderline scenario in the Val Mela torrent as a function of the spatial resolution [m].	45
Figure 47: Maximum velocity [m/s] for a simulation with the borderline scenario in the Alp da Stugl (western channel) torrent as a function of the spatial resolution [m].	46
Figure 48: Percentage of the 1 m grid based affected areas in case of an extreme event against the input DEM resolution. The given regression lines are primarily used to show trends rather than a linear correlation.	47
Figure 49: Percentage of the 1 m grid based affected areas in case of the borderline scenario event against the input DEM resolution. The given regression lines are primarily used to show trends rather than a linear correlation.	48
Figure 50: Percentage of the 1 m grid based cross-sectional areas of six transects (a-f) against the input DEM resolution at a synthetic straight channel. The thin blue line indicates the general trend line. The cyan coloured lines above and below indicate the 10% respectively 90% percentile. The red arrow points at the used channel width of 20 m.	49
Figure 51: Debris flow channel of Combatseline torrent and surrounding houses. (left) Looking upwards. (right) Looking downwards into the obstructed channel.	56
Figure 52: Illustrations of the created channel and the DEM swissALTI3D (Rhino-CAD interface)	56
Figure 53: Visualisation of the processed DEM with the included channel (Rhino-CAD interface)	57
Figure 54: Resulting maximum flow height [m] for a debris flow simulation on the original DEM (left) and the modified DEM (right) at the Combatseline torrent.	57

List of tables

Table 1: Empirical relations for estimating debris flow volume (Rickenmann, 1999).	10
Table 2: Equations for indirect determination of debris-flow peak discharge (Q_p) (Rickenmann, 1999).	10
Table 3: Definition of hazard zones or hazard levels (ARE, BWG and BUWAL, 2005).	18
Table 4: Characteristics of the study areas, approximate values (Data: swisstopo, 2019)	20
Table 5: Provided geodata	26
Table 6: Spatial resolutions of the basic DEM and the input DEMs for the subsequent modelling in RAMMS for the different real-world cases.	30
Table 7: Selected input parameters for the debris flow simulations in RAMMS according to scenario A (extreme event) and scenario B (borderline case). The channels in the artificial surfaces have a trapezoidal shape (7 m depth, 21 m top width, 60° channel bank angle) and running down a planar surface having a 10° slope.....	33
Table 8: Resulting values of cross-sectional area computation: Area [m ²], depth [m], width [m] of the different transects (see lettercode, ordered downstream)	70
Table 9: Resulting values of the affected areas [m ²] with a maximum flow height of at least 0.1 m according to the simulations at the different study sites for scenario A (extreme event) and B (borderline scenario).....	73
Table 10: Resulting values of the affected areas [m ²] with a maximum flow height of at least 1 m according to the simulations at the different study sites for scenario A (extreme event) and B (borderline scenario).....	73
Table 11: Resulting values of the affected areas [m ²] with a maximum velocity of at least 1 m/s according to the simulations at the different study sites for scenario A (extreme event) and B (borderline scenario).....	73

Abbreviations

ASTER	Advanced Spaceborne Thermal Emission and Reflection Radiometer
CAD	computer-aided design
DEM	digital elevation model
dGPS	differential Global Positioning System
DSM	digital surface model
DTM	digital terrain model
ETH	Swiss Federal Institute of Technology
GIS	Geographic Information System
LiDAR	Light detection and Ranging
RAMMS	rapid mass movement simulation
SLF	Institute for Snow and Avalanche Research
SRTM	Shuttle Radar Topography Mission
UAV	Unmanned aerial vehicle
UZH	University of Zurich
WSL	Swiss Federal Institute for Forest, Snow and Landscape Research

1 Introduction

1.1 Motivation

Tuesday night, less than two hours after midnight, there was a loud rumbling instead of the usual nights silence. The stream shoots through the sleeping village, steps over its weir, debris and boulders clog the stream bed. The immense forces of nature overrun the settlement, spilling numerous houses and streets and destroying the peaceful idyll of the beautiful village on the lake (Baumgartner, 2013).



Figure 1: Glyssibach debris flow in Brienz in summer 2005 (Swiss Air Force, 2005).

Brienz, a small village in the Bernese Oberland, has been partly destroyed by an unexpected debris flow in summer 2005. Within a few hours the appearance of the village has changed drastically. About 70'000 m³ of debris was transported into the populated area. This is equivalent to approximately 4500 truckloads. The debris flow caused two fatalities and 28 houses have been destroyed or severely damaged (Ryter, 2017).

Fast-moving flows of mud and rock are among the most numerous and dangerous types of landslides in the world. They are particularly dangerous to life and property because of their high speeds and their sheer destructive force. In Switzerland around 94% of the estimated total damage due to severe weather was caused by floods or mudflow in 2017 (Andres and Badoux, 2018). As population and settled areas are constantly increasing, the damage potential is also becoming greater. Therefore, it is of great public and private interest to define and investigate hazardous areas where future debris flows are expected to occur.

As debris flows are complex processes and difficult to understand, various approaches and methods have been developed for the hazard assessment. The main approaches and methods are (Zimmermann, 2006):

- Analysis of historical documents (e.g. maps, images, descriptions)
- Terrain analysis and interpretation
- Models which allow to calculate different parameters of debris flows

1. Introduction

All these approaches contribute to the identification and evaluation of debris flow hazards. However, events such as Brienz in 2005 show that there are major uncertainties and challenges in predicting debris flows hazard potential (Zimmermann, 2006):

- Event size
- Probability of occurrence
- Process behaviour (extent of affected area)

Today, the process behaviour is investigated in particular by means of numerical simulations. Their aim is to understand the dynamics from initiation to deposition. This should allow to predict potential deposition areas of future debris flows (Schraml *et al.*, 2015).

The downslope propagation of debris flows is strongly controlled by topography. Models simulating rapid geophysical mass movements need topographic input data. The important terrain features need to be represented in a DEM. However, many people use such tools without paying attention on how well the terrain is represented in the DEM.

Figure 2 and Figure 3 illustrate results of the numerical simulations of the debris flow in the Glyssibach in Brienz. The input volume based on the event of 2005 has been used for the simulations. The underlying topography is based on a two meter (swissALTI3D) or a 25 meter (DHM25) grid, respectively. All other parameters have been kept constant. The figures show the maximum flow height calculated in the simulations.

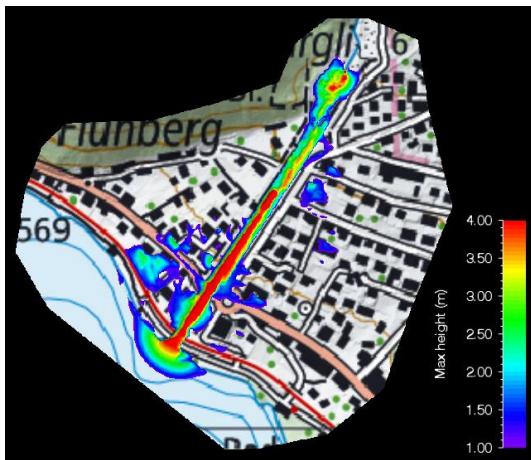


Figure 2: Resulting maximum flow height of a simulation based on a 2 m grid (RAMMS interface).

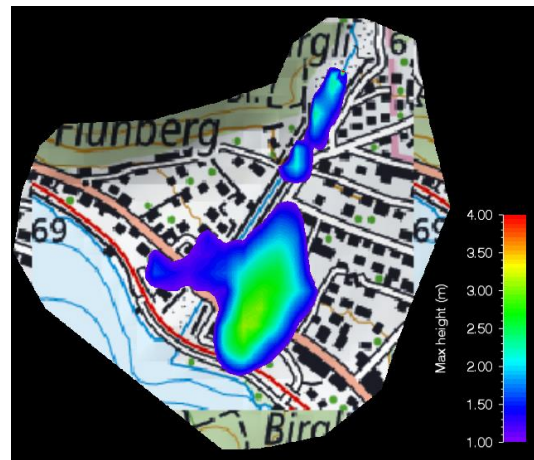


Figure 3: Resulting maximum flow height of a simulation based on a 25 m grid (RAMMS interface).

The figures show clearly diverse results. In Figure 2 the debris flow stays predominantly in the channel compared to the situation in Figure 3. The simulated runout paths differ a lot from each other. The DEM seems to have a huge influence on the modelling result.

Throughout this thesis the influence of DEM resolution on debris flow runout modelling will be assessed. A strategy for practitioners to get better simulation results by using a more appropriate DEM is then elaborated. The main goal of this thesis is:

Analyse the sensitivity of debris flow runout simulations to digital elevation model resolution.

1.2 Background of research

Downslope mass movement is the result of the force of gravity. Mass wasting processes are divided into five main groups: falls, topples, slides, spreads, and flows (Varnes, 1978). The term debris flow is used for mass wasting in which the movement is occurring throughout the flow rather than sliding as a coherent mass. This is in line with the definition given by the Swiss Federal Office for the Environment, which describes a debris flow as a slow to fast flowing mixture of water and solids with a high solids content, which often precipitates in steep channels in several phases (Bundesamt für Umwelt BAFU, 2015). The terminology describing the classification of debris flows is not very strict and some discrepancies in meaning for different languages exist (Rickenmann, 2014). This thesis focuses on channelized debris flows, not unchannelized hillslope debris flows.

Debris flows produce peak discharges which may exceed the channel capacity on the fan, resulting in widespread sediment deposition on the fan and associated hazard to buildings, infrastructure and people (Rickenmann, 1999). Several events have produced significant damage and fatalities in the Swiss Alps during recent decades (e.g. Hilker *et al.*, 2009, Hürlimann *et al.*, 2003). Such severe events are clear evidence of the kind of impact natural hazards can have on society. Records of past events are needed by insurance companies, but also by local authorities to complete the mapping of natural hazards (Hilker *et al.*, 2009). Particularly where people or essential infrastructure are vulnerable, the risk of potential debris flows needs to be considered.

Debris flow modelling allows engineering offices for comprehensive evaluation of mitigation measures to support integral risk management (Christen *et al.*, 2012). Assessing the influence of DEM resolution will provide an enhanced understanding of the modelling results. This is crucial for the determination of damage potential of possible debris flows and therefore for the planning of protection measures. Figure 4 illustrates the dependency of hazard maps and technical measures on the modelling results and thus the relevance of debris flow modelling.

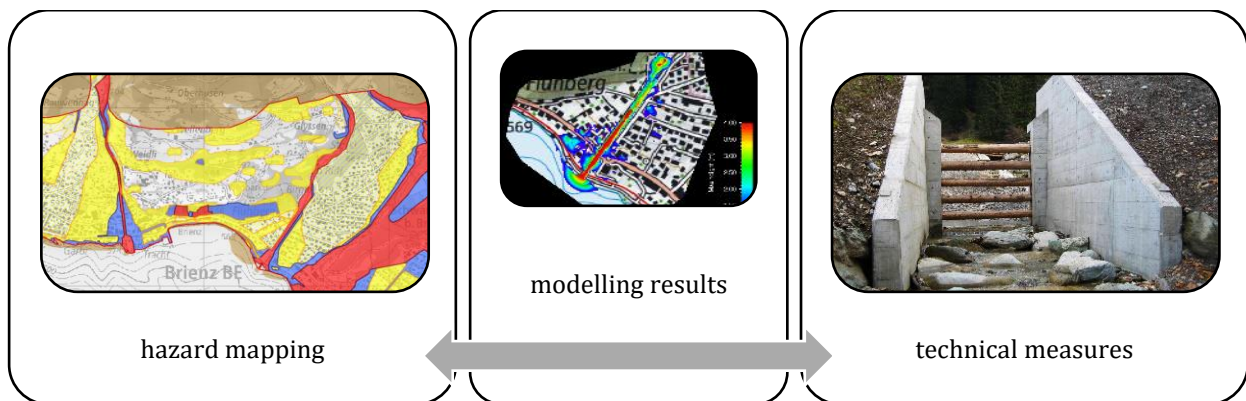


Figure 4: Relevance of debris flow modelling (own graphic representation, Images: map.apps.ch (21.02.2019), RAMMS interface, hmq-umwelt.ch (21.02.2019)).

The aim in numerical models is to understand the dynamics from initiation to deposition. Within this thesis the numerical model RAMMS is used as a simulation software. Data and empirical formulas are considered to define input parameters. The most commonly used approach for numerical modelling is based on depth-averaged conservation equations of mass, momentum and energy, which are applied to describe the dynamic motion, and a rheological model describes the material behaviour (e.g. Quan Luna, 2012). In a two-dimensional depth-averaged model the development of height and dispersion of the debris flow is mapped. Such dynamic simulation models provide the most accurate description of the flow process, including the deformation of the moving mass along the path as well as spatially and temporally detailed information on the flow parameters (Rickenmann, 2014). These values are important for the evaluation of the simulations carried out within the scope of this work.

1. Introduction

The modelling, however, can be insufficient because the terrain is not adequately represented in the DEM. Especially in a complex topography containing bumps, depressions, ridges, and gullies, the debris flow path alters, depending on the characteristics of the DEM (cf. Bühler *et al.*, 2011). The influence of grid resolution for snow avalanche runout has been investigated (Bühler *et al.*, 2011). Huggel *et al.* (2008) have evaluated ASTER and SRTM DEM data for lahar modelling and concluded that determination of hazard zones in critical areas should not be based on one DEM alone without any sensitivity analysis. Stolz and Huggel (2008) showed that the choice of the DEM in terms of resolution and quality must be evaluated carefully for debris flow modelling. They did not specifically perform an analysis of the effect of grid size and scaling on modelling results.

Therefore, an investigation of the accuracy of debris flow models using DEMs with different resolutions is important. Sensitivity studies on debris flow runout simulations linked to the DEM resolution have been done (e.g. Stolz and Huggel, 2008, Sodnik *et al.*, 2013), but to the best of my knowledge, no one has ever tried to assess these deviations in the modelling results.

1.3 Objectives

The aim of this master thesis is to analyse the sensitivity of debris flow runout simulations to digital elevation model resolution. Furthermore, this work investigates the maximum grid size for runout modelling according to the channel geometry. This aim will be addressed by the research questions and objectives under the following subsections:

Digital elevation models

How well are torrent channels represented in DEMs in common use in Switzerland?

The generic type of the DEM is a critical issue influencing the model result (Huggel *et al.*, 2008). An accurate representation of the channel geometry requires a high spatial resolution. The objectives on one hand are to assess available DEMs according to their representation qualities, on the other hand to find the minimum resolution needed for an appropriate representation of a debris flow channel.

Debris flow runout modelling

What are the debris flow transport routes and runout zones? How do they differ and vary spatially according to the used DEM?

Products of the numerical modelling in RAMMS are illustrated. The resulting runout zones are compared, and the differences will be visible. Qualitative statements about the influence of DEM resolution on modelled debris flow transport routes and runout zones are sought.

Sensitivity analysis

How is the result of the runout modelling linked to the spatial resolution of the DEM? At which grid size is the modelling error negligible?

The connection will be assessed. Bühler *et al.* (2011) demonstrated for snow avalanche simulations that elevation models with poor spatial resolution may miss important terrain features while too accurate elevation model may even lead to incorrect simulation results. The goal is to show and assess this dependency for debris flow simulations. The effects of spatial resolution on the modelling results should be quantified as far as possible.

1.4 Thesis Structure

A short overview on the research background together with the main objectives of this thesis are given in this introduction. Important information for this thesis is provided in the background chapter. After that, the study areas are introduced with a brief summary of their main characteristics. The data chapter gives an overview of the existing and self-generated datasets that have been used for analysis in this thesis. In the methods section, the technique to measure cross-sections, the creation of artificial surfaces, the modelling and the analysing procedures are described. The results chapter contains my research findings. It is followed by a discussion which embeds the thesis work into scientific context. An outlook on potential future research concepts with a practical proposal for a possible solution is described. The thesis is wrapped up by readdressing the research questions and stating the most important findings.

The three chapters methods, results and discussion all follow the structure of three entities, beginning with the digital elevation models, moving on to the debris flow runout modelling and closing with the sensitivity of the model to DEMs. These entities (see Figure 5) correspond to the research questions stated in chapter 1.3.



Figure 5: Three entities of the methods, results and discussion chapter.

1. Introduction

2 Background

2.1 Debris flow triggering mechanisms and morphology

A minimum stream gradient and a sufficiently large bedload potential are the necessary prerequisites for debris flows to occur (Rickenmann, 2014). These poorly sorted rock and soil debris are mobilized from hillslopes and channels by the addition of moisture (Costa, 1984). Rapid drainage through rainfall and snowmelt are the main moisture suppliers. Sediment sources and small steep drainage basins have the potential to transport large amounts of eroded material by debris flows. Figure 6 shows a typical watershed. The upper part is generally degraded and submitted to erosion to a more or less large extent, while the lower part is characterized by the torrent channel discharge into the alluvial fan (Ancy, 2001). These conditions can be found in Switzerland, especially in the alps. Three triggering mechanisms for channelized debris flows can be distinguished (Bundesamt für Umwelt BAFU, 2015):

- Further propagation of a hillslope debris flow within a channel
- Liquefaction of the channel bottom due to water supersaturation
- Breakthrough of a dam in the channel (e.g. by clogging by driftwood)

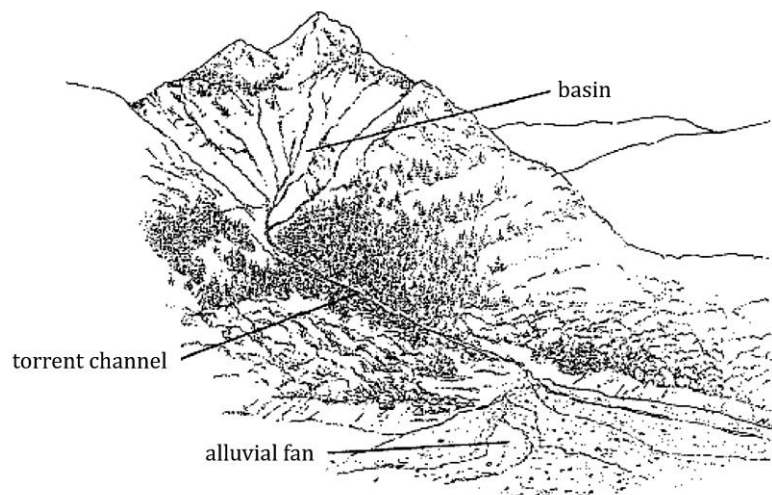


Figure 6: A typical watershed (adapted from Ancy, 2001).

The combination of component materials within debris flows leads to a rich morphology and unusual dynamics. Typical debris flows move with a speed of approximately 1 to 10 ms^{-1} and have runout distances from 100 to 1000 m (eg. Turnbull *et al.*, 2015). However, as it is a wide-spread hazardous phenomenon in mountainous terrain the magnitude and therefore speeds and runout distances depend primarily on the characteristics of the channel (Hungri *et al.*, 2014). As the flow moves down the slope, the larger particles segregate upwards and then move towards the front. Behind the relatively dry and deep granular head, forms a thinner and more fluid-rich region in the bulk of the flow (Pierson, 1986). Figure 7 shows the architecture of a debris flow.

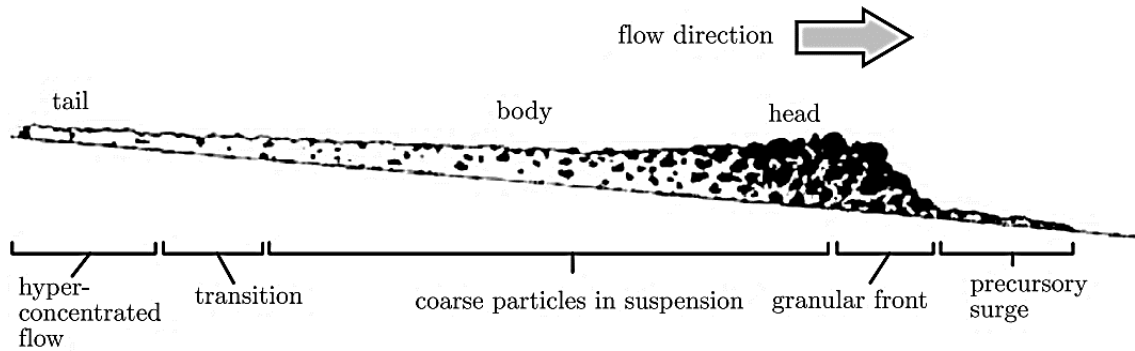


Figure 7: Schematic of a granular front debris flow (Pierson, 1986).

2.2 Climate impact on debris flow activity

In Switzerland climate change particularly plays a role for the amplification of debris flow activity. At the end of the last millennium scientists, such as Beniston and Haeberli (1998), warned that debris flows of various magnitudes may happen due to the new climatic conditions. Volcanic activity depositing ash, land-use changes such as deforestation and climate change generate new vulnerabilities. Several recent case studies in Switzerland have shown an unusually large increase in debris flow frequency, and sometimes also magnitude, for catchments with recent sediment input from rock fall or rock avalanches (e.g. Baer *et al.*, 2017).

The exact reason for this increase in debris flow frequency is still unclear. In the Swiss Alps, evidence has been presented that the number of extreme rainfall events capable of triggering debris flows in summer has increased (Harris *et al.*, 2009). The rise in atmospheric temperatures observed in the last decades is associated with permafrost degradation and glacier retreat, both factors tending to increase the sediment supply during debris flow events (Haeberli and Zimmerman, 1992). However, in the case study on the connection between debris flow activity and permafrost degradation realized by Sattler *et al.* (2011) no statistically-significant evidence has been found for this link. Nevertheless, a connection between the development of new initiation zones and the thickening of the active layer as a reaction to the melting of a former glacier is thought to be possible in this case.

2.3 Debris flow processes

In order to comprehend the role of topography in the numerical modelling of debris flows, an understanding of different processes is essential. The topography is subject to constant change, whereby a debris flow can temporarily accelerate this transformation. Processes differ during formation, transport and deposition of debris flows. The following subchapters provide an overview on two main processes and introduce parameters which describe the flow behaviour.

Debris flow is distinct from other types of landslides in that it occurs on an established path, usually gullies and drainage channels (Hungr *et al.*, 2014). A typical characteristic of the flow properties of debris flows is their wave-like discharge, usually in several phases, with the formation of a front consisting of coarse blocks (e.g. Costa, 1984). The type of movement and therefore the flow behaviour and its parameters are determined by the following factors (Tognacca, 1999):

- Solid phase material composition
- Solids concentration
- Characteristic of the liquid phase

These factors control erosion and deposition of material. Entrainment and deposition are thus responsible processes for topographic changes of the channel bed and other affected areas. Parameters are used to evaluate the effects of such processes.

2.3.1 Entrainment

Once soil material begins to move in a steep channel, the bed becomes subject to rapid undrained loading, often so that even coarse material can liquefy, or at least suffer a significant increase in pore-pressure. The bed material will become entrained in a growing surge. As the surge moves downstream, further material is added to the flow. The bulk of the material involved in a debris flow event usually originates from entrainment from the path (Hungri *et al.*, 2014; Frank *et al.*, 2016).

In addition to the bed entrainment, the destabilization of the banks provides material for a debris flow. Steep stream and gully channels are often being actively incised and thus their banks may exist in a state of marginal equilibrium that is easily disturbed by lowering of the bed, such as often occurs during passage of a debris flow surge (Hungri *et al.*, 2005). As a result, a shallow landslide might be released directly into a surge or provides material for incorporation in a next debris flow.

The debris yield rate is the amount of material entrained per unit of length of the channel. If divided by channel width, this key indicator gives an average thickness of the entrained material or the erosion depth (Hungri, 2005). As debris flows can transform from an initially small flow to a large, hazardous flow by entraining sediment several studies have been made to measure this erosion (e.g. Berger *et al.*, 2011; Hungri *et al.*, 2005).

2.3.2 Deposition

The main deposition area of a debris flow usually occurs on an established fan as a result of a combination of slope reduction and a loss of confinement (Hungri, 2005). As the debris flow front slows down, steepens and may be partly expelled to the margins of the channel many debris fans accumulate material in the form of levees (see Figure 8) or abandoned boulder fronts (Hungri *et al.*, 2014). This deposition is thus an archive of past flow magnitude, timing, composition and depositional pattern. Shifts in the active channel of a debris flow fan, termed avulsions, provide important implications for hazard assessment on debris flow fans (de Haas *et al.*, 2018).

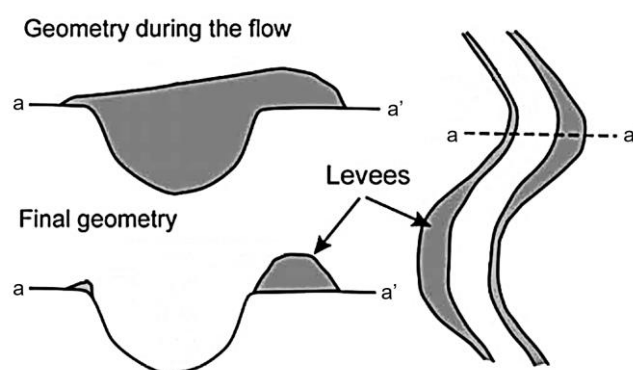


Figure 8: Schematic view of levees near channel bends. (right) Seen from top. (left) In cross section. (adapted from Johnson and Rodine, 1984)

2.3.3 Parameters

The flow behaviour of debris flows can be described with a number of different parameters. They are useful for hazard assessment and can often be derived from empirical formulas. These are used in this work to define meaningful input parameters for the numerical modelling.

Volume

For the evaluation of a potential hazard, the debris flow volume is one of the most important parameters. However, the spectrum of possible debris-flow volumes is wide and many attempts have been made to estimate an average or maximum debris-flow volume for a given torrent catchment (Rickenmann, 1999). These empirical equations are usually based on the most important morphometric characteristics of a catchment. Table 1 gives an overview on such empirical relations.

Table 1: Empirical relations for estimating debris flow volume (Rickenmann, 1999).

Formula	Number of events	Source
$M = K A_c 100 S_c$	1420	Kronfellner-Kraus (1984)
$M = 27000 A_c^{0.78}$	~ 65	Zeller (1985)
$M_a = 150 A_c (100 S_f - 3)^{2.3}$	15	Hampel (1977)
$M = L_c (110 - 250 S_f)$	82	Rickenmann and Zimmermann (1993)
$M_a = 136000 A_c^{0.61}$	551	Takei (1980)
$M_a = 29100 A_c^{0.67}$	64	D'Agostino (1996)
$M_a = 45 A_c^{0.9} S_c^{1.5} I_G$	64	D'Agostino (1996)

M	Maximum event magnitude [m ³]	S _f	Mean fan slope [-]
M _a	Average event magnitude [m ³]	L _c	Length of active channel [m]
A _c	Catchment area [km ²]	K	Torrentiality factor [-]
S _c	Mean channel slope [-]	I _G	Geologic index [-]

Because these equations may overestimate the actual debris flow volume by up to a factor of 100 it is recommended to make a geomorphologic assessment of the sediment potential rather than using these equations (Rickenmann, 1999). However, since this work has a different objective and no geomorphological studies are carried out, these formulas are useful for determining the input volume needed in the simulation.

Velocity and maximum discharge

The velocity is decisive for the maximum flow required to determine whether a channel has sufficient flow capacity. If no information on the discharge at different times at a given location is available, empirical relationships between total volume and maximum discharge can be used. Table 2 gives an overview on possible equations. Note that the equation according to Rickenmann (1999) is used for the calculation of hydrographs for the modelling part in this project (cf. chapter 2.5.2).

Table 2: Equations for indirect determination of debris-flow peak discharge (Q_p) (Rickenmann, 1999).

Equation	Author
$Q_p = 0.135 V^{0.78}$ (bouldery debris flows)	Mizuyama and Kobashi (1992)
$Q_p = 0.019 V^{0.79}$ (muddy debris flows)	Mizuyama and Kobashi (1992)
$Q_p = 0.04 V^{0.90}$ (boulder debris flows)	Bovis and Jakob (1999)
$Q_p = 0.003 V^{1.01}$ (volcanic debris flows)	Bovis and Jakob (1999)
$Q_p = 0.293 V_w^{0.56}$	Costa (1988)
$Q_p = 0.016 V_w^{0.64}$	Costa (1988)
$Q_p = 0.1 V^{0.83}$	Rickenmann (1999)

V	Debris flow volume
V _w	Water volume behind the natural dam

2.4 Elevation models

Digital elevation models are often used in geographic information systems (GIS) as a representation of a terrain's surface. The terms digital elevation model (DEM), digital terrain model (DTM) and digital surface model (DSM) are often assumed to be synonymous in scientific literature (e.g. Li *et al.*, 2004). However, the term DSM actually refers to a representation of the earth's surface which includes all objects on it. In contrast to a DSM, the digital terrain model (DTM) represents the bare ground surface without any objects like plants and buildings (see Figure 9). DEM is often used as a generic term for DSMs and DTMs, only representing height information without any further definition about the surface. All datasets which are captured with flying platforms are originally DSMs. It is possible to compute a DTM from high resolution DSM datasets with complex algorithms (Li *et al.*, 2004).

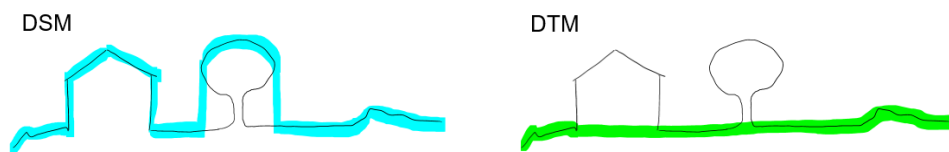


Figure 9: Difference between DSM (blueish) and DTM (greenish).

A DEM can be represented as a raster or as a vector-based triangular irregular network. For this work only raster DEMs are used. Surface altitude information is depicted in terms of elevation values for each pixel.

2.4.1 Production

DEM are acquired through different techniques. Frequently, remote sensing methods are rather used than direct survey data (e.g. interpolation of contour maps). Some of the most important techniques to generate DEMs are described in this chapter.

Radar technology is often used in space-born systems. Data can be received independently of the time since microwave signals do not require an external light source. Another advantage is the wavelength, because the radiation can penetrate the atmosphere virtually uncorrupted, so radar systems can operate independently of the weather. The three-dimensional orientation of a ground pixel cannot be unambiguously determined with only one radar image. Two images must be recorded from different positions and then combined. Representative for this technology is the Shuttle Radar Topography Mission (SRTM), which is an international research effort that obtained DEMs on a near-global scale by using radar technology. (eg. DLR, no date; Makineci and Karabörk, 2016)

Photogrammetry is a set of measurement and evaluation methods used in remote sensing to determine the spatial position or three-dimensional shape of an object from photographs. To create DEMs photogrammetric technology can be applied on stereo pairs of aerial images. Measurement can be made either semi-automatic with human intervention or fully automatic taking advantage of the image matching algorithm (Ismail and Jaafar, 2013). The surface models generated by the image matching procedure in photogrammetry are most likely to be those of DSMs. Therefore, non-terrain features above the ground surface such as vegetation canopy or man-made objects are visible. This especially is the case in DEMs created by using drones to collect images. Drones or unmanned aerial vehicles (UAV), can get much closer than conventional aircraft and therefore provide a significantly higher resolution which translates to a better ground sampling distance. During operation, UAV takes hundreds of photos at relatively low cost in order to create an orthomosaic respectively DSM (Flener *et al.*, 2013). Some of the DEMs used in the scope of this thesis have been made by flying with drones for the purpose of creating high resolution DSMs.

LiDAR (light detection and ranging) is based on distance measurement and precise orientation between a sensor and a reflecting object (Flener *et al.*, 2013). This method can be used to make digital 3-D representations.

2. Background

Wavelength varies to suit the target. This allows to filter out reflections from vegetation from the point cloud to create DTMs. Airborne LiDAR respectively airborne laser scanning is currently the most detailed and accurate method of creating DEMs. The high resolution DTM swissALTI3D, which covers Switzerland and Liechtenstein is based on LiDAR data for areas below 2000 m a.s.l. (Swisstopo, 2018).

2.4.2 Resampling

When scaling a raster graphics image such as a DEM, a new image with a higher or lower number of pixels must be generated. This process of deriving pixel values for a new image from an existing image is called resampling and is crucial for this thesis.

One resampling technique is the bilinear interpolation. It is often used for continuous data (e.g. DEM). The method assigns the output cell value by taking the weighted average using the four nearest neighbouring cells. Therefore, the output raster grid will get smoothed. RAMMS uses bilinear interpolation to set the simulation resolution (see chapter 2.5.2). This method can also be applied to prepare the input DEMs which have different grid sizes. These elevation models must be based on the same data, otherwise the results of the modelling would not be comparable. Figure 10 illustrates the effect of down-sampling on the input DEM and the effect of up-sampling on the simulation resolution. The figure shows a segment of a torrent channel at which the elevation values are displayed exaggerated. The smoothing is clearly visible. Although the original DEM has the same resolution as the DEM for the simulation, it looks different and therefore has different elevation values. Due to down-sampling and subsequent up-sampling, the original DEM goes through the smoothing process of bilinear interpolation twice and the original values are lost.

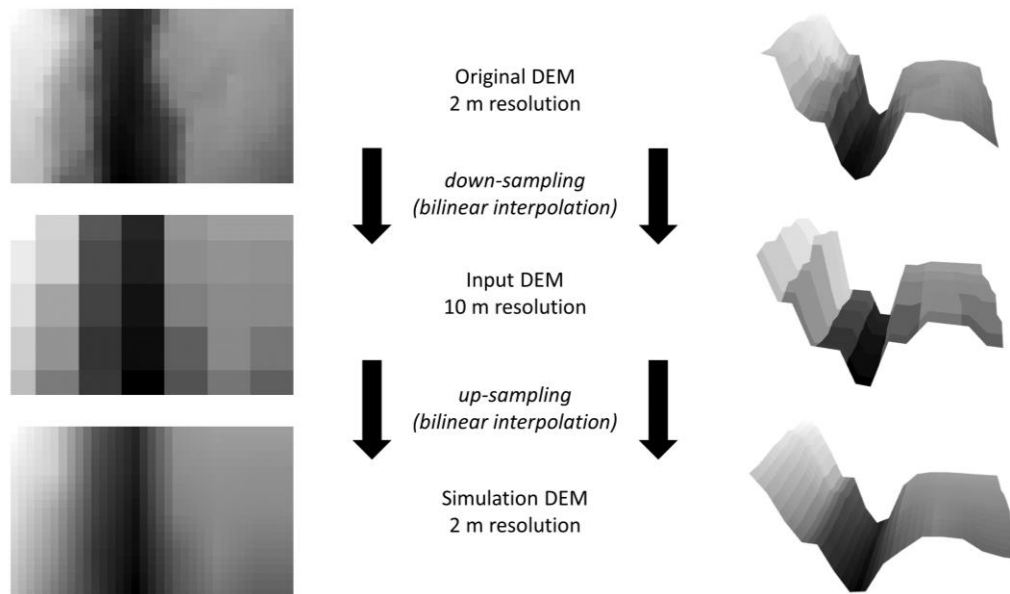


Figure 10: The process from the original DEM to the simulation DEM by using bilinear interpolation resampling technique (elevation values are displayed threefold vertically exaggerated).

However, when using bilinear interpolation as resampling technique, the output raster grid still contains a lot of information of the original DEM, since this method uses elevation values of the neighbouring cells for the calculation. In this thesis, the goal is to research about the influence of DEM resolution on debris flow runoff modelling. Therefore, the DEMs used for the simulations should not include too much extra information. One must assume that no high-resolution DEM is available. Hence another resampling technique needs to be applied. An appropriate method is called nearest neighbour. This approach assigns the value of the closest input pixel to the corresponding output pixel. As a result, linear features (e.g. torrent channels) might disappear partly or completely. This behaviour is intended because such channels are often invisible in DEMs with a relatively coarse grid size. Figure 11 shows the same as Figure 10 but the down-sampling method used this time

is the nearest neighbour resampling technique. The input DEM and the simulation DEM have consequentially changed and even more information about the original DEM is lost. To be exact, the input DEM in this example contains only height values of the original DEM every 10 m in X and Y direction (10 m grid). By resampling this case to a finer spatial resolution using bilinear interpolation, the channel becomes visible again.

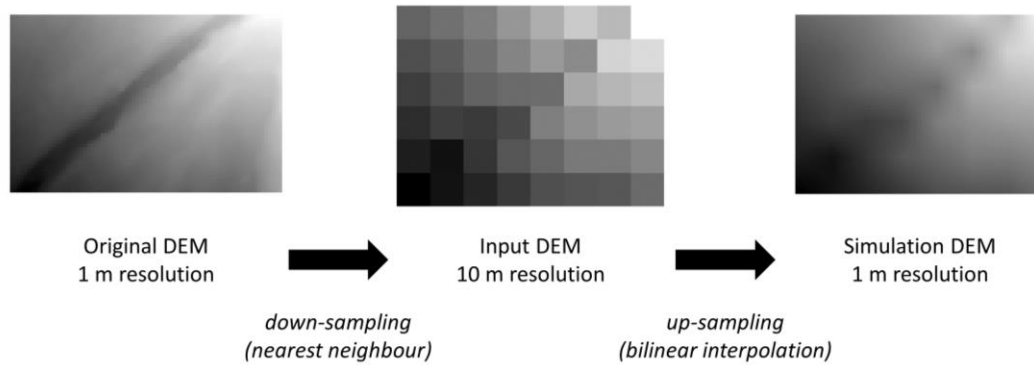


Figure 11: The process from the original DEM to the simulation DEM by using nearest neighbour resampling technique followed by bilinear interpolation.

As one can see in Figure 12, the channel gets a stepwise shape in the simulation DEM. This is typical for DEMs in which the spatial resolution is too limited that channels are clearly visible.

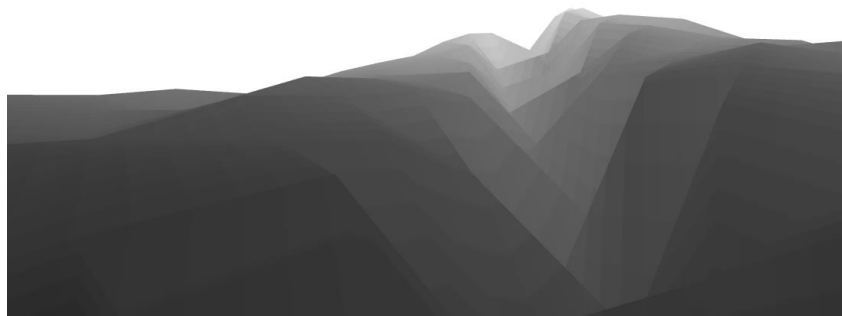


Figure 12: Visualisation of the simulation DEM.

2.5 RAMMS

As already mentioned, debris flows are a very complex hazard process. The RAMMS (RAPid Mass MovementS) program is used to simulate debris flows as accurately as possible. This numerical simulation software was developed by the WSL Institute for Snow and Avalanche Research SLF for the modelling of mass movements (Christen *et al.*, 2010). Currently, the software package consists of three process modules:

- RAMMS::AVALANCHE
- RAMMS::ROCKFALL
- RAMMS::DEBRISFLOW

For this project the module RAMMS::DEBRISFLOW (Version 1.7.20) was used. The RAMMS software needs input data, which then is used for the calculation. Several parameters which describe the debris flow are available as an output. Figure 13 shows the RAMMS project workflow. The following subchapters describe how the model works in general, what input data it uses, and what results it can produce.

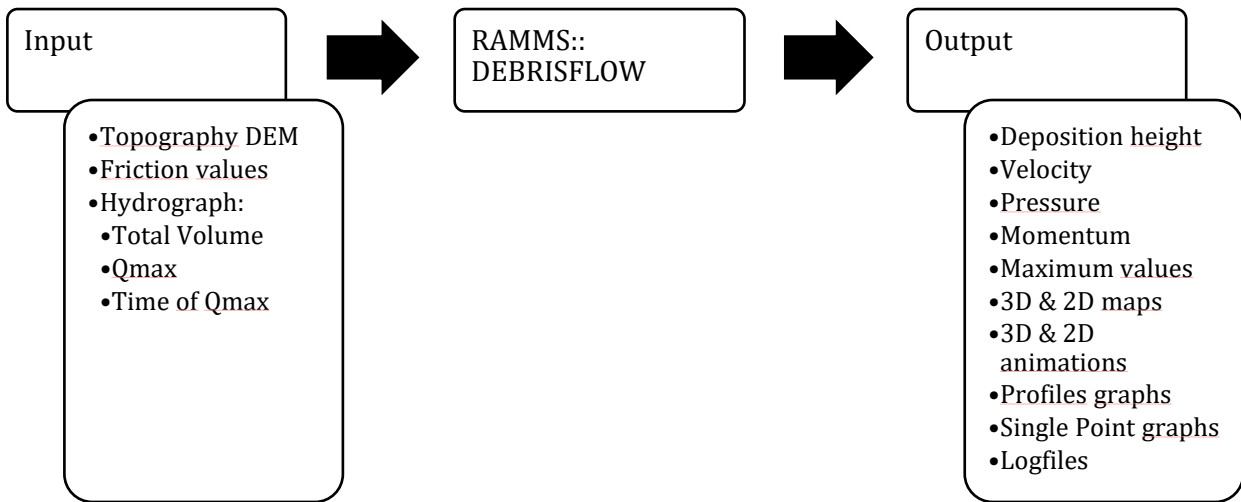


Figure 13: RAMMS project workflow (adapted from Christen et al., 2012)

2.5.1 General

RAMMS::DEBRISFLOW modules are used to calculate the motion of the movement from initiation to runout in three-dimensional terrain. The model uses depth-averaged equations and predicts the slope-parallel velocities and flow heights (Bartelt *et al.*, 2013).

The core of the program is a solution for the 2D shallow water equations adapted to the granular flow (Christen *et al.*, 2012). The rheology is described the Voellmy relation, which describes the friction behaviour of the flow process based on the Coulomb friction (μ) and the velocity squared dependent turbulent friction (ξ) (Christen *et al.*, 2012). This so-called Voellmy-Salm-model is based on the assumption of a fluid phase without shear deformation, where the flow mass moves as a block with uniform velocity along a slip plane (Cesca and D'Agostino, 2008). This is a very simplified approach, which greatly reduces the computing time. The formula for the friction resistance S is:

$$S = \mu * \rho * H * g * \cos(\theta) + \frac{\rho * g * U^2}{\xi}$$

whereby

- S [Pa]: Friction resistance
- ρ [kg m^{-3}]: Density of the moving mass
- H [m]: Flow height
- g [m s^{-2}]: Gravitational acceleration
- θ [$^\circ$]: Slope angle of slip plane
- U [m s^{-1}]: Flow velocity
- μ [-]: Coulomb friction coefficient for dry friction
- ξ [m s^{-2}]: Friction coefficient for the turbulent flow

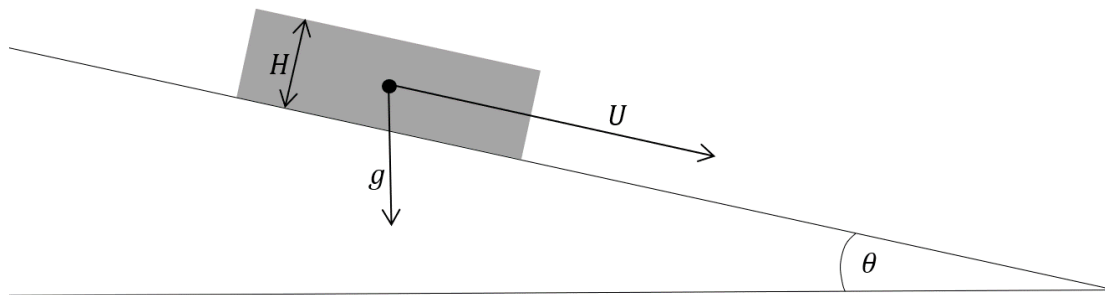


Figure 14: Block model by Voellmy and Salm (inspired by Oggier, 2011)

The friction parameter μ shows a clear negative correlation with the range of the debris flows. The turbulent friction parameter ξ correlates especially with the flow velocity. Since the Voellmy-Salm model is only an approximation of the rheology, the real friction values of the existing terrain can differ from the friction values used in RAMMS. Therefore, it is very important to calibrate the model against previous events or at least to use empirical values (Bartelt *et al.*, 2013).

Since version 1.6.20 the basic Voellmy equation has been modified to include cohesion and the normal force includes centrifugal forces arising from terrain curvature (Bartelt *et al.*, 2013). For simulations carried out in the scope of this work, no additional yield stress (cohesion) was used. The curvature was activated and therefore the centrifugal force is considered in this model.

2.5.2 Input information

Various input data and parameters are required for modelling debris flows in RAMMS. This chapter describes which data and parameters have been used and what purpose they serve.

(1) Elevation models:

The elevation models are by far the most important input data for this project. Therefore, this thesis contains more background information on elevation models in different chapters. It is important for modelling in RAMMS that the models represent the topography adequately.

(2) Maps and orthophotos:

This function is mainly used to facilitate orientation and to present the results in an understandable way. The map or orthophoto is placed over the elevation model.

(3) Simulation Parameters:

- Simulation resolution: The grid resolution for the simulation in RAMMS can be set manually. The default is the value of the spatial resolution of the input DEM. Adjusting this value changes the resolution of the original DEM by grid resampling through bilinear interpolation (Bartelt *et al.*, 2013). With a smaller grid resolution, the calculation time increases, and a larger storage capacity becomes necessary.
- End time: The end time can be used to limit the calculation time for the simulation. If the end time is reached before stop criterion, the simulation ends. With the help of the channel length and an assumption about the average velocity, an estimation about the duration of the debris flow process can be made.
- Dump step: The dump-step interval only has a limited influence on the calculation time and has no effect on the simulation results. For a smooth animation of the simulation the dump-step interval should be chosen relatively short.

2. Background

- Density: For the simulation of debris flows a density of 2000 kg/m^3 is used. This corresponds to the default value of the software. According to Iverson (1997) bulk densities of natural debris flows seldom range outside of 1800 to 2300 kg/m^3 .
- Lambda (λ): The parameter λ modifies the longitudinal pressure gradients driving the flow. This value is not changed for the simulations, since it is not recommended and the influence is very small (Bartelt *et al.*, 2013).

(4) Friction parameters:

The friction parameters μ and ξ belong to the most important data along with the input topography. They are varying depending on the material properties of the debris flow, the volume and the soil composition. As mentioned in chapter 2.5.1, the two values have a decisive influence on the speed and range of the simulated event. The values are kept constant throughout the entire event. In practice, they are determined by calibrating the model using previous events. In the context of this work, values from the literature are used. If they aren't available, the following approach is an appropriate option:

- Set μ to $\tan(\alpha)$, where α is the slope angle in the deposition zone (Mc Ardell, personal communication).
- Set ξ to 200 m/s^2 , which is suggested by Bartelt *et al.* (2013) if the type of flow is not known.

(5) Release parameters:

For the release mechanisms one can choose between block release and hydrograph. Since this work is limited to the runout of channelized debris flows, only hydrographs were applied. This leads to more realistic input conditions for large debris flows. Another advantage is the reduced simulation time, as the calculation domain can be made smaller to include only the geographical area of interest. The hydrographs were positioned preferably slightly higher than the fan apex. The discharge is defined by a 3-point-hydrograph calculation by using the following values:

- The total volume is set according to literature for specific events or if not available after empirical equation (cf. section 2.3.3). However, a volume was defined for the borderline case, that means any larger discharge would end in a channel overflow (see chapter 5.2.2).
- The maximum discharge (Q_{\max}) is calculated automatically according to Rickenmann (1999): $Q_{\max} = 0.1 V^{0.83}$, where V is the debris flow volume. However, this empirical relationship only makes sense for extreme events. According to the staff from the WSL and their observation stations, typical peak discharges of debris flows in Switzerland are by a factor of ten lower than what Rickenmann predicts (McArdell, personal communication). Therefore, the maximum discharge has been adjusted according to the observations for the borderline cases.
- For the time at which the maximum occurs (t_{\max}) a typical value of 10 s is set, and the velocity is set to 5 m/s as this has no significant influence on the simulation result (McArdell, personal communication).

(6) Additional functions: Several additional functions are available for RAMMS. For example, the forest effect can be considered by adjusting the friction parameters in the forest areas. It is also possible to simulate the entrainment of material (Frank *et al.*, 2016). However, this has not been done in this project.

2.5.3 Output

RAMMS offers different functions to visualize the simulation results respectively the different parameters. For this project the flow height and flow velocity are of importance. These results can be displayed in two- or three-dimensional view. For further analysis in GIS, an export as ASCII-File or Shapefile is possible.

2.5.4 Alternative models

Beside RAMMS there are other physically based, dynamic models. All of them solve the equations of motion using the depth-averaged shallow-water equations in 2D. Some of the models described below (RAMMS, DAN3D) include an additional centripetal acceleration term which helps them behave more like 3D models, especially over natural terrain (McArdell, personal communication). The models differ, among other things in the description of the rheology or frictional behaviour, which is decisive (eg. Stricker, 2010). Some of the models consider the erosion and deposition of sediment in the channel bed, which is also important in some cases. Because all these models solve the equations on a natural topography available on a grid, results obtained within the scope of this thesis using the RAMMS models are transferable to similar models, e.g.:

DAN3D, which was developed by Scott McDougall as a part of his PhD thesis at the University of British Columbia (McDougall and Hungr, 2004),

Flo-2D, which was developed by O'Brien at Colorado State University and combines hydrologic and hydraulic models to simulate flooding problems and muddy debris flows (O'Brien *et al.*, 1993), and

r.avaflow, which was developed in the framework of a German Research Foundation (DFG) project, and which uses open-source software (GRASS GIS and the R Project for Statistical Computing) for visualization (Mergili *et al.*, 2017).

It has been shown that the most complete characterization of debris flow processes is provided by such continuum based dynamic runout methods (Scheidl *et al.*, 2013). These models allow an estimation of flow depth and mean velocity, parameters that are often required for a more detailed hazard assessment. Comparisons between different debris flow models have been carried out by numerous authors (e.g. Rickenmann *et al.*, 2006; Cesca and D'Agostino, 2008; Schraml *et al.*, 2015), the various rheological or friction coefficients can typically be adjusted to achieve similar results for a given field case.

2.6 Hazard mapping

Based on Swiss federal law, the cantons are obliged to provide hazard maps and to consider these for spatially relevant projects. Hazard maps should allow a prediction about the threat posed by natural events. They act as a guideline for communal planning and the implementation of protective measures. Debris flow is one hazard type which can influence the map. (e.g. Raetzo *et al.*, 2002; Zimmermann *et al.*, 2005; Tobler and Krummenacher, 2013)

The hazard levels in a hazard map are derived from the intensity and the probability (respectively return period) of the different hazard types. Therefore, parameters for debris flows are defined, which describe the magnitude of an event and its frequency. The hazard classification is based on the diagram shown in Figure 15.

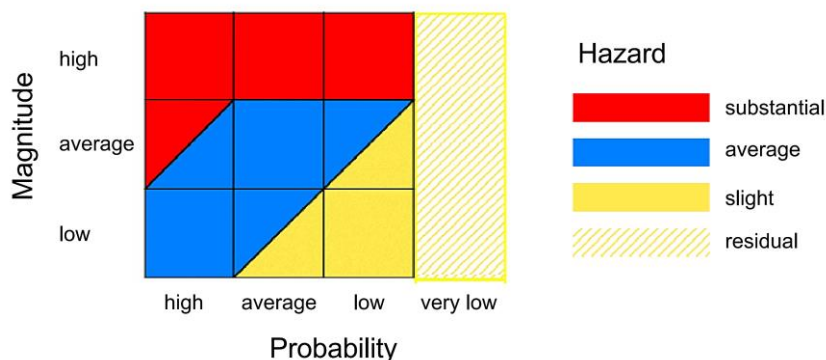


Figure 15: Diagram of hazard levels as a function of probability and intensity (e.g. BAFU, 2016).

2. Background

Three levels of magnitudes are considered, i.e. “high, average and low”. Regarding probability, four levels “high, average, low and very low” are used, with the corresponding return periods “1 – 30, 30 – 100, 100- 300 and >300 years”. For a potential hazard, its magnitudes therefore have to be determined for the chosen levels of probability at selected points of a specified area of investigation. This is achieved by various means, for instance by modelling the underlying process (e.g. numerical modelling in RAMMS). The magnitude of debris flow depends on the thickness of debris front (D) and the flow velocity (v) (BAFU, 2016):

- Low intensity: --
- Average intensity: $D < 1$ m and $v < 1$ m/s
- High intensity: $D > 1$ m and $v > 1$ m/s

Based on the results of the modelling process and with respect to Figure 15, the expected hazard level can be determined for any location on a given hazard map. The four classes of hazard levels (substantial, average, slight and residual) can be interpreted according to Table 3.

Table 3: Definition of hazard zones or hazard levels (ARE, BWG and BUWAL, 2005).

Substantial	<ul style="list-style-type: none"> ➤ Persons are endangered both within and outside buildings. ➤ The sudden destruction of buildings may occur. ➔ Prohibited area
average	<ul style="list-style-type: none"> ➤ While persons are hardly at risk inside buildings, they are so outside. ➤ Damage to buildings must be expected, but sudden collapse is unlikely in this area provided that certain requirements on building design are fulfilled ➔ Restricted area
slight residual	<ul style="list-style-type: none"> ➤ Persons hardly at risk ➤ Slight damage to buildings and/or obstructions must be anticipated, however substantial damage to buildings are possible ➔ Warning area

For this thesis the differentiation of danger zones is of importance, since the results of the numerical simulations for the maximum flow height over 1 m and for velocities over 1 m/s are sometimes shown separately. Thus, areas with substantial danger are addressed and investigated with more detail.

3 Study areas

A total of five study areas were selected for this project. They are all located in Switzerland (see Figure 16). The Illgraben is by far the best-known case and is situated in the canton of Valais near Leuk. The other four cases are situated in the canton of Graubünden and are considerably smaller in terms of catchment area, alluvial fan size and width of the torrent channel. Thus, the study sites include various characteristics. Some key indicators are listed in Table 4. Figure 17 gives an overview of the study areas.

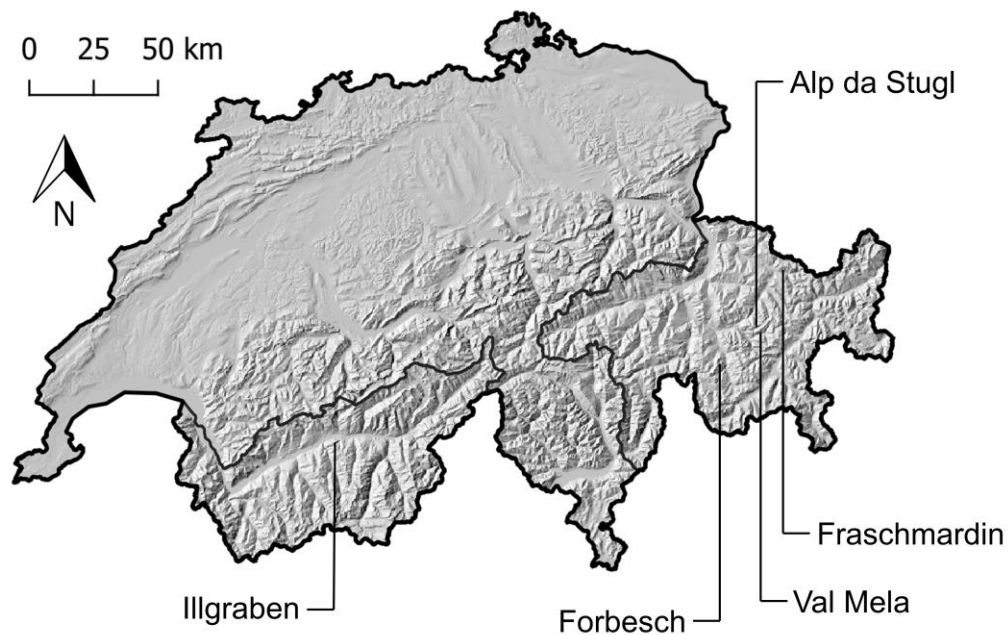


Figure 16: Locations of the study areas (swisstopo, 2018).

Due to the topography of the Alps, Switzerland is predestined for debris flow processes. Many historical settlements have been developed on debris flow fans. The elevated terrain offers protection against flooding of the valley floors. The houses are located mainly in areas that are far away from the channel, which keeps the risk of debris flow relatively low. However, economic growth and settlement pressure have led to an expansion of the exposed objects (*PLANAT*, no date). Due to the severity of the possible consequences of a debris flow, more is being invested in research. The selected study areas are part of various research projects of the WSL. In particular, the Illgraben was and is the subject of numerous investigations. As a result, detailed data are already available. High-resolution DEMs were produced for the cases in the canton of Graubünden, which are used in this thesis. This data availability is the main reason why the investigation areas, described in more detail below, were selected.

3. Study areas

Table 4: Characteristics of the study areas, approximate values (Data: swisstopo, 2019)

	Illgraben	Fraschmardin	Val Mela	Alp da Stugl ¹ West / East	Forbesch
Catchment area [km ²] ²	9.0	1.0	0.7	0.6 / 0.4	1.3
Highest point of the catchment area [m a.s.l.]	2716	2670	2954	2806	3261
Altitude at fan apex [m a.s.l.]	867.5	1556	1902	2071 / 2103	2000
Main exposition	North	South	South	South	Southeast
Channel length on the fan [m]	2800	1050	600	200 / 290	450
Average slope of the fan [%]	9	25	25	29 / 27	18
Alluvial fan size [km ²]	8.5	0.5	0.1	unknown	0.1
Mean channel width on the fan [m]	16	6	9	4 / 3	9

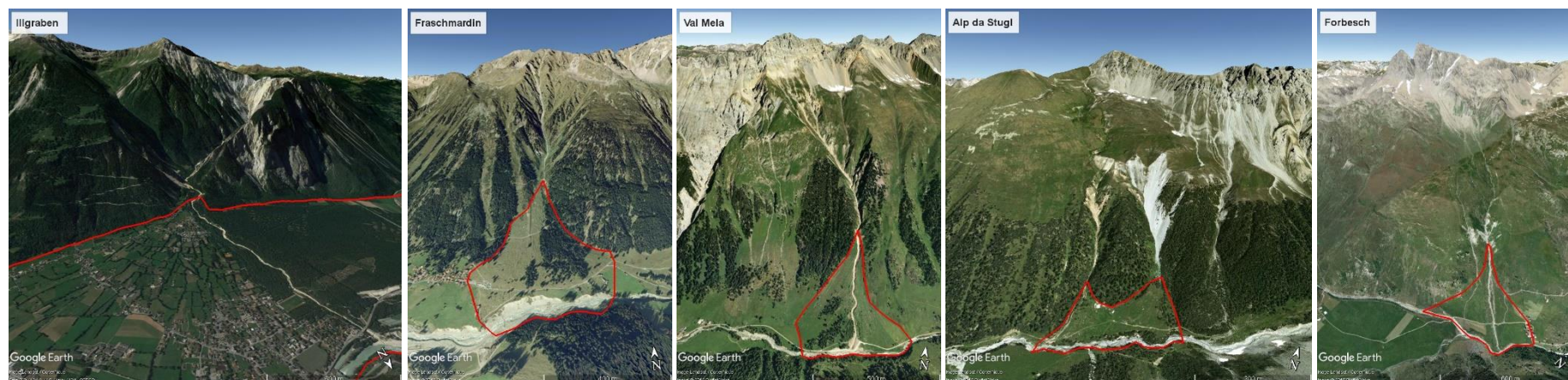


Figure 17: Study areas and approximate alluvial fans outlines in red (created with Google Earth).

¹ Two channels, two overlapping alluvial fans

² Catchment area until the fan apex

3.1 Illgraben

Several times per year the Illbach torrent rises with intensive precipitation and carries debris flows into the main valley. This extraordinary activity has led to the torrent piling up a huge debris flow fan into the valley of Rhone. While the eastern part of the debris fan is farmed with grasslands and acres, the western part is home to the Pfywald forest. The channelized part is strongly influenced by the regular debris flows, therein no permanent vegetation can form inside the channel due to the strong erosion (see Figure 18 and Figure 19).

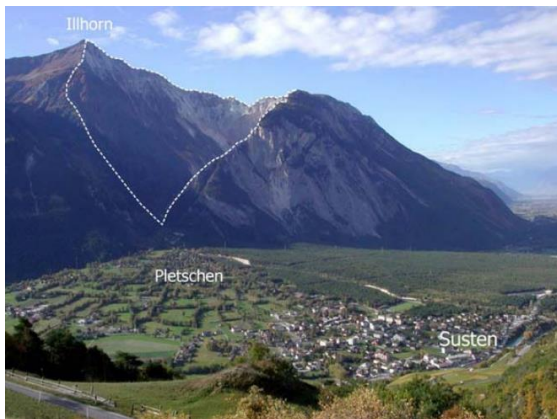


Figure 18: Illgraben debris fan with the village of Susten and confluence with Rhone River in foreground and the catchment in the background (F. Dufour, WSL). The area enclosed by the dashed line shows the active part of the catchment (Badoux *et al.*, 2009).



Figure 19: Typical view of the Illgraben debris flow channel. No vegetation can form inside the channel due to strong erosion.

The village of Susten is located on the fan and thus in the immediate danger zone. After devastating events in 1961, a protection concept was developed and implemented. A main dam and 29 other smaller dams are intended to stop the masses of debris as far as possible (Missbauer, 1971). Since 2000, the WSL has been monitoring spontaneous debris flows on the Illgraben and in 2007 a multi-stage warning system was set up for the municipality (Badoux *et al.*, 2009). A wide variety of flow types has been recorded at this station (see Figure 20).

According to Badoux *et al.* (2009) debris flows at Illgraben can generally be grouped into small debris flows which entirely remain within the channel, intermediate debris flows with limited overbank flow and large debris flows that could reach populated areas. The upper limit for small debris flows has been estimated using unpublished consulting reports at $75'000 \text{ m}^3$. This value is of importance for the simulation of the borderline case (cf. section 5.2.2). For a very unlikely and rare event, hence an extreme event, a debris flow volume of $500'000 \text{ m}^3$ can be expected (Berger *et al.*, 2012).



Figure 20: Arrival of the debris-flow front upstream of check dam 29 during the July 28, 2006 event (C. Gwerder, WSL). (Badoux *et al.*, 2009)

3.2 Cases in Graubünden

The cases in the canton of Graubünden are far less known for debris flows than the Illgraben. However, they are characterised by highly active torrent channels, which was well noticeable during field visit. The relatively narrow channels have a typical trapezoidal shape. All of them are at high altitudes, which is why they often serve as avalanche channels and, depending on the conditions, snow remains in the channel throughout the summer. During field work in May 2019 significant snow was within the torrent channels, especially for the cases situated above 1500 m a.s.l..

Fraschmardin

Fraschmardin is an easily accessible torrent near Klosters. The hamlet of Monbiel is close to the debris fan. At the end of winter, the snow disappears, and the torrent channel becomes visible. The fan apex is at an altitude of 1560 m a.s.l.. When looking down from there, one sees an artificial dam on the right-hand side which is intended to protect Monbiel from a possible debris flows or snow avalanches. The actual channel runs first along a forest until it flows completely into it. Finally, the torrent flows into the Landquart river after crossing a road.



Figure 21: Situation when looking down from the fan apex at the Fraschmardin torrent. The location of the actual channel is marked in blueish colour, while the protection dam is coloured in a yellowish colour.

The debris flow channel has a relatively constant width of about 5 meters on the entire fan. Very steep banks partly made it impossible to measure the cross sections. Figure 22 and Figure 23 show the trapezoidal channel shape representative for Fraschmardin.



Figure 22: Fraschmardin torrent with its typical trapezoidal shape within the forest.



Figure 23: Fraschmardin torrent with its typical trapezoidal shape along the forest.

Val Mela

The Val Tuors mountain valley near Bergün is accessible by a small gravel road. Shortly before the end of the road, the Val Mela channel must be crossed. It mostly serves as a track for huge avalanches. Due to natural hazards, few people have settled in Val Tuors. In order to reach the houses at the end of the valley by land, you have to pass dangerous avalanche cones with your skis in winter. In summer, the road may be temporarily unusable due to debris flows or other slope processes.



Figure 24: Val Mela torrent partly filled with snow just before it crosses the road.



Figure 25: Val Mela torrent channel filled with avalanche snow.

Alp da Stugl

Alp da Stugl is situated in the uninhabited Val da Stugl near Bergün. Two small debris flow channels (approx. 3 to 4 m wide) make their way down into the valley. Due to snow conditions this area could not be visited during the field campaign in May 2019.

Forbesch

Forbesch is a one-hour hike from the village of Mulegns. This debris flow channel can be accessed through the Val Faller. The torrent is named after the Piz Forbesch mountain just close by. The area near the debris flow fan is used as an alpine pasture. Some small houses and a chapel belong to the hamlet of Tga in Val Faller. During the visit in May 2019 there was still snow in the valley.



Figure 26: The Forbesch torrent channel partly filled with snow (in front). The hamlet TGA is located just on the side of the debris fan (in background).

3. Study areas

4 Data

This thesis investigates the optimal resolution of DEM for debris flow modelling. That is why a variety elevation data was used, ranging from provided and self-created height models to field data which was acquired through intensive fieldwork (see Figure 27).

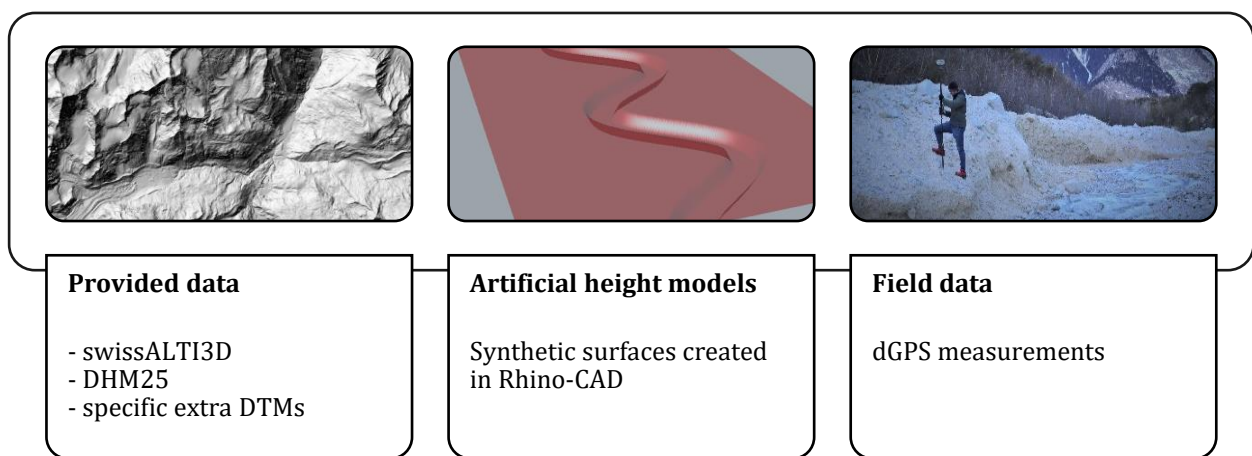


Figure 27: Elevation data (own graphic representation, Images: geodata4edu.ch (26.02.2019), Rhino-CAD interface (26.02.2019), Brian McArdell (22.01.2019).

4.1 Geodata

In order to answer the research questions, data provided by various institutions and individuals were used. The different elevation models are crucial for this study. In addition, maps and orthophotos were included for the analysis. In particular the product swissALTI3D by swisstopo was used. Furthermore, swisstopo provided the elevation model DHM25 as well as different maps and orthophotos. These basic data could be obtained from the geodata4edu website (<http://geodata4edu.ethz.ch/>, last access: 09.04.2019) in GeoTIFF format. This is a geodata service for Swiss universities established by the institute of cartography and geoinformation of the ETH Zurich.

For the cases in Graubünden Dr. Yves Bühler from the SLF provided high resolution DSMs (10 cm spatial resolution). In addition, the corresponding orthophoto with a spatial resolution of 5 cm was provided. A high-resolution DEM (5 cm spatial resolution) for the Illgraben in the canton of Valais was obtained by Prof. Tjalling de Haas, University of Utrecht. These data were recorded within the scope of different measurement campaigns by using UAV.

An overview of the provided geodata which was used in this thesis can be found in Table 5. Note that all data is in raster format and have different accuracies depending on the surveying method.

Table 5: Provided geodata

Dataset	Spatial resolution	Year	Source	Comment
swissALTI3D	2, 5, 10 m	2018	swisstopo	DTM
DHM25	25 m	variable	swisstopo	DTM
National map 1:25000	762 dpi	variable	swisstopo	with relief
National map 1:50000	762 dpi	variable	swisstopo	with relief
SWISSIMAGE	1 m	variable	swisstopo	Orthophotomosaic
DEMs Graubünden	0.1 m	2018	SLF (Yves Bühler)	DSM
Orthophotos Graubünden	0.05 m	2018	SLF (Yves Bühler)	-
DEM Illgraben	0.05 m	08/11/2018	University of Utrecht	DTM

4.2 Artificial height models

To investigate the influence of the spatial resolution of the elevation model on the simulation result, artificially generated surfaces were used. These were created with the help of a tool called Docofossor in Rhino-CAD (see chapter 5.2.1). The elevation models are output in raster format and are the topographic data basis for the simulation in RAMMS.

The raster format in Docofossor allows to calculate Boolean operations within the 2.5D distance field. The data structure is based on a single list that defines a regularly spaced quad grid from topographic data. A header part defines the properties of the grid such as the cell size, the number of rows and columns, and the coordinates of the origin of the grid. The elevation data in form of z-values is in column-major order starting bottom left. This raster format is roughly based on the Esri ASCII grid (Bernhard and Hurkxkens, 2018).

4.3 Field data

Especially to answer the first research question (*How well are torrent channels represented in DEMs in common use in Switzerland?*) and to complement the readily available datasets, in-situ measurements have been done by using dGPS (see chapter 5.1.1). The data was acquired in fieldwork on the 22nd of January at Illgraben, and on the 21th and 22nd of May in 2019 at the field sites in the canton of Graubünden. Furthermore, the approximate geometry of the torrent channel Combatseline in the valley of Nendaz was measured on the 29th of May 2019. This data contains cross-section transects of the torrent channels. Over four hundred measurement points were taken in total. Along with the coordinates and the elevation, meta data on the locations and interesting features have been collected. Photographs were taken to illustrate the study sites.

The data was imported into a GIS to be able to analyse the data in regard to the research questions. The spatial analyses are performed in QGIS, while the statistical analysis and data visualisations are made in RStudio.

5 Methods

5.1 Digital elevation models

This section covers the methods that have been used to assess the representation of torrent channels in different DEMs. Torrent channel cross-sections have been measured in the field by using dGPS. The data gathered was used to generate detailed profiles which then were compared to the cross-sections at the same locations, which are derived from various DEMs. The comparison gives an insight into the characteristics of the channel geometries and its digital representation. Since the spatial behaviour of debris flow events is affected by the channel capacity, a method was developed to estimate the channel area, which is necessary to define the carrying capacity of the channel. Basically, the cross-sectional areas of the transects have been computed. Plotting these results against the grid resolution provides an indication regarding the representation of debris flow channels in DEMs.

5.1.1 Field work

The study sites were visited to get an overall impression and to carry out cross-section measurements of the torrent channels. Several photographs were taken to illustrate the different situations with their characteristics.

The measurement of channel cross-sections provides information about the geometry of the torrent channels and their flow capacity. It is important to take at least one cross section per homogenous channel area to be able to interpolate information between the sampled locations (Willi *et al.*, 2015). Thus, an effort was made to measure one cross section per homogeneous channel area on the entire debris fan. However, due to reasons of accessibility, time and hazard potential, it was not always possible to achieve this. Especially significant snow often made it impossible. Nevertheless, several cross-section measurements have been taken.

The measurements contain information on position and height. Depending on the channel geometry, different numbers of measuring points were recorded for each cross-section. The aim was to record as many measuring points that an accurate representation of the channel is possible. In addition, metadata about specific properties of the profile were recorded. Figure 28 illustrates how the measurements were made.



Figure 28: Cross-section measurement at Illgraben (Photo: Brian McArdell)

5. Methods

As a measuring instrument the “Leica GPS1200” was used (see Figure 29). A lightweight and compact antenna (see Figure 30) enables the reception of a signal which allows to determine an accurate and repeatable position to be calculated. The accuracy of the position is increased with the aid of a correction signal received by a conventional mobile phone. This method is called dGPS. It makes use of reference stations whose exact position has been clearly determined by classical surveying methods. The actual travel times of the signals for each satellite can be determined very precisely from the deviation of the actual and the received position. With this information the mentioned correction signal can be generated. The metadata of the measurements showed, that the accuracy of the position and height was determined with minor inaccuracies of a few centimetres.

However, real time measurements were not possible for some field sites in Graubünden. The reason is a lack of communication signals to the Swisscom-network or to the GPS-satellites. Therefore, some points were taken in postprocessing mode, this means that a measurement for such a point is based on around 300 signals. This took up to ten minutes per measurement point.



Figure 29: Leica GPS1200



Figure 30: Antenna of Leica GPS1200

5.1.2 Cross-section visualisation

The results of the measurements with the dGPS are used to answer the first research question. They give exact information about the location of the channel. For these measuring points, elevation values were subsequently read out from various existing elevation models (see chapter 4.1) using a GIS. With this, cross sections for the same locations and the different DEMs could be generated and compared. The spatial resolution of the DEMs used in this project range from a few centimetres to 25 meters. The swissALTI3D-DEMs are all frequently used in practice. The results obtained with the DHM25 are also of importance since in other countries the DEM with the highest spatial resolution may even be worse than 25 meters.

The comparative representation of the cross-sections was created in R-Studio. The corresponding script can be found in the appendix.

5.1.3 Channel capacity

Since the channel capacity is also decisive for the propagation of debris flows, a method was developed to calculate it for the derived cross sections. This allows a further insight into how well torrent channels are represented in DEMs which are commonly used in Switzerland.

The flow behaviour of debris flows is complex and difficult to understand (see chapters 2.1 and 2.3). They can exceed the bank height without leaking out. They also move at different speeds. Therefore, the channel capacity cannot be calculated conclusively. Instead, simplified assumptions must be made to answer the first research question. For this purpose, the cross-sectional area was calculated. Hence, a simple comparison of the cross-

sectional areas, which are based on the transects of the different elevation models, is possible. The calculation is based on the assumption that the debris flow behaves like a normal river. It was done in RStudio (see appendix for script). The following steps are performed automatically for each cross-section (the numbers in the brackets correspond to the one shown in Figure 31):

- Define the lowest point of the cross-section (1).
- Define the highest point left and right of the lowest point (2).
- Take the lower of these two points (2).
- Fill the cross-section until this point is reached. The result is the cross-sectional area desired (blue area in Figure).

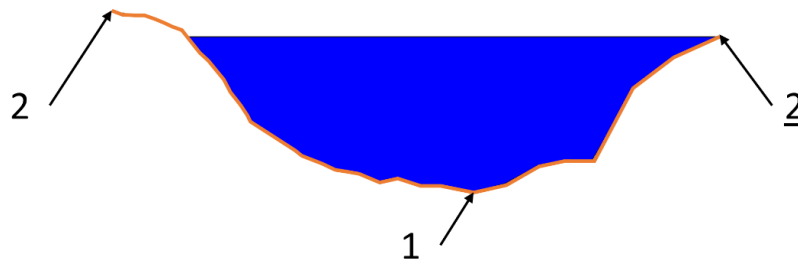


Figure 31: Visualisation of a calculated cross-sectional area (blue area in figure). The orange line illustrates the cross-section. The numbers correspond to the description given in the text.

This method also allows the determination of the maximum filling level. Together with the corresponding channel width, this provides additional indicators of how well a channel is represented in the different DEMs.

5.1.4 Evaluation

In order to evaluate and compare the cross-sections, the calculated cross-sectional area, channel width and depth were collected in a table (Table 8 in appendix). The data based on the dGPS measurements serve as a basis for comparison in the analysis. This is because these point measurements are accurate to within a few centimetres and therefore represent the position and shape of the channel best. The cross-sectional area, width and depth determined from the dGPS data per transect are thus used as comparative values and indicators.

In a first step, the cross-sectional area values calculated on the basis of the different DEMs are compared to the reference value. Using the program RStudio, the results are displayed in a grouped bar chart.

Since a relationship between the channel width and an adequate representation of the cross-sectional area dependent on the DEM resolution is assumed, the second step serves to compare the previously computed area percentages with the dGPS-based widths. RStudio was applied for the presentation of this scatter plot with regression lines.

5.2 Debris flow runout modelling

5.2.1 Preparation of the input DEMs

In order to perform the planned modelling, the elevation models needed to be prepared. This was done for two types of topography: The real-world cases and the synthetic surfaces.

Real-world cases

For the real cases, the highest resolution DEM forms the basis. These were subsequently converted to the requested resolution. The procedure used for resampling was the nearest neighbour method (see chapter 2.4.2). The reason why existing elevation models with a different resolution (e.g. DHM25, swissALTI3D) were not used, is due to the different data-recording times. Because the ground contours changes over time, the simulation results would not be comparable regarding the research questions. The resampling was performed in QGIS and the new DEMs were saved in GeoTIFF format. Table 6 shows the resolution of the original DEM and the resolutions of the input DEMs for the subsequent modelling in RAMMS. The resolution of the input DEMs was doubled until a resolution of 32 m (64 m for the Illgraben) was reached.

Table 6: Spatial resolutions of the basic DEM and the input DEMs for the subsequent modelling in RAMMS for the different real-world cases.

	Illgraben ³	Fraschmardin	Val Mela	Alp da Stugl	Forbesch
Resolution of original DEM [m]	0.05	0.1	0.1	0.1	0.1
	1	0.1	0.1	0.1	0.1
	2	0.25	0.25	0.25	0.25
	4	0.5	0.5	0.5	0.5
	8	1	1	1	1
Resolution of input DEMs [m]	8	2	2	2	2
	16	4	4	4	4
	32	8	8	8	8
	64	16	16	16	16
		32	32	32	32

Synthetic surfaces

The synthetic surfaces and artificial height models were generated within the program Rhino-CAD. Rhinoceros (abbreviated Rhino) is a commercial 3D computer graphics and CAD application software developed by Robert McNeel & Associates (*Rhinoceros*, no date). Currently running on version 6.0 it is used in industries including architecture, industrial design, product design, multimedia and graphic design. For the purpose of this work the Grasshopper-Plugin has been used. Grasshopper is a graphical algorithm editor tightly integrated with Rhino's 3-D modelling tools (*Grasshopper*, no date). This plugin allows generation of 3-D geometries in a relatively simple way by dragging program components onto a canvas. The outputs of these components are then connected to the inputs of subsequent components.

Docofossor is a collection of landscape modelling components in 2.5D with distance fields which can be used as a component library for Rhino 3D Grasshopper. Originally it was developed to model cut and fill operations by a robotic excavator in landscape architectural design. However, as these components allow a continuous transformation of the topography by point, path area or volume operations on a DTM, it is used for this project

³ For the Illgraben the high-resolution DEM had to be merged to the swissALTI3D DEM, because it only covers the area of the channel.

to create the synthetic surfaces. Docofossor is open-source and Python-based. The authors are Matthias Bernhard and Ilmar Hurkxkens from the ETH Chair of Landscape Architecture led by Professor Christophe Girot (Bernhard and Hurkxkens, 2018).

Figure 32 shows the components within the Grasshopper interface which have been used and how they are connected to create a synthetic surface.

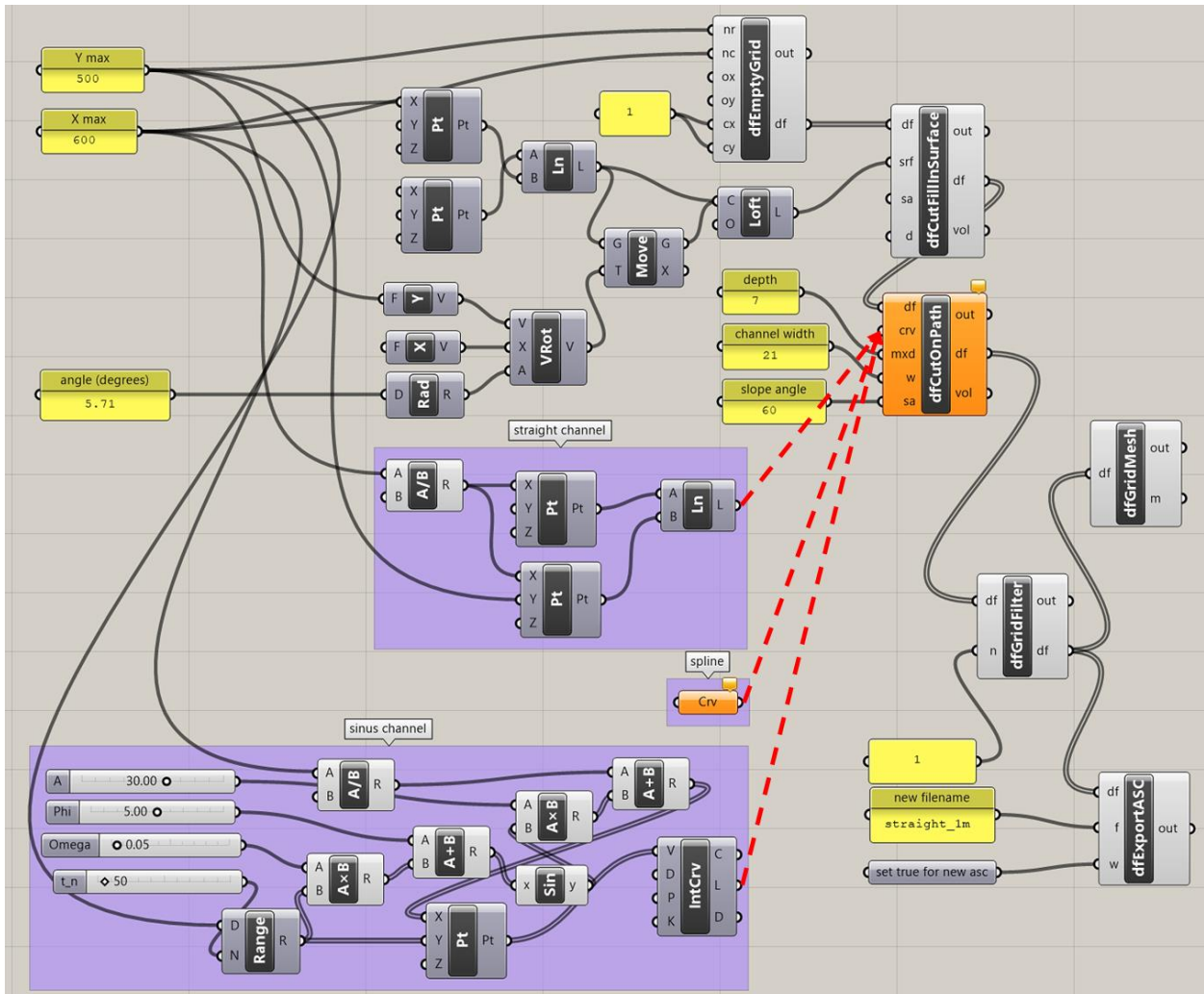


Figure 32: Components which have been used to create the various synthetic surfaces (Grasshopper interface). The red dashed lines indicate links of components that need to be established in order to specify the desired channel path.

Different steps were required to create the artificial surface. The first step was to define a flat surface of a certain size. Then it was tilted at a desired angle. In order to integrate a channel on it, its path had to be defined. In this case three possibilities were provided: A straight channel, a free form that can be drawn by hand and a channel in the form of a sinusoidal curve. Furthermore, the definition of the channel width, depth and bank inclination is necessary. Thus, the cross sections of the created channels have a trapezoidal shape. The spatial resolution as well as the grid to be exported could be determined by using further components.

Figure 33 illustrates how the artificial surface which was defined in Grasshopper may be represented within the Rhino-CAD interface.

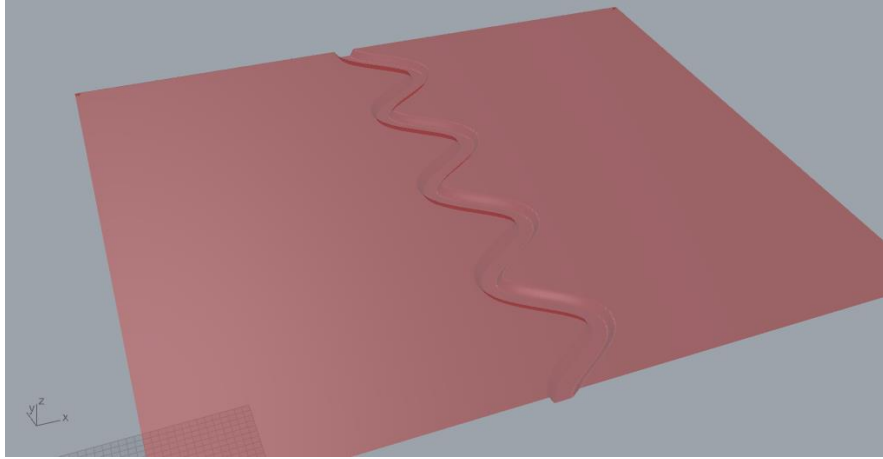


Figure 33: Representation of a synthetic surface with a sinus channel in the 3D-view (Rhino interface).

5.2.2 Modelling in RAMMS

With the RAMMS module the speed and spatial extent of debris flows are predicted (see chapter 2.5). The prepared input DEMs with several various resolutions have been used as topographic input data for the runout modelling. All other input parameters have been kept constant to evaluate the differences in the runout zones for the following two predefined scenarios:

- Extreme event (A):

As no specific data is available except for the Illgraben, the empirical formula⁴ according to D'Agostini (1996) was used for the input volume. The advantage of this formula is that it depends only on the size of the catchment area, which can be easily calculated in GIS. As the volume of this magnitude is not decisive for the modelling results, the received values were rounded generously. All other input parameters were determined based on recommendations (cf. chapter 2.5.2). Experience has shown that such empirical formulas often overestimate the debris flow volume (see chapter 2.3.3). Thus, the term extreme event is used for this scenario.

- Borderline scenario (B):

In the borderline scenario any larger discharge would end in a noticeable channel overflow. Therefore, the input volume was adapted and μ has been set to a value which allows the debris flow to reach the end of the channel on the fan. One tenth of the value proposed by Rickenmann was applied for the peak discharge Q_{max} . This is a more typical value (explanation see chapter 2.5.2). The borderline case is based on the simulation using the input DEM with one-meter spatial resolution. This scenario was applied, because it was observed in the results of the first part of the thesis that the channel capacity usually decreases, if a DEM with a larger grid size is used. As a result, it's expected to detect significant channel overflows when the other input DEMs are considered.

All parameters used for the simulations are listed in Table 7. The input hydrograph was placed into the channel slightly above the fan apex. All simulations were then carried out on a 1 m grid. This means RAMMS converts the resolution of the input DEM to the simulation resolution of 1 m. This is an essential procedure to ensure that the resulting runout zones are comparable for the purpose of this research. The simulation stop criterion is the time, that the debris flow needs to reach the end of the fan or a barrier which prevents the debris flow of further propagation. The end time was set accordingly. The modelling results were saved as ASCII files for further analysis. The maximum flow height and the maximum velocity were considered.

⁴ $M_a = 29100 A_c^{0.67}$, see chapter 2.3.3

Table 7: Selected input parameters for the debris flow simulations in RAMMS according to scenario A (extreme event) and scenario B (borderline case). The channels in the artificial surfaces have a trapezoidal shape (7 m depth, 21 m top width, 60° channel bank angle) and running down a planar surface having a 10° slope.

Input parameter	Scenario	real-world					artificial		
		Illgraben ⁵	Fraschmardin	Val Mela	Alp da Stugl West	Alp da Stugl East	Forbesch	Sinus	Freeform
Sim resolution [m]	A	1							
	B								
End time [s]	A	1000	380	250	50	180	250	80	60
	B	2500	600	300	80	250	400	-	-
Dump step [s]	A	50	5						
	B								
Density [kg/m ³]	A	2000							
	B								
Lambda	A	1							
	B								
ξ [m/s ²]	A	400	200						
	B								
μ [-]	A	0.07	0.25	0.25	0.29	0.27	0.18	0.07	0.07
	B		0.13	0.13	0.14	0.12	0.1	-	-
Inflow direction	A	30	260	280	270	280	315	225	310
	B								
Volume [m ³]	A	500'000	30'000	25'000	20'000	15'000	35'000	100'000	100'000
	B	110'000	12'000	14'000	5'000	2'000	12'000	-	-
Qmax [m ³ /s]	A	5587.8	536.3	460.8	382.6	301.1	609.8	1462.2	1462.2
	B	158	25	28	12	6	25	-	-
t1 [s]	A	10							
	B								
V _{initial} [m/s]	A	5							
	B								

5.2.3 Visualisation of runout zones

To visualize and analyse the results of the RAMMS modelling, the ASCII files were read into RStudio. As a background for the simulation results orthophotos of swisstopo (SWISSIMAGE) with a spatial resolution of 1 m were used. These were converted to grayscale images in order to clearly visualize the varicoloured results. A grid corresponding to the Swiss national coordinates (CH1903) was inserted to provide scale and orientation.

Since the values for the flow height and the velocity of the debris flows vary and contain outliers, the values have been coloured appropriately for the purpose of illustration. Flow heights below 0.1 m are never displayed or used for further analysis. According to McArdeLL (personal communication) such a thin overflow is unlikely and rather single debris boulders might stop in this range. These thin layers cannot be avoided in the original results due to the computing formulas in RAMMS. In some illustrations only flow heights above 1 m or velocities

⁵ The friction parameters (ξ , μ) and the volume for scenario A for the Illgraben are based on Berger, McArdeLL and Lauber (2012). The volume for scenario B set a bit higher than the channel-capacity given by Badoux *et al.* (2009)

above 1 m/s are displayed, as this corresponds to a high intensity magnitude of debris flows in hazard mapping (see section 2.6). The R-script used for the mapping is in the appendix.

5.3 Sensitivity of the model to DEMs

Since the simulation results indicate general trends, some of these are analysed in more detail. The size of affected area is related to the channel deformation. These links between the DEM resolution and the modelling results are shown by different graphs. Finally, these results allow a statement about the necessary grid resolution for which the modelling error becomes negligible.

5.3.1 Affected area

To assess the influence of the grid resolution on the affected area the pixels of the simulation results were counted. Pixels having a minimum value of 0.1 m respectively 1 m for the flow height and a minimum value of 1 m/s for the debris flow velocity were considered. Each pixel corresponds to 1 m², because for the modelling exactly this simulation resolution was chosen. Therefore, the number of pixels equals the affected area in square meters. This procedure was done in RStudio for the simulation results of the real-world cases. The data was summarized in a table (Tables 9, 10 and 11 in appendix).

To compare the data, it was necessary to normalize the area values. Therefore, the affected area at a resolution of 1 m is 100%. All data are in relation to this value. This concerns the graphs for the maximum flow height over 0.1 m and over 1 m and for the maximum velocity, respectively. The percentages corresponding to the affected areas are represented on the y-axis and the input DEM resolution by the x-axis.

Graphs were created separately for the extreme event simulation results and for the borderline scenario simulation results. Channel overflow is likely in the borderline scenario using the one-meter grid, because the affected area changes a lot more in the simulations based on the borderline scenario. At a coarser grid size, it is even more probable and therefore the affected area is expected to increase.

5.3.2 Channel deformation

In the simulation results, the formation of apparent pools in the channel was detected. This phenomenon of channel deformation depends on the grid resolution of the input DEM and the resampling technique, respectively. To analyse the behaviour in more detail, DEMs with different resolutions were created with an artificial channel in it. The basic DEM was created in Rhino-CAD by using the Docofossor tool of the Grasshopper-plugin (explained in chapter 5.2.1). A spatial resolution of 1 m was chosen. The channel had a trapezoidal shape. The top width was 20 m, the depth 6 m and the banks are 50° steep. The course of the channel was straight and downhill but not parallel to the DEM cells.

The basic DEM (with 1 m resolution) was resampled within Q-GIS by using nearest neighbour technique to various spatial resolutions up to 30 m. Because RAMMS uses bilinear interpolation technique for resampling the input DEM to the simulation resolution, all DEMs have been resampled this way back to a one-meter grid. As a result, several DEMs were available in the same grid scale for the analysis.

By taking cross-sections within these DEMs at the same location, a comparison (similar to the one described in chapter 5.1.3) is possible. Therefore, several cross-sectional areas were calculated. The areas based on the basic DEM are the most precise and are used as a reference. This analysis allows detection of the grid size, where the cross-sectional area begins to change or vary and therefore at which grid size the forming of pools becomes visible.

6 Results

6.1 Digital elevation models

To demonstrate how the channels are represented in the different DEMs, line plots of the various transects were created. The dGPS measurement gives the start and the end point of a transect line and represents the actual channel margins. Hence, the x-axis represents the horizontal line of the transect, meaning the horizontal profile axis. The y-axis represents the surface elevation. Figure 34 shows the representation of a channel cross-section of the Val Mela torrent depending on different data origins. The yellow line always indicates what has been measured with the dGPS during fieldwork. The other coloured lines are based on data derived from the various DEMs, which range from a spatial resolution of 0.1 m to 25 m in this case.

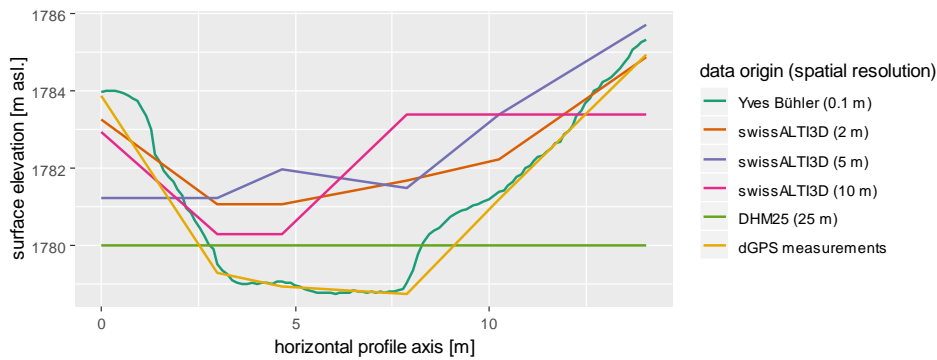


Figure 34: Representation of a channel cross-section in Val Mela depending on different data origins.

The dark-green line is derived by the UAV-DEM from the SLF (Yves Bühler) and has a similar pattern to the dGPS measurements-based line. In the swissALTI3D DEMs the channel is also recognizable, but the representation is clearly worse in the 5 m resolution DEM than in the 10 m resolution DEM. In the DHM 25, however, the channel disappears completely. This can be confirmed by the results of the calculations for the cross-sectional areas (see Figure 35). For the dGPS and the UAV-DEM cross-section the channel reaches approximately the same capacity. For the other DEMs the cross-sectional area is reduced drastically or even disappears completely.

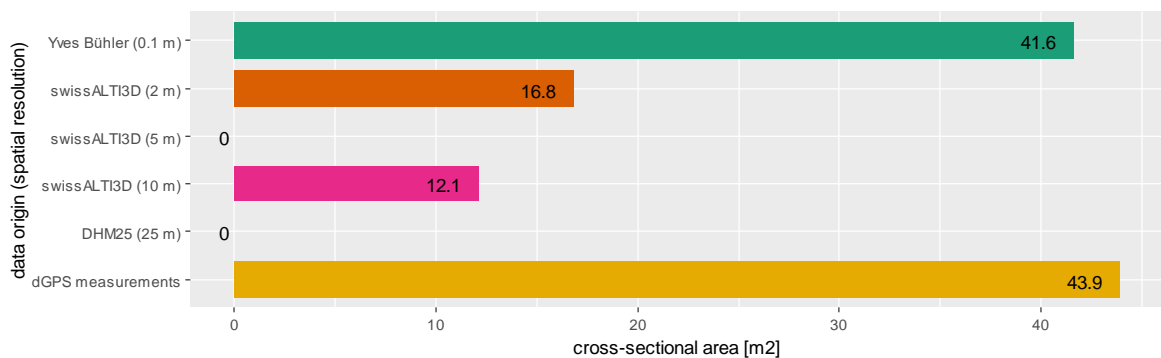


Figure 35: Cross-sectional areas [m²] of the channel cross-sections based on the same data as Figure 34.

6. Results

In Figure 35 the cross-sectional area of the transect based on swissALTI3D with 5 m spatial resolution has a value of 0 m² although a small channel is visible. This can be explained by the chosen method for computing the cross-sectional area (see chapter 5.1.3): If the lowest point of the transect is not within the channel, a calculation is impossible.

Only a selection of cross-section representations is shown within the next figures, because many transects were measured. The results of the calculated cross-sectional areas are summarized in Figure 38 and Figure 39 later in this chapter.

At Illgraben a total of eight transects were measured. With an average channel width of well above 10 m, it is more likely that the channel will be recognized at DEM's with relatively poor spatial resolution (e.g. 10 m or more). The southernmost illustrated cross section shown in Figure 36 is at a large check dam. In this graph the influence of a coarser grid resolution is clearly visible: While the UAV-DEM from the University of Utrecht and the swissALTI3D with 2 m resolution have a quite similar profile line as the one based on the dGPS measurements, the cross-sections for the DEMs based on a resolution of 5 m, 10 m and particularly 25 m deviate more. The other illustrated transects are showing similar results for the representation of cross-sections whereas in the profile-lines based on the DHM25 the channel is nearly invisible for both cases. For the northernmost illustrated cross-section diagram, however, a striking difference in the channels lowest point should be noted for the DEMs with a small grid size. This is probably due to different recording times of the DEMs which is discussed in chapter 7.1.2.

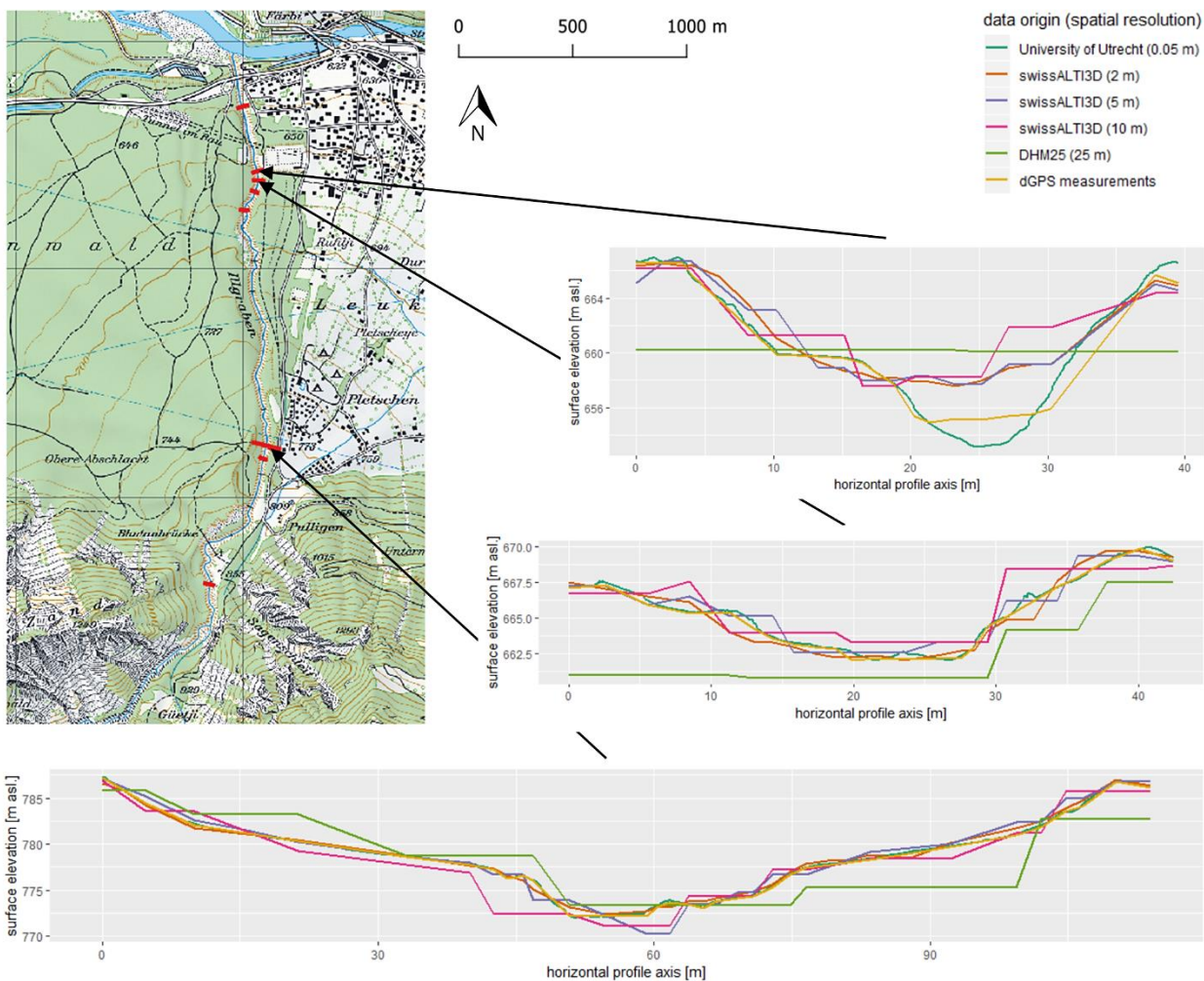


Figure 36: Selection of cross-section representations at Illgraben (map: swisstopo 2018)

In contrast to the Illgraben, the Fraschmardin torrent has a much smaller channel width of approximately six metres on average. As a result, a channel can not be detected in the DHM25. Only in the swissALTI3D with 2 m grid size or even better resolved DEMs is a channel usually recognizable in the cross sections (Figure 37). Additionally, the cross section based on the UAV-DEM from the SLF (Yves Bühler) shows a strongly-elevated area starting at an x-axis value of about 8 m. Because it is a DSM, the vegetation is part of the representation in the DEM, which makes interpreting the results more difficult. The cross-section illustration at the bottom right is also remarkable, where the DHM25 is indicating a completely different height compared to the other DEMs.

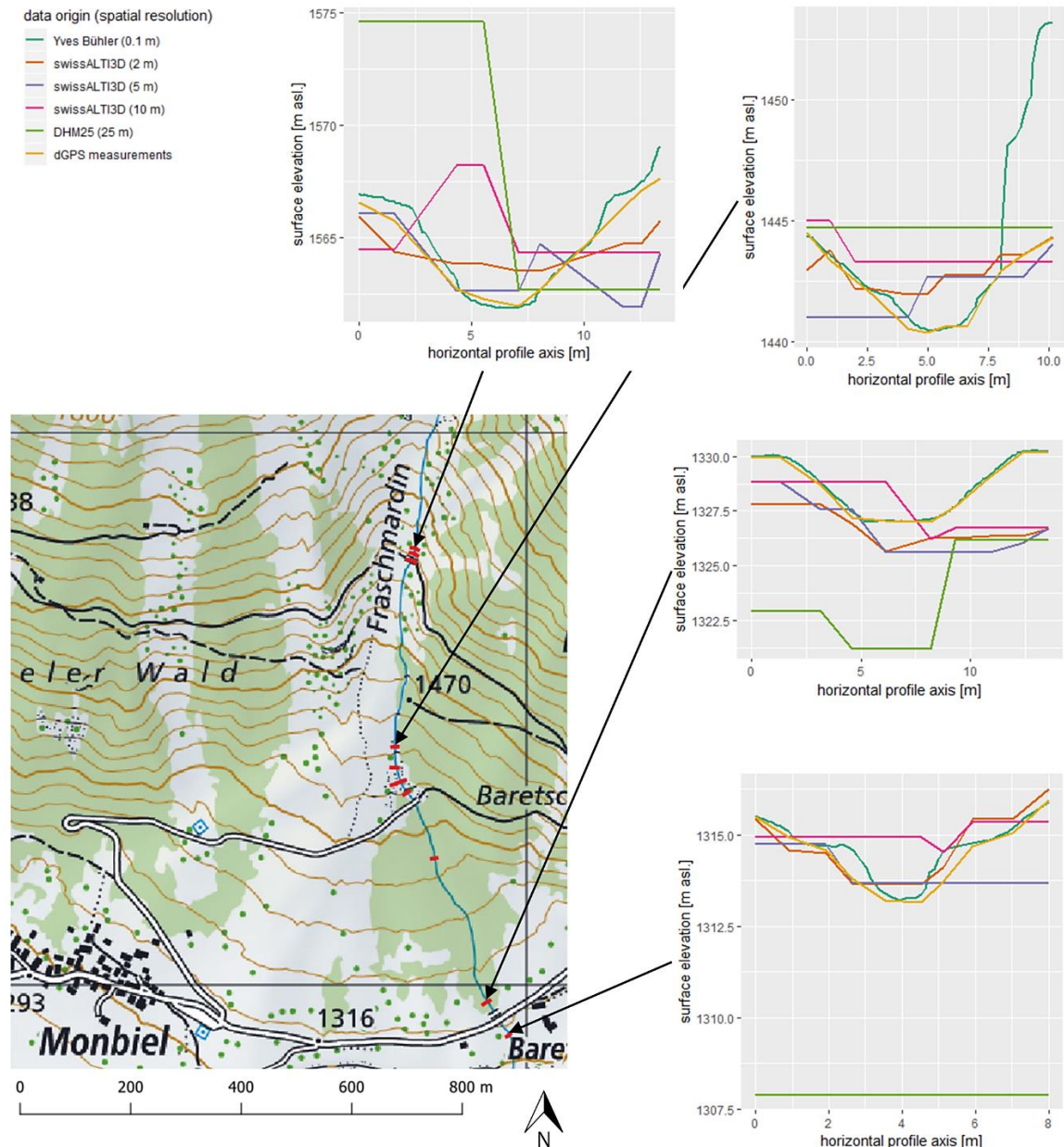


Figure 37: Selection of cross-section representations at Fraschmardin (map: swisstopo 2018)

For all transects (many of them are not illustrated above) the cross-sectional areas have been computed. The area values were compared to the dGPS based cross sectional area which serves as a basis for the comparison. For more detail, the width and filling height is also included in the analysis. The resulting graph is a grouped barplot (see Figure 38). Each group indicates a transect and each bar the cross-sectional area percentage in relation to the dGPS based cross-sectional area. As it can be seen easily, the dark green bars fluctuate relatively close to 100% with a few exceptions, meaning that the high-resolution UAV DEMs from SLF and the University of Utrecht have approximately the same cross-sectional area values. No regularity can be detected for this

6. Results

fluctuation. However, the deviations of the dark-green bars towards the upper end are probably due to altitude values in the DEM, which represent the vegetation. In the swissALTI3D DEM with 2 m resolution, channel cross-sections could be determined for all transects investigated, but their area is often well below 100%. This is especially the case where the width falls below a value of about 15 m. With a grid size of 5 m or more, the representation of the cross-sectional areas is usually insufficient. There seems to be a connection with the channel width: The wider the channel, the more likely it is that the values of the bars reach around 100% indicating an accurate representation of the channel cross-section area. This relationship is further investigated in a next step. Outliers can be detected for the swissALTI3D with 10 m resolution: The bars sometime reach higher percentages in the analysed cases than the swissALTI3D with 5 m resolution. In the DHM25, on the other hand, no channel is detected in most of the transects.

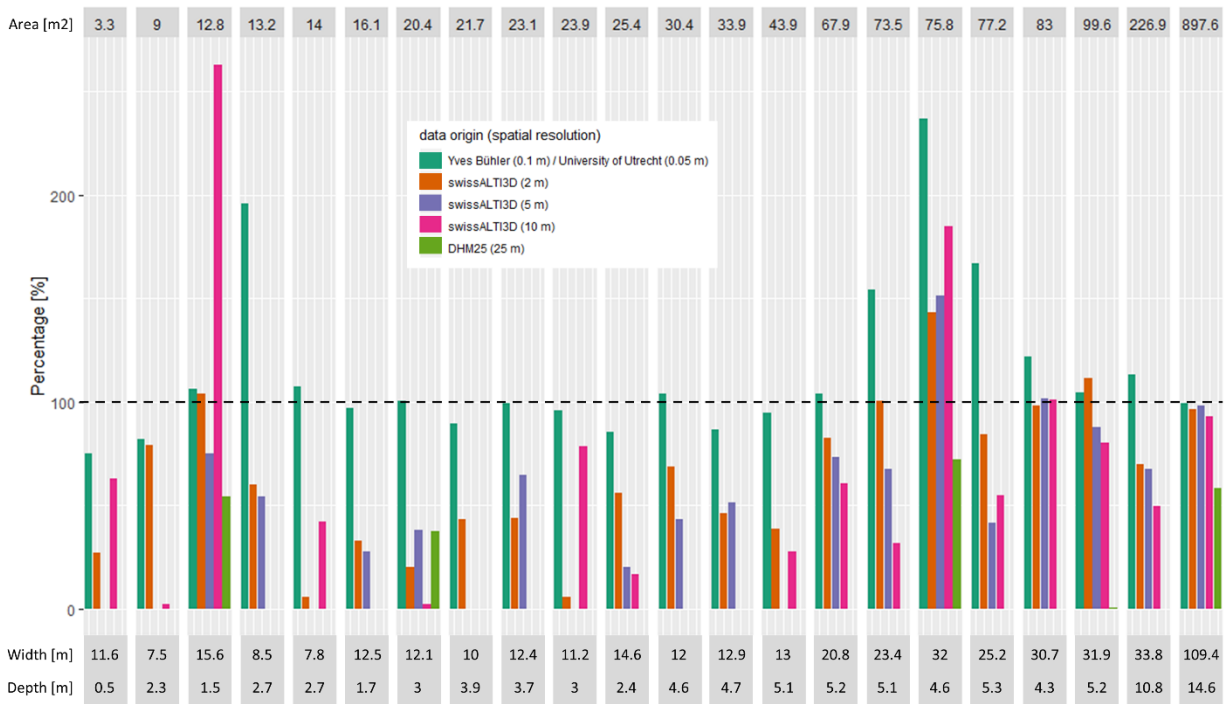


Figure 38: Calculated cross-sectional areas for all field sites where measurements were taken (field sites not separately labelled) based on the different DEMs as a percentage of the dGPS-based cross-sectional area (sorted ascending). The absolute calculated cross-sectional area based on the dGPS data is in the top row. The corresponding width and depth of this transect are in the bottom rows.

To study the relationship between the existing cross-sectional areas and the channel width in more detail, a scatterplot was created (Figure 39). The y-axis represents a percentage of the dGPS based cross-sectional area. This time, however, the x-axis is representing the channel width according to the dGPS data. Therefore, each point in the scatterplot indicates a specific DEM-based cross-sectional area which is sorted according to the channel width. Thus, there are five points on top of each other, which represent the computed areas of the same transect. A regression line allows to make a statement about the connection between the spatial resolution and the actually represented cross-sectional area. Outliers have been excluded for this analysis: Percentage value above 150 % have been removed. This was done to minimize the influence of errors due to vegetation in the UAV-DEMs and to ignore randomly large values, whose impact on the result is immense due to the sample size.

Looking at the points and in particular on the regression lines in Figure 39 the expected behaviour is clearly visible. The 100% line is reached when the channel is wide, and the grid size of the DEM is relatively small. In detail, the fluctuation around 100% for the UAV-DEM points is visible. For the swissALTI3D with 2 meters resolution a first point achieves 100% at approximately 15 meters channel width. The first point reaching 100% for the 5m-DEM is at a channel width of 30 meters. Since most of the debris flow channels are up to 10 m width it is difficult to make more precise conclusions. However, it can be said that for the investigated cases

and therefore for most cases in Switzerland the swissALTI3D with 2m resolution, underestimates the channel capacity. Even though this is the best publicly available DEM in Switzerland at the moment, debris flow simulations based on this dataset might be critical.

According to the gathered data and its analysis the following rule of thumb can be applied: In order to ensure that the cross-sectional area respectively the capacity of a torrent channel is represented in the correct measure in a DEM, the channel width should be at least ten times as large as the spatial resolution of the DEM.

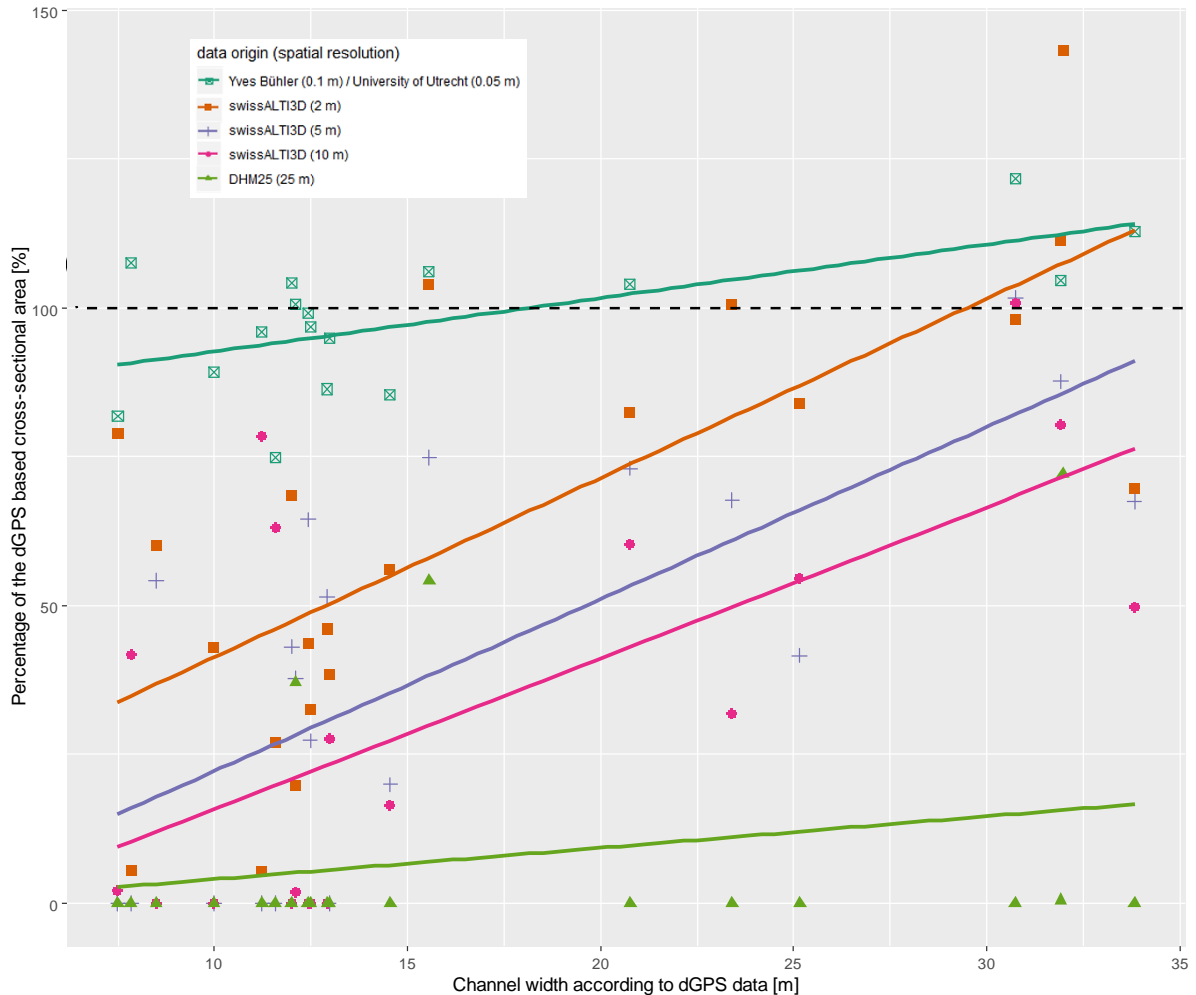


Figure 39: Percentage of the dGPS based cross-sectional areas against the channel width according to dGPS data. The regression lines are primarily used to show trends rather than a linear correlation.

6.2 Debris flow runout modelling

In order to illustrate which transport routes and runout zones the debris flows have, the simulation results are visualized. Depending on the spatial resolution of the DEM used for the modelling, different results are obtained, in which some general trends can be identified. As these are easily recognisable in the artificial cases, these results are shown first. Only a selection of the results is visualized in this thesis. As described earlier, all simulations are made on a one-meter computational grid.

6.2.1 Artificial cases

Sinus channel

The modelling results of an extreme event for the surface with a sinus channel demonstrate the general trends in a very clear way. The main part of the debris flow stays within the channel with some exceptions. If the channel has insufficient capacity, the debris flow tends to flow over the outer banks and overflow the area behind. This happens particularly in these cases where the speed and or the debris flow volume exceeds a certain limit. However, the spatial resolution of the DEM used for the simulation has a significant influence. The larger the grid size, the worse the channel is represented. As a result, the area affected by the debris flow is increasing and the impact on the area just behind the curves is more dramatic. This behaviour is illustrated in Figure 40 which shows the maximum flow height of a simulated debris flow as a function of the spatial resolution on such a surface with a channel having a sinus course.

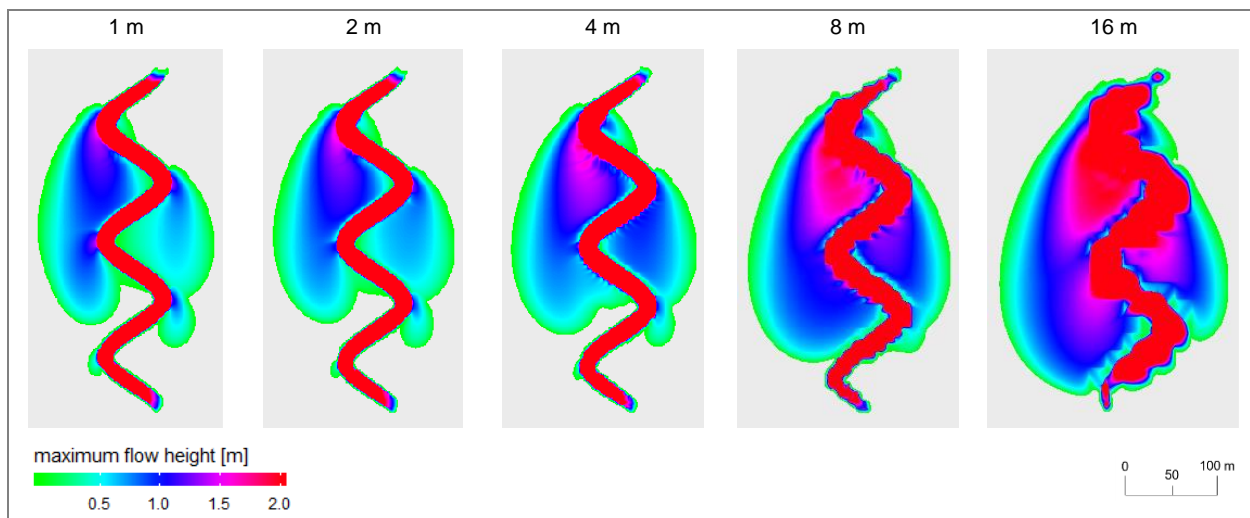


Figure 40: Maximum flow height [m] of a simulated debris flow as a function of the spatial resolution (on top of each simulation result) on a surface with a channel in a sinus course.

The channel has a width of 21 m, is 7 m deep and the banks have a slope angle of 60°. All maximum flow heights above a value of 2 m are coloured red in Figure 40. This colouring has the advantage, that the behaviour in the flooded areas outside the channel are clearly displayed. The flooded areas are a consequence of the overflow of the debris flows at the curve. Further down the hill (lower part in the figure) the maximum flow height gets thinner due to the lower volume inflow respectively the limited range.

The simulation results for the DEMs with relatively coarse mesh resolution are remarkable. The values for the maximum flow height are showing an unnatural behaviour. It seems as if the shape of the channel has changed and the banks have become jagged. This can be explained by the resampling technique (see chapter 2.4.2). Due to the degraded resolution, information about the channel geometry is lost. Typically, small pools with steep banks are formed before the channel geometry gets lost completely. The impact on the simulation result can be seen in particular in the values for the maximum velocity. Figure 41 illustrates the maximum velocities for

the same simulations as Figure 40. The results based on the 8 m and 16 m DTM clearly show the increased speed at pool transitions.

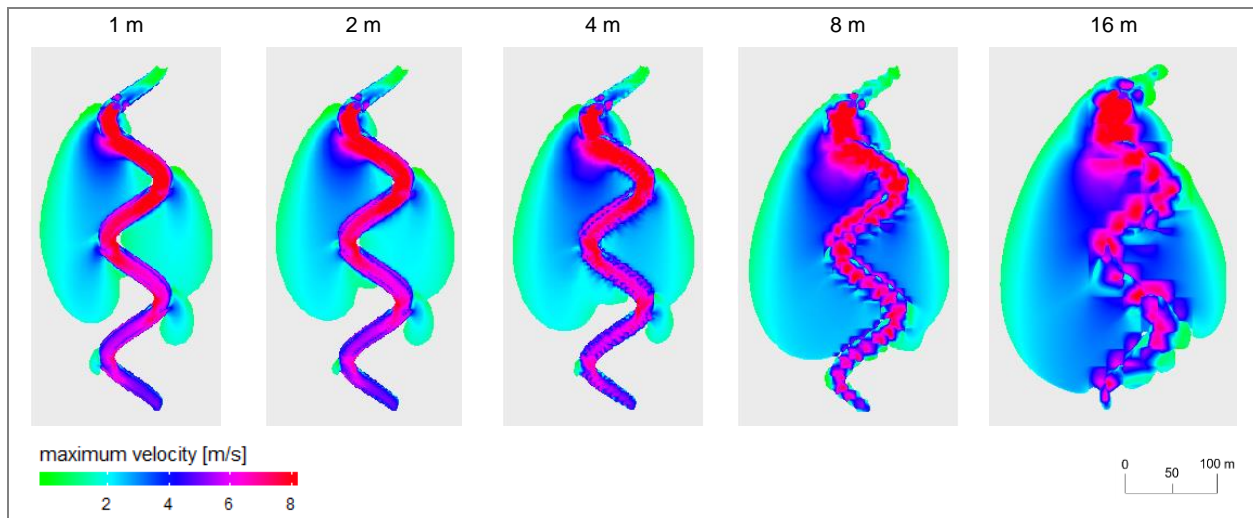


Figure 41: Maximum velocity [m/s] of a simulated debris flow as a function of the spatial resolution (on top of each simulation) on a surface with a channel in a sinus course.

Freeform

To further verify the detected general trends, another artificial surface was created, with a channel course which is closer to a natural torrent channel. The input DEMs are shown as shaded reliefs next to the simulation results of the maximum flow height to illustrate the channel geometry (see Figure 42).

The shaded reliefs clearly show the change in the input DEMs. The shape of the channel is no longer exactly defined in the coarser DEM. A further consequence of the general trend caused by the spatial resolution can be observed in the results for the freeform: The modelled debris flow has a greater runout distance for the 1 m DTM than for 16 m DTM within the same time period. This is an indication for a correlation between the debris flow runout distance and the spatial resolution in the modelling.

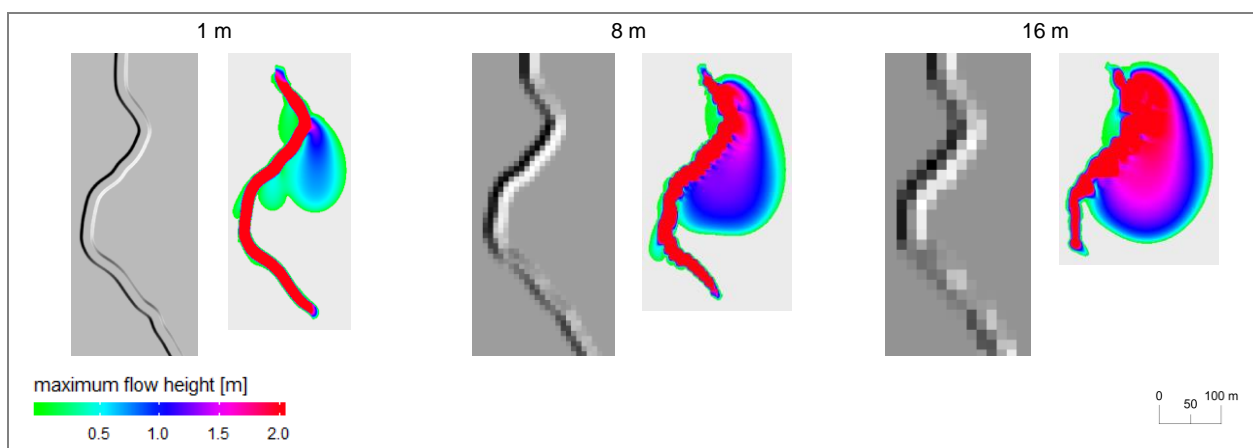


Figure 42: Shaded reliefs of a surface with a random channel course as a function of the spatial resolution and the corresponding results for the maximum flow height [m] of a simulated debris flow on these surfaces.

6.2.2 Real world cases

The general trends and correlations observed should be apparent in the real-world cases. For each study location a selection of the visualisations is illustrated which show at least one important aspect. The results indicate the different debris flow transport routes according to the used DEM and therefore how they differ from each other. On the basis of these results the key observations were noted, which are generally valid:

The coarser the DEM resolution, ...

- ... the less a debris flow follows the actual channel.
- ... the wider is the debris flow channel and the larger are the apparent pools in it.
- ... the smaller is the debris flow runout distance in a given simulation time.
- ... the more debris flows out of the actual channel.
- ... the straighter is the resulting debris flow runout path.

Fraschmardin: Channel disappearance

The coarser the DEM resolution, the less a debris flow follows the actual channel.

According to the simulations for an extreme event in the Fraschmardin torrent a significant overflow occurs on the right side of the channel when looking downstream (see Figure 43). The area in between the dam and forest would be affected. This behaviour seems to be independent of the resolution. However, when using a coarser DEM grid size, the channel tends to disappear. Furthermore, the debris flow does not make its way through the forest in the channel or has difficulties to do so.

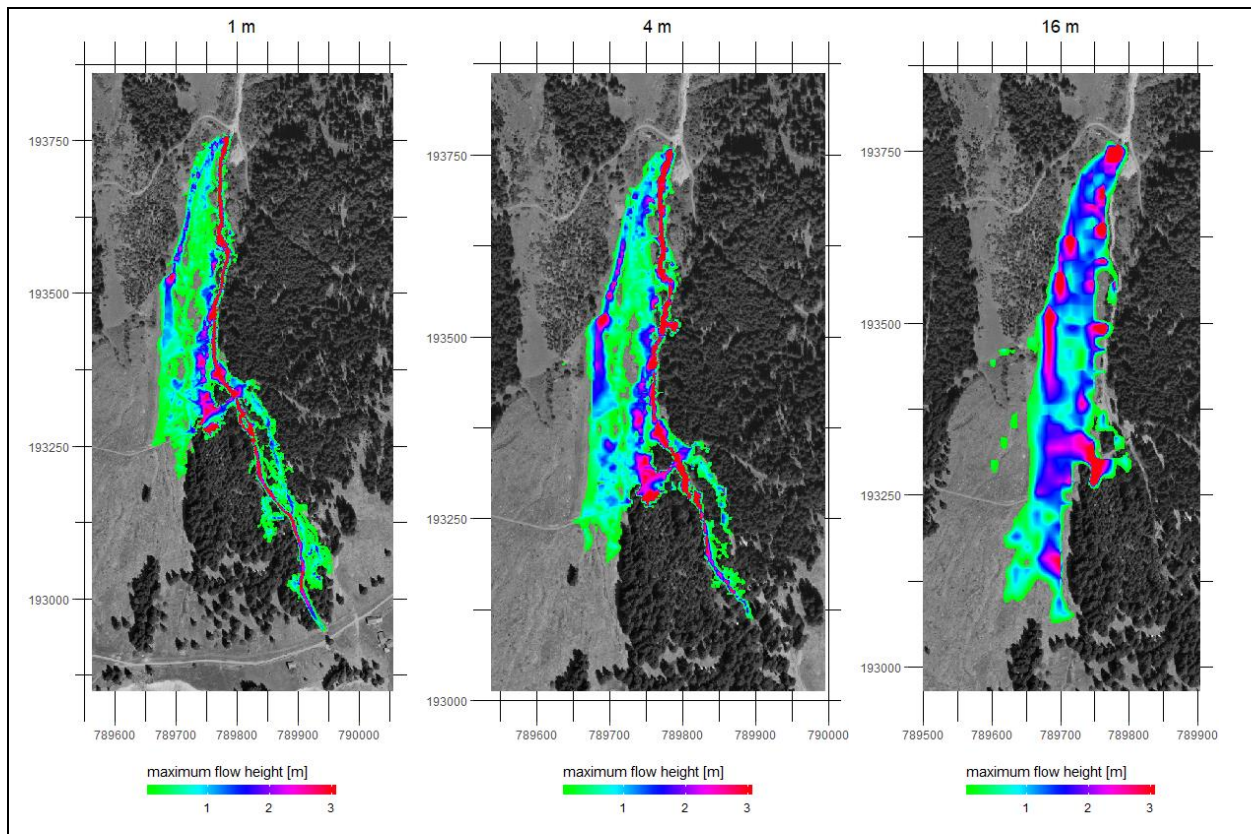


Figure 43: Maximum flow height [m] for an extreme event simulation in the Fraschmardin torrent as a function of the spatial resolution [m].

Forbesch: Channel deformation

The coarser the DEM resolution, the wider is the debris flow channel and the larger are the apparent pools in it.

At the Forbesch torrent the area affected by a debris flow doesn't change as dramatically compared to other study sites in case of an extreme event. A huge part of the debris fan would be inundated according to the simulations. The effect of the spatial resolution on the simulation result of the maximum velocity is clearly visible because the Forbesch torrent has a straight channel (see Figure 44). Starting at a resolution of 4 m, the building of pools can be seen within the channel. This is where the highest velocities usually are. The coarser the DEM grid becomes, the larger are the pools and the wider the channel appears. The explanation on why these pool form in the DEMs in the resampling process can be found in chapter 2.4.2.

What cannot be seen in Figure 44 is the influence of the small bridge just located before where the torrent reaches the bottom of the main valley. It has a similar effect to the one of a dam, since a bridge represents a higher elevation in the DSM compared to the elevation values within the channel just next to it.

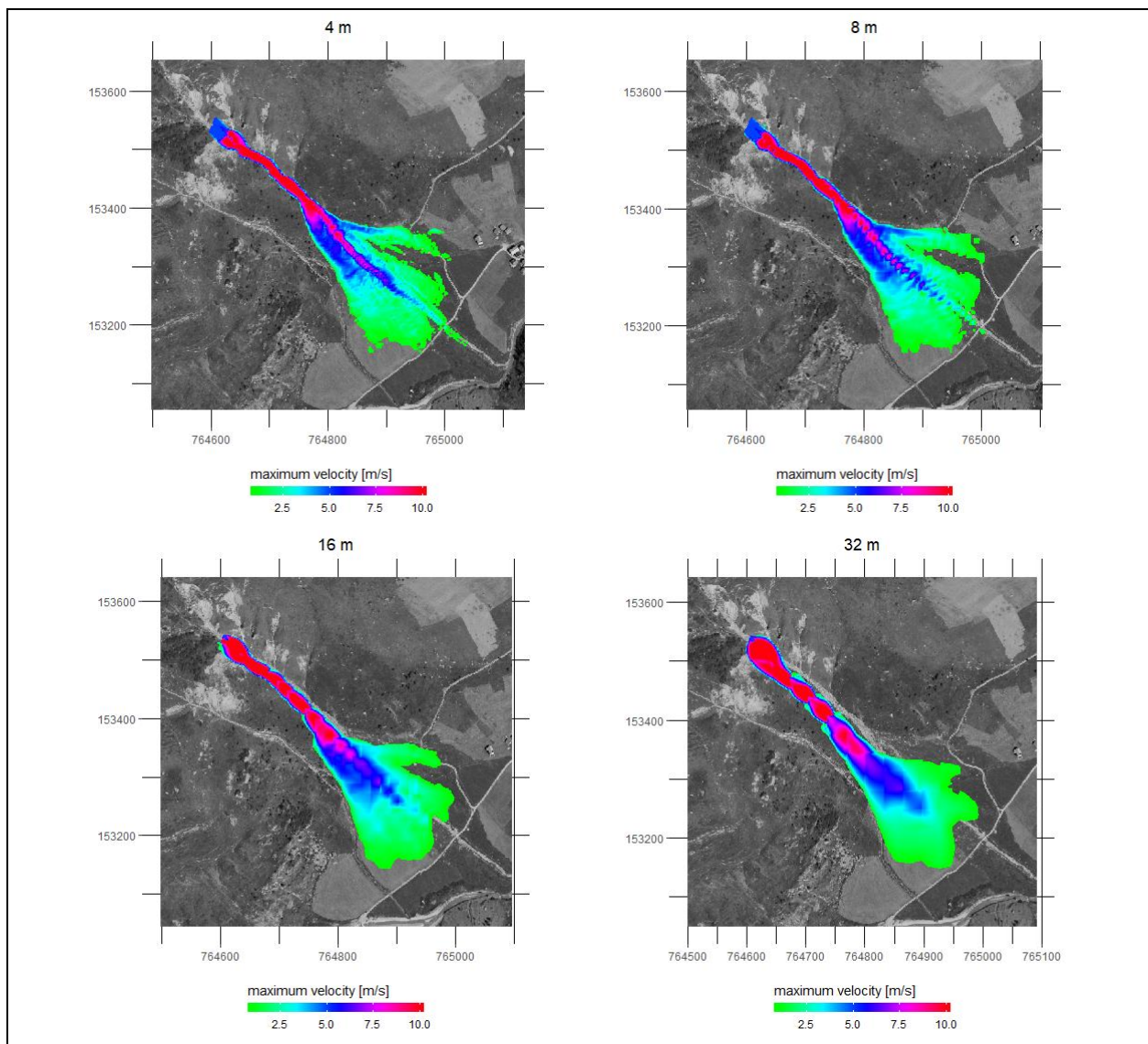


Figure 44: Maximum velocity [m/s] for an extreme event simulation in the Forbesch torrent as a function of the spatial resolution [m].

Illgraben: Debris flow runout distance

The coarser the DEM resolution, the smaller is the debris flow runout distance in a given simulation time.

The Illgraben is substantially larger than the other cases. Therefore, the effects of a coarser DEM grid resolution appear at another scale. However, it is predestined to illustrate the influence of the grid size of the input DEM on the runout distance of a debris flow in a given simulation time. In Figure 45 the flow height (if above one meter) can be seen for a simulation based on the borderline scenario for 2500 seconds after it started. While the debris flow reaches the Rhone in the 8 m DTM it does not do so for the 32 m DTM. Beside this trend the building of pools and a light shift of the actual channel can be observed in these results.

The velocity change is a consequence of channel deformation. The forming of pools can be compared to the building of dams, which have an influence on the debris flow speed. Since this behaviour is heavily dependent on the topography and the magnitude of the debris flow, it is difficult to assess it precisely.

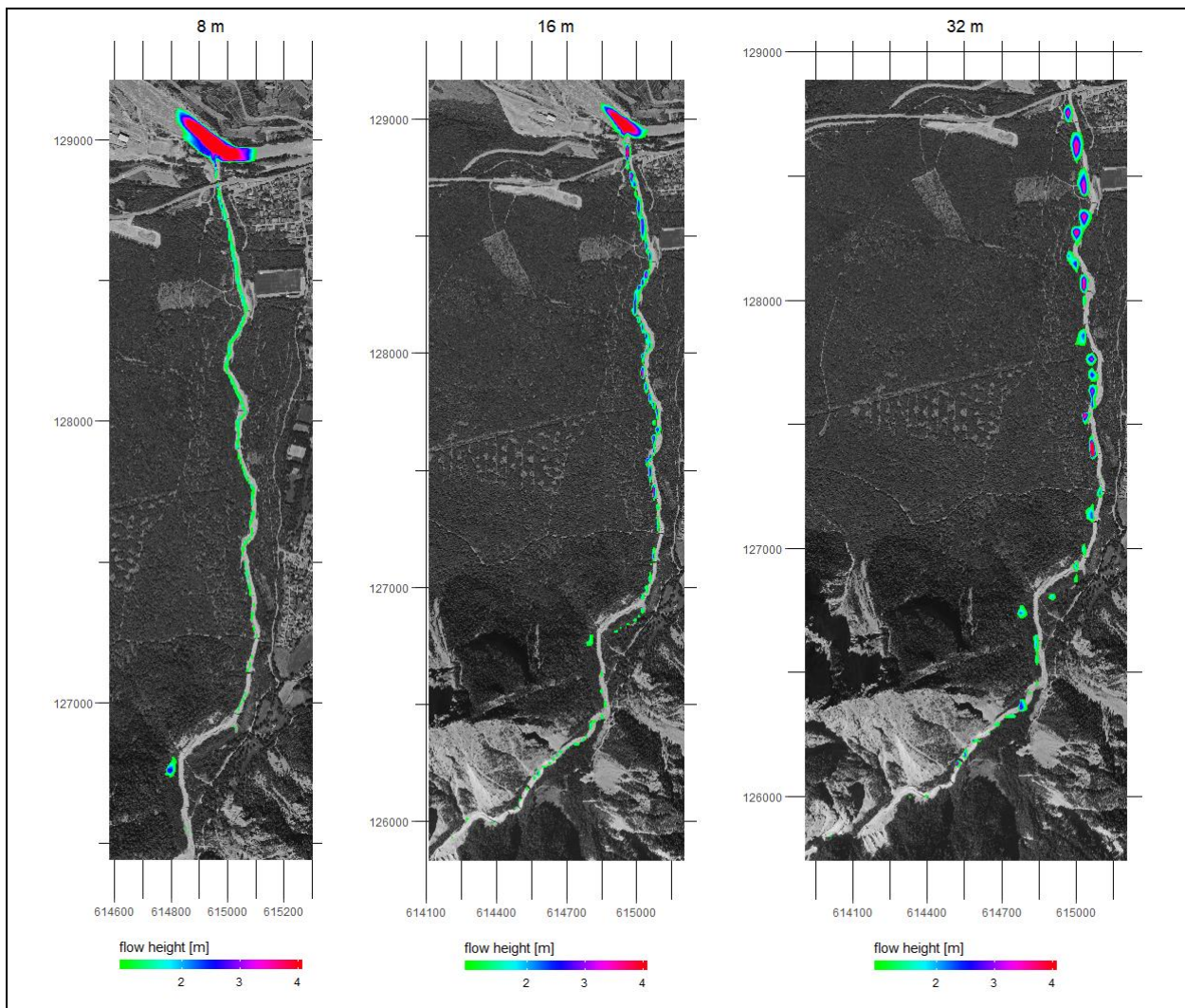


Figure 45: Flow height [m] above 1 m for a simulation with the borderline scenario at a specific timestep in the Illgraben torrent as a function of the spatial resolution [m].

Val Mela: Channel overflow

The coarser the DEM resolution, the more debris flows out of the actual channel.

The effect of the grid size on the channel overflow can be illustrated by showing the results for the maximum flow height in the simulation of the borderline scenario for Val Mela torrent (see Figure 46). In the one-meter DEM the debris flow stays within the channel. Some outflows on the lower part of the fan are visible in the 8 m DEM. Additionally, a building of pools can be observed. The 16 m DEM allows even more outflows, the channel is shifted and straightened. These effects in the simulation based on the 32 m DEM are extreme. The debris flow follows a straight path and is even wider, since the channel isn't clearly detectable anymore within this DEM.

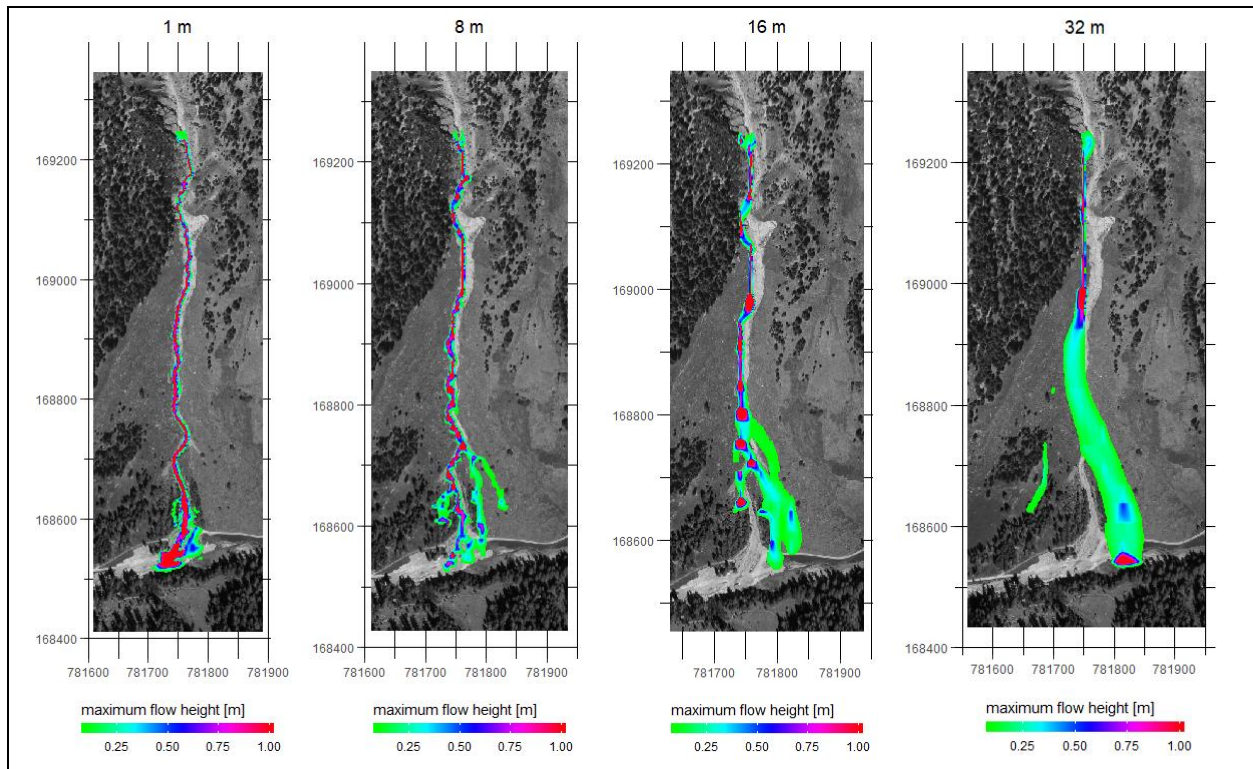


Figure 46: Maximum flow height [m] for a simulation with the borderline scenario in the Val Mela torrent as a function of the spatial resolution [m].

Alp da Stugl: Channel straightening

The coarser the DEM resolution, the straighter is the resulting debris flow runout path.

The western channel at Alp da Stugl study site has an average width of approximately 4 m. Therefore, a channel overflow and the building of kind of a second channel is already visible in the simulation based on a 4 m DEM. In the results for the 8 m DEM the debris flow just takes a straight path down the fan. Figure 47 shows the maximum velocity for the borderline scenario simulation within the western torrent channel of Alp da Stugl. The described behaviour is clearly visible. Furthermore, large velocities can be detected at spots where the flow thickness is large in the simulation results.

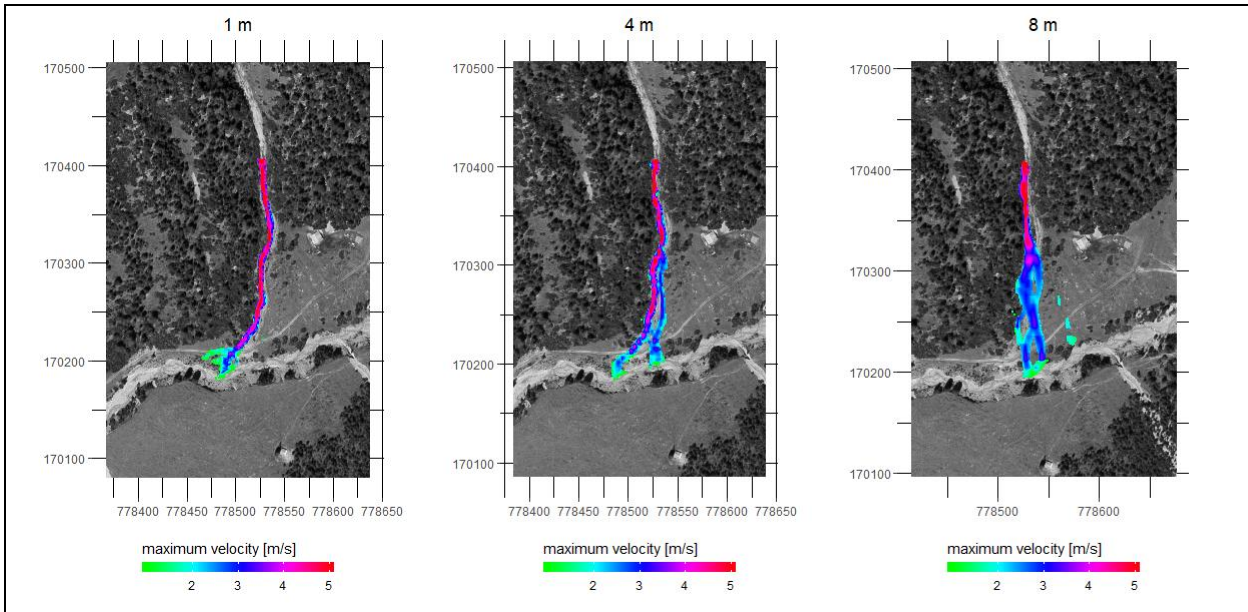


Figure 47: Maximum velocity [m/s] for a simulation with the borderline scenario in the Alp da Stugl (western channel) torrent as a function of the spatial resolution [m].

6.3 Sensitivity of the model to DEMs

The sensitivity analyses confirm the results which are described in the previous chapter. The area affected by a debris flow increases significantly with coarse grid resolution, especially in the case of a scenario in which the channel capacity is barely visible in the elevation model. Furthermore, the resolution plays an essential role for the representation of the channel and for the building of unrealistic pools in it. A computer experiment has shown that the DEM resolution should be at least a quarter of the channel width in order that its capacity can be approximately correct. A coarser grid resolution can lead to both an under- and overrepresentation of the channel and thus to a formation of pools.

Therefore, the answer to the research question, at which grid size the modelling results gets negligible, must be differentiated. The affected area usually increases with coarser resolution, whereby the debris flow volume in relation to the channel capacity is decisive. At a resolution of more than a quarter of the channel width, its capacity becomes too small or too large, resulting in an even stronger influence on the affected area.

The following two subchapters show the results in detail.

6.3.1 Affected area

In most of the cases the affected area gets larger when the input DEM becomes coarser. This trend can be detected in the computed values for the simulations of extreme events (see Figure 48). The affected area by a maximum velocity of at least 1 m/s is increasing the strongest when using a coarser grid. The influence on the affected area with a maximum flow height of at least 0.1 m is rather small. Overall the effect of grid size on the amount of affected area doesn't play a big role for extreme events. Additionally, some outliers at relatively coarse grid sizes have a positive influence on the trendlines.

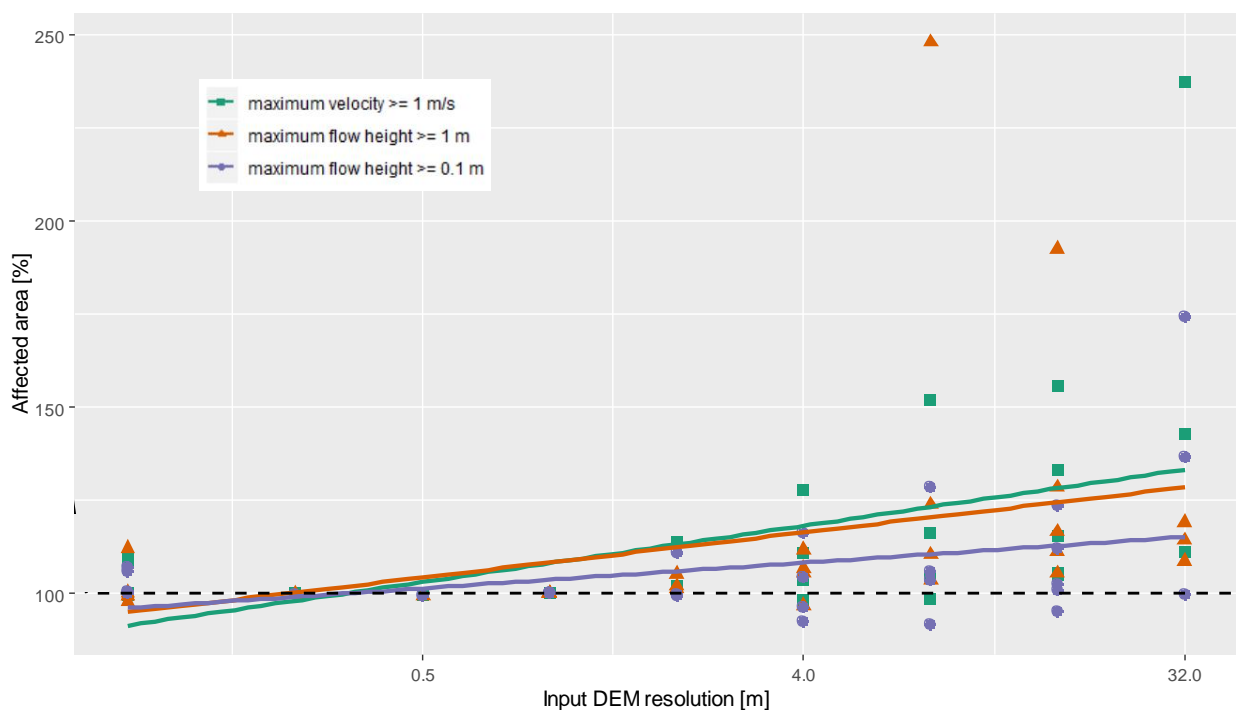


Figure 48: Percentage of the 1 m grid based affected areas in case of an extreme event against the input DEM resolution. The given regression lines are primarily used to show trends rather than a linear correlation.

The grid size does not have such a large influence on the affected area in case of an extreme event scenario, because almost any area which is not higher elevated is flooded. The borderline scenarios corresponding to a 30-year event, show a greater influence on the size of the affected area.

6. Results

Due to the fact that a channel overflow occurs at a coarser grid resolution than 1 m, the affected area increases. Figure 49 shows this for the affected area with a maximum velocity of at least 1 m/s and for the maximum flow height of at least 0.1 m. The area affected by at least 1 m, on the other hand, becomes smaller. With a coarser grid resolution, the simulated debris flows occupy a larger area of less thickness.

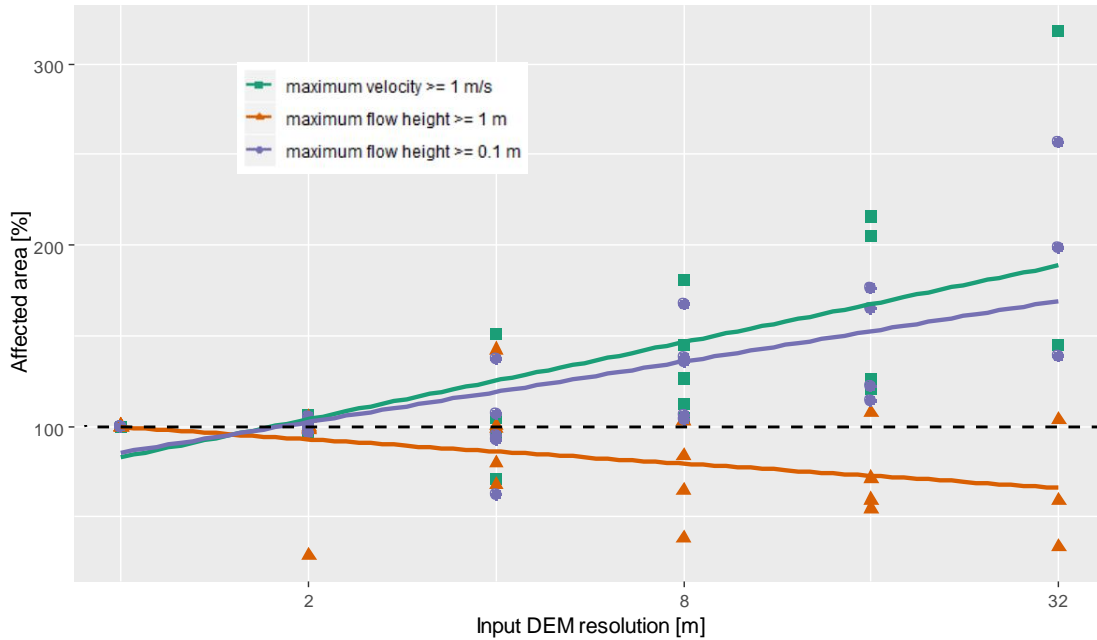


Figure 49: Percentage of the 1 m grid based affected areas in case of the borderline scenario event against the input DEM resolution. The given regression lines are primarily used to show trends rather than a linear correlation.

6.3.2 Channel deformation

The formation of pools until the complete disappearance of channels as the DEM resolution decreases could be observed in the simulation results. The question raised is at which grid size do these effects start. The computer experiment shows a clear pattern. Until a DEM grid size of 5 m, no significant change was detectable within the cross-sectional areas. At larger DEM grid sizes however, the cross-sectional area starts to vary stronger and stronger (Figure 50). On one hand, the channel capacity increases with a coarser grid resolution, on the other hand a decrease is also observable. It can be assumed, that the general trend goes towards a cross-sectional area of zero square meters, since with an infinitely large resolution, the detection of the channel becomes increasingly unlikely.

This result means for debris flow runout modelling that the maximum resolution should be at least a quarter of the channel width in order to avoid the formation of pools.

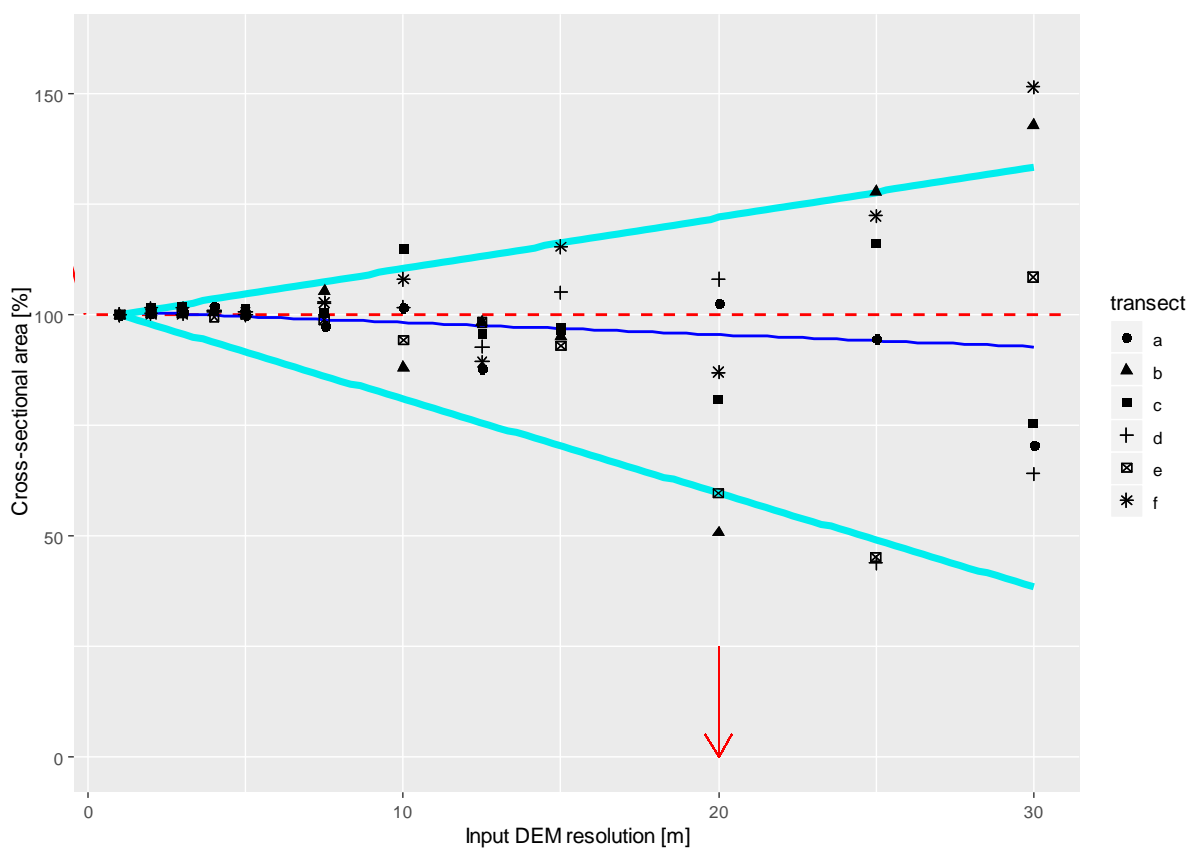


Figure 50: Percentage of the 1 m grid based cross-sectional areas of six transects (a-f) against the input DEM resolution at a synthetic straight channel. The thin blue line indicates the general trend line. The cyan coloured lines above and below indicate the 10% respectively 90% percentile. The red arrow points to the used channel width of 20 m.

7 Discussion

7.1 Digital elevation models

The various DEMs are the central focus of this thesis. Their influence on the debris flow modelling is crucial. Different types exist, they represent the landscape differently. Therefore, not only the spatial resolution is decisive, whether a torrent channel is detectable or not. The quality of the representation is also affected.

In the following subchapters, the results and methods used for the first part of this thesis will be discussed. As the DEM type plays an important role on how well torrent channels are represented, this becomes a first focus. The second and third areas of focus will be more on the methods used. DEMs recorded at different times serve as data basis for the cross-section comparison. However, the topography changes over time, particularly if a debris flow event occurs. The cross-sectional area calculation method used, is another factor which influences the results. It is based on the assumption, that the torrent channel capacity is limited by the lower bank height and that the debris flow surface is flat across the width of the channel.

7.1.1 DEM type

Existing DEM types and possible production techniques are introduced in chapter 2.4. The DEMs used for this work are mainly DTMs with exception for the DSMs provided by the SLF. In torrent channels does usually not grow vegetation. Hence, a DSM shouldn't have other elevation values than a DTM at these locations. However, some differences are detectable in cross-section comparisons (e.g. at Fraschmardin torrent). The elevation value of the DSM is significantly higher at the channel banks due to overlapping vegetation. As a result, the channel might get less wide compared to the reality and artificially higher banks seem to exist when studying a specific transect.

The technology to create high-resolution DTM, in which channels are well represented, is available. For example LiDAR technology enables the acquisition of high spatial resolution datasets (Bühler *et al.*, 2012). However, airborne or spaceborne optical sensors can cover large areas at considerably lower costs and allow to create DSMs by using photogrammetric methods. There are hardly any trees left in areas above 2000 m a.s.l. and thus it does not matter, that only a DSM but no DTM can be surveyed. Nevertheless, some study areas are situated below 2000 m a.s.l. and contain trees. Consequentially, cross-section data which have been clearly influenced by vegetation has been neglected for analysis in this thesis.

Studies have shown, that in general the generic type of the DEM is a critical issue influencing the model result beyond the grid resolution alone (e.g. Stolz and Huggel, 2008; Stevens *et al.*, 2003). According to the findings in the scope of this work this is true. But indeed, the grid size is decisive, whether a continuous channel can be detected in the DEM at all. This underpins the results of Sodnik *et al.* (2013): In their study about the quality of input topographic data on the debris flow modelling results, they concluded that higher resolved topographic data promises better representation of torrential channel on torrential fans (narrow, deep channels). Furthermore, computed results (velocities, depth) are generally better estimated and therefore delineation of hazard area into corresponding zones is of higher accuracy for a selected debris flow scenario. Since in some DEMs (most of all in the DHM25) no channel could be detected at all, it makes sense to use a high-resolution DEM for

the modelling. Otherwise, the debris flow path in the simulation results would likely follow the channel and would not produce realistic results.

7.1.2 Temporal changes in channel geometry

In the diagrams comparing cross-sections of a certain transect some striking differences are exist, which cannot be explained only with the different grid sizes of the DEMs. The comparative representation of the cross-sections is based on DEMs containing elevation data recorded at different times. That's why this comparison must be interpreted with caution.

A debris flow event leads to surface changes within the channel. Erosion and deposition of channel bed material are important aspects of debris flow processes (see chapter 2.3). Studies on factors influencing volume changes due to a passage of a debris flow were done (e.g. Weber, 2004; Iverson *et al.*, 2010), however, there is a lack of detailed observation data on channel modifications (Willi *et al.*, 2015). Only a few investigations are made on compiling detailed quantitative data on erosion and accumulation within the different channel reaches. Schürch *et al.* (2011) detected a volume change of $87 \pm 5 \text{ m}^3$ over an area of $\sim 4900 \text{ m}^2$ caused by one event down a 300 m reach of the Illgraben channel. Since several flood and debris-flow events are observed at the Illgraben each year and the DEM-data ranges from the 1980s (DHM25) to 2018, one can assume a significant change in this complex topography. Nevertheless, the results are important regarding the research question. The primary aim is to find out whether, the torrent channels in the DEMs are recognizable at all. As most of the DEMs date from a period of less than one year just before the field work was done, it is possible to make a statement about the quality of their channel representation. A change in the course of the debris flow channel during this short time or a shift of the channel banks is rather unlikely. More probable is a change in the channel depth caused by an event. This could be observed in some transects of the Illgraben torrent when comparing the dGPS measurements-based cross-section to the high-resolution DEM based cross-section by the University of Utrecht (see Figure 36).

7.1.3 Cross-sectional area calculation

The computed cross-sectional areas were used as the main indicator, to examine whether a DEM is representing the torrent channel in a correct measure or not. In this discussion, capacity is defined by the cross-sectional area of the channel (m^2) and not explicitly the discharge capacity (m^3/s) used by e.g. engineers. The available capacity of a debris flow channel is decisive for a possible overflow of the banks. Hence, a small cross-sectional area leads to a corresponding small capacity. The results have shown that in addition to the grid resolution of the DEM, that the channel width is crucial for a correct representation of the cross-sectional area. The channel width must be at least ten time as large as the spatial resolution of the DEM in order to ensure that the channel's capacity is accurately represented.

To calculate the cross-sectional area, a bank-full definition originating from the hydrological research field on rivers, was chosen. The bank-full discharge at a river cross-section is the flow which fills the channel to the tops of the banks and therefore marks the condition of incipient flooding (Williams, 1978). Since various concepts of this term exist, a definition was chosen, which allows an easy coding for the computation. According to Schumm (1960) and Bray (1975) bank-full is the elevation of the "low bench". Based on this definition the computation procedure was set up: By drawing a line from the lower bank horizontally to the other bank a cross-sectional area is created. However, the geometry of a debris flow during the flow, is a bit different (see Figure 8 and clarifications in chapter 2.3). Therefore, the calculated values do not reflect the effective capacity at a specific channel transect. A comparison of the capacities according to the different resolved DEMs is rather possible. Regarding the evaluation of the representation of the torrent channels, this method turned out to be reasonable.

7.2 Debris flow runout modelling

The modelling part took the most time by far. By identifying the transport routes and runout zones of the debris flows, general trends were detected. Beside the input topography other input parameters needed to be defined which played a role. The simulations in RAMMS with its computing characteristics led to the results. All these factors have an influence on the modelling results and their interpretation.

7.2.1 Input topography

Numerical models such as RAMMS need precise DEM datasets with a high spatial resolution covering complex alpine terrain (Bühler *et al.*, 2011). This is in line with the findings discussed under 7.1.1. Therefore, always the highest resolution DEM available was used as the basic topography. The conversion to other resolutions in order to obtain the input DEM for RAMMS was done by using the nearest neighbour resampling technique. As described (see chapter 2.4.2), it is used when the elevation values of the resampled DEM need to be based on single pixels. Since the assumption is made that the quality of the DEM only allows a certain grid size, taking more information out of the original DEM (e.g. through bilinear interpolation resampling technique) would lead to a qualitative better DEM for practical applications. As mentioned earlier, this interpolation had to be avoided for this thesis project.

However, the quality of a DEM can't be described simply. It depends on its intended purpose. A DEM for debris flow modelling requires not only a certain grid resolution, it requires a sufficient representation of the terrain roughness and therefore an appropriate vertical resolution. An evaluation of the vertical accuracy of open source DEMs was done by Mukherjee *et al.* (2013). They concluded that the vertical accuracy of the DEMs is affected by the terrain's morphological characteristics. Terrain roughness influences the vertical accuracy negatively. Furthermore, the slope characteristic of the terrain has a significant impact. Related studies came to similar results (e.g. Su and Bork, 2006).

To evaluate the vertical accuracy of DEMs used for debris flow modelling, could be a future research topic. It would go far beyond the main goal for this thesis. However, it is important to consider that a qualitative DEM does not only depend on the grid resolution itself. For this reason, a publicly available DEM (e.g. DHM25, swisSALTI3D) might represent the topography better than the by nearest neighbour technique down-sampled DEMs with the same grid resolution.

7.2.2 Scenario definition

The scenario definition for the simulations was a challenge. While for the extreme events simple input parameters could be chosen which were based on analysis from different regions, adjustments had to be made for the borderline scenario. The main question was the magnitude of the event. Numerous simulation runs were performed to reach the borderline scenario as good as possible. Beside the magnitude of the event (input hydrograph, peak discharge) the resistance coefficient μ usually needed to be reduced. This corresponds to the study of Frank *et al.* (2016), who found that the parameter ξ has a relatively small influence on the flow behaviour compared to the Coulomb friction term μ .

The discharge a debris flow channel can handle cannot be determined conclusively by means of simulations. It depends on rheological characteristics of potential debris flows and therefore on the friction parameters. These are very hard to estimate. At least, the volumes represent an approximate order of magnitude.

7.2.3 RAMMS

Except for the Illgraben, no data on past events was available. Therefore, the modelled flow heights and velocities for the debris flows could not be compared to data of past events. The parameters used are based on recommendations and had to be partially adjusted to achieve more realistic results. This calibration took a long

time, because there were many possibilities to set different values for the input parameters. A large number of simulations were carried out.

RAMMS must process large amounts of data. The computer needs a relatively large internal memory and a fast processor. For simulations with a rather large process domain and a high simulation resolution, the calculation of a simulation can still take several hours. E.g. the modelling of the Illgraben debris flows in RAMMS took approximately 48 hours on the workstation at the WSL.

The achieved simulation results with the determined general trends show the strengths of RAMMS. But there are also limits which only allow qualitative statements about the influence of grid resolution on the simulation results. On one hand due to the model itself (e.g. assumption of a homogeneous material), on the other hand by the simplifications that have been made (e.g. neglected erosion).

Another crucial factor is, that a too good spatial resolution can even lead to unrealistic simulation results. For the modelling of snow avalanches, it has been found that higher resolutions DEMs provide more accurate simulations, but the results are not improved significantly with a resolution less than 5 m (Christen *et al.*, 2008). This is not applicable for debris flows, as their channel capacity cannot be represented in the DEM adequately, when the spatial resolution is too low compared to the channel width. According to the RAMMS user manual, the topographic data is the most important input requirement (Bartelt *et al.*, 2013): *“The simulation results depend strongly on the resolution and accuracy of the topographic input data. Before you start a simulation, make sure all important terrain features are represented in the input DEM.”* Thus, an appropriate selection of the spatial resolution, which is neither too high nor too low, is a challenge. In addition, caution is advised when using DEM datasets with a very high spatial resolution acquired a certain time ago, because they may not represent the correct terrain for the simulated avalanche event (Bühler *et al.*, 2011). This is also true for a simulated debris flow event. The temporal topographic change has been discussed previously.

This means for the results of this study, that no generally valid recommendation can be made at which spatial resolution the simulation is optimal. It suggests a minimum resolution relative to the width of the channel and shows the consequences of using a lower or higher resolved DEM for the simulations.

7.3 Sensitivity of the model to DEMs

The simulation results showed a significant increase of the affected area for the borderline scenario, when a coarse grid resolution is used. This effect was rather small for the extreme event simulations. However, these results alone do not confirm a change in channel capacity. This would require a different methodology. It indicates a strong sensitivity of the modelling results to the DEM resolution.

The debris flow channel should be decisive for the flow path. As in the simulations a channel deformation by building of pools was detected, an effort was made to quantify at which grid size this happens. It was found that the maximum resolution of the DEM should be a quarter of the channel width to avoid the formation of pools.

The results of this thesis imply for small debris flow channels the need of high-resolution DEMs in order to get accurate simulation results. Otherwise a reliable hazard assessment seems to be impossible. As the production of DEMs is usually very time- and cost-intensive, a possible solution was elaborated and tested. It includes a time-efficient improvement in the representation of the channel within an already available DEM.

7.3.1 Sensitivity analysis

A strong sensitivity of the modelling results to the DEM resolution has been demonstrated. Stolz and Huggel (2008) could not directly observe the influence of DEM resolution on the predicted inundation. However, it was clear for them that the inundation area, predicted by mass-conservation models mimicking mass movements such as landslides or debris flows, depend on how mass is distributed and therefore, which grid size the DEM has. By assessing the dependency of the affected area on the grid resolution, this relationship could be demonstrated for the first time. In all cases, a trend towards a larger affected area with coarser DEM resolution could be detected. The only exception is the area affected with at least 1 m flow height for the simulations with the borderline scenario. The decrease can be explained by an increase in the affected area with a lower flow height.

The results in chapter 6.1 have already shown an underrepresentation of channels within different DEMs commonly used in Switzerland, particularly for DEMs with coarse grid resolution. The related capacity change was also assumed to be the main reason for the effect on the affected area. By the computer experiment on the channel deformation, the behaviour could be analysed in more detail. Having a coarser resolution than a quarter of the channel width leads to a formation of pools. The bottlenecks between the pools result in a debris flow leaving the channel in the simulations. As the entire volume rarely flows back into the channel, the debris flow spreads over a larger area.

Reflections were made on a different analysis procedure. The debris flow volumes outside the channel could be compared for a specific timestep of the simulation. To perform this, the channel area must be defined exactly first, so the volume inside can be subtracted. Since the channel areas change due to the DEM resampling, this should be done separately for all DEMs. This process could have been facilitated with the help of a GIS tool. The "River Bathymetry Toolkit", a plugin running on ArcGIS Desktop software, allows users to describe and measure river channels using high resolution DEMs (*River Bathymetry Toolkit (RBT) - ESSA*, no date). There have been attempts to determine the channel area with this tool. First, the DEM needs to be detrended in order to remove the longitudinal valley slope. By varying the water level in the detrended DEM, the stream area can be investigated. However, this raises the question about the bank-full definition again. Furthermore, debris flow channels do have a comparable geometry to river channels but are different. All these factors lead to a time-consuming manual adaptation of the polygon shapefile which should cover the torrent channel as accurate as possible. Nevertheless, this could be an exciting starting point for future research on this topic.

7.3.2 Outlook: A possible solution

The need for a high-resolution DEM for modelling debris flows is a major issue. The topographic surveying is traditionally associated with high capital and logistical costs, exacerbated by the remoteness and inaccessibility of many field sites, so that data acquisition is often passed on to specialist third party organisations (Westoby *et al.*, 2012). The relatively new photogrammetric technique, termed “Structure-from-Motion”, allows to create high-resolution DEMs from extensive photosets, obtained using a digital camera fixed on a UAV. The DEMs produced by the SLF (Yves Bühler) and the University of Utrecht are based on this technique. However, as seen in this thesis the usefulness of these DEMs was limited by high vegetation. Another factor is the time. The raw “Structure-from-Motion” output has a significant post-processing load which must be taken into account when choosing this application (Westoby *et al.*, 2012).

Therefore, the choice of the DEM surveying technique must often be weight against the factors of time and costs. For cases, where a short-term and cost-effective hazard assessment must be made, a possible solution is presented here. It is a method to improve the representation of the debris flow channel in an insufficient resolved DEM, which could allow better simulation results.

The methodology was tested in the canton of Valais. The Combatseline torrent in Val de Nendaz passes by meadows, houses and chalets, before entering in La Printse (see Figure 51). The lower part of the debris flow channel is obstructed and very narrow (1.2 m). The catchment area is relatively small (0.17 km²). A debris flow event in 1995 had a volume of 1500 m³. The data are from a study of the WSL comparing three numerical simulation models for debris flows, including this torrent as a study site (Raymond Pralong *et al.*, 2018).



Figure 51: Debris flow channel of Combatseline torrent and surrounding houses. (left) Looking upwards. (right) Looking downwards into the obstructed channel.

The dGPS was used to record cross-sections between homogenous channel sections, each consisting of four points. Two points at the top of the banks and the other two at the edges of the channel bottom; on one transect. The surveyed points were then read into Rhino CAD together with the DEM swissALTI3D (2 m spatial resolution) by using the Docofossor tool. A first impression of how the points are situated compared to the DEM could be obtained. The next step was the transformation of the points to a channel shape. For this purpose, both bank lines and the channel bottom side lines were created from the points. The channel shape was obtained by placing the surfaces between the lines. Figure 52 illustrates what it looked like in the Rhino-CAD interface.

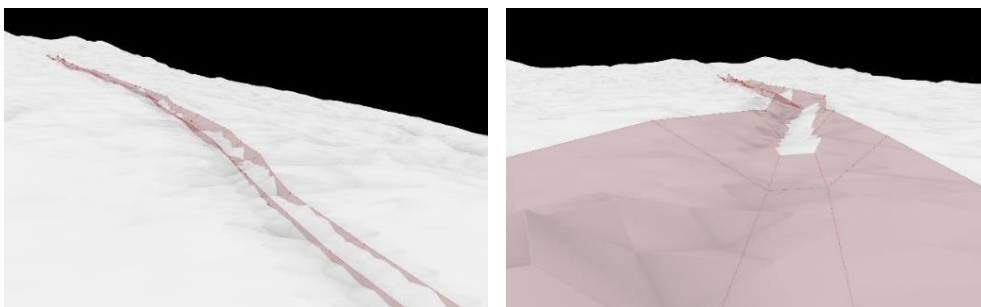


Figure 52: Illustrations of the created channel and the DEM swissALTI3D (Rhino-CAD interface)

The created channel shape was subsequently integrated into the DEM. For the channel banks which situated higher or lower than the DEM, an adaptation was made. It was set, that the angle to reach the DEM outside the channel from the channel banks is 10° . This prevented an abrupt level change. Finally, the new DEM was exported as an ASCII-file. Figure 53 shows how the new DEM was visualised within Rhino-CAD-interface. It has a spatial resolution of 0.5 m. In this case, the original swissALTI3D-DEM with 2 m spatial resolution was resampled by bilinear interpolation to 0.5 m in a previous step.

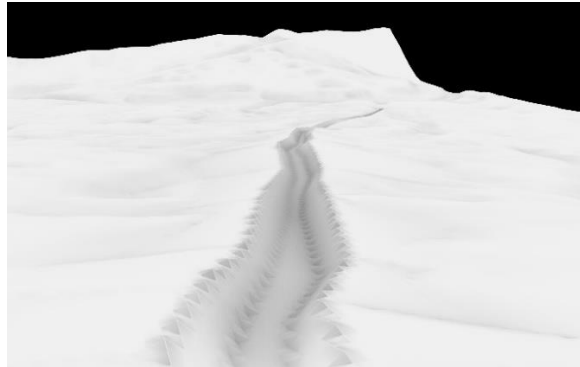


Figure 53: Visualisation of the processed DEM with the included channel (Rhino-CAD interface)

The modification on the DEM seems enormous at first glance. By modelling debris flows in RAMMS on the original and modified DEM the effects on the simulation results could be compared. The used input parameters were taken from extra information of the study by Raymond Pralong *et al.* (2018). The volume applied (1500 m^3) corresponds to the event of 1995. Both simulations have been done with a simulation resolution of 0.5 m and show different results. As expected, the modelled debris flow on the modified DEM follow the channel more clearly (see Figure 54). One consequence is, that less deposits have been modelled on the left side of the channel (looking downhill). Due to the adapted topography, the debris flow reaches the road with the obstruction in a shorter time.

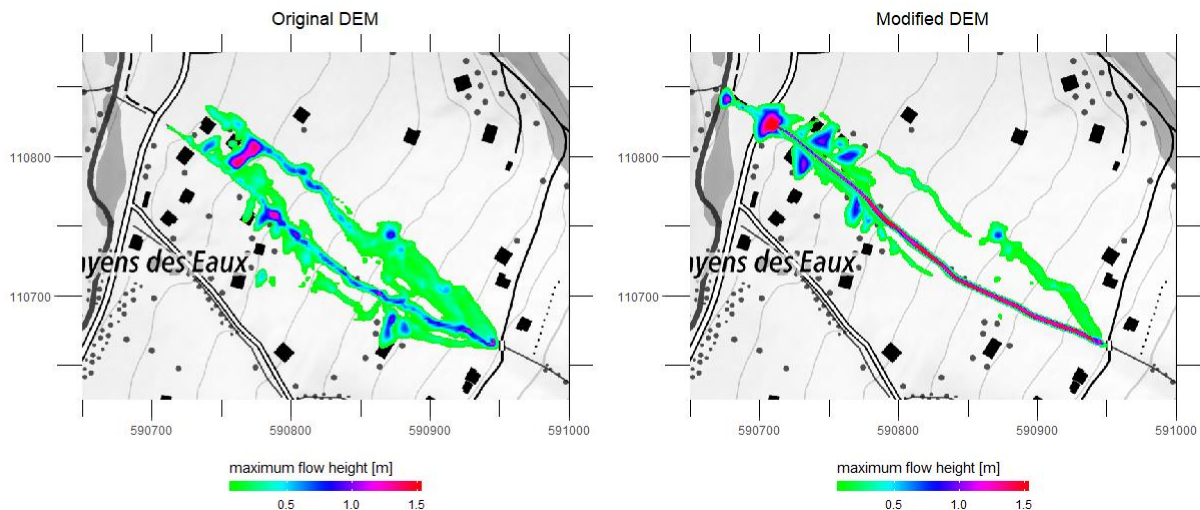


Figure 54: Resulting maximum flow height [m] for a debris flow simulation on the original DEM (left) and the modified DEM (right) at the Combatseline torrent.

If the simulation results are more realistic when adapting the DEM applying this method was not investigated. However, if the DEM is of even worse quality, at least the channel can be implemented. Thus, the main flow path of the modelled debris flow should be correct. Further research needs to be done on this topic.

8 Conclusion

The main objective of this thesis was to analyse the sensitivity of debris flow runout simulations to digital elevation model resolution. For that purpose, the maximum grid size for a torrent channel to be represented in the correct measure in a DEM was elaborated. Furthermore, the influence of the grid resolution on the affected area and the formation of unrealistic pools was analysed in detail.

Previous observations and modelling results made in connection with the influence of digital elevation model data on debris flow runout modelling have been confirmed by new measurement series and RAMMS simulation results. This study shows that the representation of the particular topography is crucial to determine debris flow hazard zones when applying results of numerical simulations.

By addressing the research questions the following conclusions were drawn:

How well are torrent channels represented in DEMs in common use in Switzerland?

The representation of torrent channels in DEMs depends on the channel width and on the DEM characteristics itself. The channel capacities and related cross-sectional areas derived by different DEMs serve as a key indicator to assess whether a channel is represented adequately.

Currently, swissALTI3D with a 2 m resolution is the best publicly available DEM in Switzerland. For the investigated cases and therefore for a lot of similar torrent channels, this DEM underestimates the channel capacity. In order to ensure that the cross-sectional area is represented in the correct measure in a DEM, the channel width must be at least ten times as large as the spatial resolution of the DEM.

However, the findings must be interpreted with caution, as changes of channel geometry over time might influence the results. Furthermore, DEMs have a specific recording time and are generated using different techniques. The type of DEM, i.e. DSM or DTM, combined with its quality are critical.

What are the debris flow transport routes and runout zones? How do they differ and vary spatially according to the used DEM?

The DEM resolution greatly affects the topography of the area and the geometry of the debris flow channel. This has a direct influence on the behaviour of the debris flow in terms of velocity and flow height. By investigating simulation results of debris flows on artificial surfaces it could be demonstrated that the by a debris flow affected area is increased when a coarser grid resolution is used. The impact on the area just behind the curves in the channel is more severe.

The transition of the underlying topography resulting from a degraded resolution drastically affects the channel geometry. Typically, small pools with steep banks are formed or continuous channels get lost completely. For the simulations this means an increased speed at pool transitions and a corresponding decrease within the pools, and varying flow heights within the channels.

8. Conclusion

Based on several simulation results with the same input parameters but different DEM-resolutions generally valid trends were observed: The coarser the DEM resolution, ...

... the less a debris flow follows the actual channel.

... the wider is the debris flow channel and the larger are the apparent pools in it.

... the smaller is the debris flow runout distance in a given simulation time.

... the more debris flows out of the actual channel.

... the straighter is the resulting debris flow runout path.

How is the result of the runout modelling linked to the spatial resolution of the DEM? At which grid size is the modelling error negligible?

The area affected by a debris flow increases significantly with coarse grid resolution, especially in the case of a modelling scenario in which the channel capacity is barely visible in the DEM. For extreme events this trend is much smaller. Another effect of a different grid resolution is a redistribution of the mass. For example, the same debris flow can occupy a larger area if its thickness is decreased. This was observed in particular for simulations on coarser resolved DEMs.

A computer experiment has shown that the resolution of a DEM should be at least a quarter of the channel width in order to avoid the appearance of pools within channels. This result does not state the maximum grid size at which the modelling error becomes negligible. However, a coarser resolution leads to unnatural artefacts in a DEM which significantly influences simulation results.

The number of cases investigated in this thesis is relatively small and many of the field cases are of similar size, so it is difficult to establish a general rule. Nevertheless, the use of a DEM resolution smaller than a quarter of the channel width should be aimed at. Even better would be a tenth, to ensure an adequate representation of the channel's capacity.

For narrow torrent channels high-resolution DEMs are essential, which is a major issue. A time- and cost-effective solution to improve the channel representation within existing DEMs was elaborated. Whether better simulation results can be achieved using this method needs to be investigated. First debris flow simulation results on an adapted DEM seem promising.

9 Literature

- Ancey, C. (2001) 'Debris Flows and Related Phenomena', in *Geomorphological Fluid Mechanics*, pp. 528–547. doi: 10.1007/3-540-45670-8_21.
- Andres, N. and Badoux, A. (2018) 'Unwetterschäden in der Schweiz im Jahre 1990', *Wasser, Energie, Luft*, pp. 67–74.
- ARE, BWG and BUWAL (2005) *Empfehlungen - Raumplanung und Naturgefahren*. Bern: Reihe Naturgefahren.
- Badoux, A. et al. (2009) 'A debris-flow alarm system for the Alpine Illgraben catchment: design and performance', *Natural Hazards*, 49(3), pp. 517–539. doi: 10.1007/s11069-008-9303-x.
- Baer, P. et al. (2017) 'Changing debris flow activity after sudden sediment input: a case study from the Swiss Alps', *Geology Today*, 33(6), pp. 216–223. doi: 10.1111/gto.12211.
- BAFU (2016) *Schutz vor Massenbewegungsgefahren. Vollzugshilfe für das Gefahrenmanagement von Rutschungen, Steinschlag und Hangmuren*. Bern.
- Bartelt, P. et al. (2013) *RAMMS - rapid mass movements simulation, A numerical model for debris flows in research and practice, User Manual v1.7.0, Debris Flow, Manuscript update November 2017*. WSL Institute for Snow and Avalanche Research SLF.
- Baumgartner, F. (2013) *Unwetter Brienz 2005: Analyse des Planungsprozesses zu den raumplanerischen Massnahmen*. Universität Fribourg. Available at: http://www.unifr.ch/geoscience/geographie/assets/files/bachelor-theses/BA_FionaBaumgartner.pdf (Accessed: 18 July 2019).
- Beniston, M. and Haeberli, W. (1998) 'Climate change and its impacts on glaciers and permafrost in the Alps', *AMBIO - A Journal of the Human Environment*. Jun1998. doi: 10.2307/4314732.
- Berger, C., Mcardell, B. W. and Lauber, G. (2012) *MURGANMODELLIERUNG IM ILLGRABEN, SCHWEIZ, MIT DEM NUMERISCHEN 2D-MODELL RAMMS MURGANMODELLIERUNG IN DER PRAXIS*. Available at: www.interpraevent.at (Accessed: 16 May 2019).
- Berger, C., Mcardell, B. W. and Schlunegger, F. (2011) 'Direct measurement of channel erosion by debris flows, Illgraben, Switzerland', *Journal of Geophysical Research: Earth Surface*. John Wiley & Sons, Ltd, 116(F1), p. n/a-n/a. doi: 10.1029/2010JF001722.
- Bernhard, M. and Hurkxkens, I. (2018) *DOCOFOSSOR. Designing a dynamic alpine landscape*. ETH Zurich.
- Bovis, M. J. and Jakob, M. (1999) 'The role of debris supply conditions in predicting debris flow activity', *Earth Surface Processes and Landforms*, 24(11), pp. 1039–1054.
- Bray, D. I. (1975) 'Representative discharges for gravel-bed rivers in Alberta, Canada', *Journal of Hydrology*. Elsevier, 27(1–2), pp. 143–153. doi: 10.1016/0022-1694(75)90103-1.
- Bühler, Y. et al. (2011) 'Sensitivity of snow avalanche simulations to digital elevation model quality and resolution', *Annals of Glaciology*, 52(58), pp. 72–80. doi: 10.3189/172756411797252121.
- Bühler, Y., Marty, M. and Ginzler, C. (2012) 'High Resolution DEM Generation in High-Alpine Terrain Using Airborne Remote Sensing Techniques', *Transactions in GIS*, 16(5), pp. 635–647. doi: 10.1111/j.1467-9671.2012.01331.x.

9. Literature

Bundesamt für Umwelt BAFU (2015) *Hochwasser und Murgang - Faktenblätter Gefahrenprozesse*.

Cesca, M. and D'Agostino, V. (2008) 'Comparison between FLO-2D and RAMMS in debris-flow modelling: A case study in the Dolomites', *WIT Transactions on Engineering Sciences*, 60, pp. 197–206. doi: 10.2495/DEB080201.

Christen, M. *et al.* (2008) 'Calculation of Dense Snow Avalanches in Three-Dimensional Terrain with the Numerical Simulation Program Ramms', *Proceedings Whistler 2008 International Snow Science Workshop September 21-27, 2008*, p. 709. Available at: <http://arc.lib.montana.edu/snow-science/item/119> (Accessed: 9 July 2019).

Christen, M. *et al.* (2012) 'Integral hazard management using a unified software environment numerical simulation tool " Ramms "', *12th Congress Interpraevent*, pp. 77–86. doi: ISBN 978-3-901164-19-4.

Christen, M., Kowalski, J. and Bartelt, P. (2010) 'RAMMS: Numerical simulation of dense snow avalanches in three-dimensional terrain', *Cold Regions Science and Technology*. Elsevier, 63(1–2), pp. 1–14. doi: 10.1016/J.COLDREGIONS.2010.04.005.

Costa, J. E. (1984) 'Physical Geomorphology of Debris Flows', in *Developments and Applications of Geomorphology*. doi: 10.1007/978-3-642-69759-3_9.

Costa, J. E. (1988) 'Floods from dam failures', in Baker, V. R. and Patton, P. C. (eds) *Flood Geomorphology*. New York: John Wiley & Sons, pp. 439–463.

D'Agostino, V. (1996) 'Analisi quantitativa e qualitativa del trasporto solido torrentizio nei bacini montani de Trentino Orientale', *Scritti dedicati a Giovanni Tournon*.

DLR (no date) *How is a digital elevation model made?* Available at: https://www.dlr.de/eoc/en/Portaldata/60/Resources/dokumente/7_sat_miss/srtm_DEM_generierung_en.pdf (Accessed: 5 April 2019).

Flener, C. *et al.* (2013) 'Seamless Mapping of River Channels at High Resolution Using Mobile LiDAR and UAV-Photography', *Remote Sensing*. Multidisciplinary Digital Publishing Institute, 5(12), pp. 6382–6407. doi: 10.3390/rs5126382.

Frank, F. *et al.* (2016) 'Debris flow modeling at Meretschibach and Bondasca catchment, Switzerland: sensitivity testing of field data-based erosion model', (September), pp. 1–28. doi: 10.5194/nhess-2016-295.

Grasshopper (no date). Available at: <https://www.grasshopper3d.com/> (Accessed: 10 April 2019).

de Haas, T., Kruijt, A. and Densmore, A. L. (2018) 'Effects of debris-flow magnitude–frequency distribution on avulsions and fan development', *Earth Surface Processes and Landforms*, 43(13), pp. 2779–2793. doi: 10.1002/esp.4432.

Haeberli, W. and Zimmerman, M. (1992) 'Climatic change and debris flow activity in high- mountain areas: a case study in the Swiss Alps', *Catena Supplement*, 22(January 2016), pp. 59–72.

Hampel, R. (1977) 'Geschiebewirtschaft in Wildbächen', *Wildbach- und Lawinenverbau*, 41(1), pp. 3–34.

Harris, C. *et al.* (2009) 'Permafrost and climate in Europe: Monitoring and modelling thermal, geomorphological and geotechnical responses', *Earth-Science Reviews*. Elsevier B.V., 92(3–4), pp. 117–171. doi: 10.1016/j.earscirev.2008.12.002.

Hilker, N., Badoux, A. and Hegg, C. (2009) 'The swiss flood and landslide damage database 1972-2007', *Natural Hazards and Earth System Science*, 9(3), pp. 913–925. doi: 10.1002/asl.183.

Huggel, C. *et al.* (2008) 'Evaluation of ASTER and SRTM DEM data for lahar modeling: A case study on lahars from Popocatepetl Volcano, Mexico', *Journal of Volcanology and Geothermal Research*, 170(1–2), pp. 99–110. doi: 10.1016/j.jvolgeores.2007.09.005.

Hungr, O. (2005) 'Classification and terminology', in *Debris-Flow Hazards and Related Phenomena*. Heidelberg, Germany: Springer Verlag. doi: 10.1007/3-540-27129-5_2.

Hungr, O., Leroueil, S. and Picarelli, L. (2014) 'The Varnes classification of landslide types, an update', *Landslides*, 11(2), pp. 167–194. doi: 10.1007/s10346-013-0436-y.

- Hungr, O., McDougall, S. and Bovis, M. (2005) 'Entrainment of material by debris flows', *Debris-Flow Hazards and Related Phenomena*, pp. 135–158.
- Hürlimann, M., Rickenmann, D. and Graf, C. (2003) 'Field and monitoring data of debris-flow events in the Swiss Alps', *Canadian Geotechnical Journal*, 40(1), pp. 161–175. doi: 10.1139/t02-087.
- Ismail, Z. and Jaafar, J. (2013) 'DEM derived from photogrammetric generated DSM using morphological filter', in *2013 IEEE 4th Control and System Graduate Research Colloquium*. IEEE, pp. 103–106. doi: 10.1109/ICSGRC.2013.6653284.
- Iverson, R. M. (1997) *The physics of debris flows*, *Reviews of Geophysics - REV GEOPHYS*. doi: 10.1029/97RG00426.
- Iverson, R. M. *et al.* (2010) 'Positive feedback and momentum growth during debris-flow entrainment of wet bed sediment', *Nature Geoscience*, 4. doi: 10.1038/NCEO1040.
- Johnson, A. M. and Rodine, J. R. (1984) 'Debris flow', in Brundsen, D. and Prior, D. B. (eds) *Slope Instability*. New York: John Wiley, pp. 257–361.
- Kronfellner-Kraus, G. (1984) 'Extreme Feststofffrachten und Grabenbildungen von Wildbächen', in *Proc. Int. Symp. Interpraevent*. 2nd edn. Villach, Austria, pp. 109–118.
- Li, Z. *et al.* (2004) *Digital Terrain Modeling*. CRC Press. doi: 10.1201/9780203357132.
- Makineci, H. B. and Karabörk, H. (2016) 'EVALUATION DIGITAL ELEVATION MODEL GENERATED BY SYNTHETIC APERTURE RADAR DATA', *The International Archives of Photogrammetry, Remote Sensing and Spatial Information Sciences*, XLI-B1. doi: 10.5194/isprsarchives-XLI-B1-57-2016.
- McDougall, S. and Hungr, O. (2004) 'A model for the analysis of rapid landslide motion across three-dimensional terrain', *Canadian Geotechnical Journal*. NRC Research Press, 41(6), pp. 1084–1097.
- Mergili, M. *et al.* (2017) 'r. avaflow v1, an advanced open-source computational framework for the propagation and interaction of two-phase mass flows', *Geoscientific Model Development*. Copernicus GmbH, 10(2), p. 553.
- Missbauer, P. (1971) 'Stützmauer für die Wildbachverbauung im Illgraben', *Schweizerische Bauzeitung*, 89(40), pp. 1003–1006.
- Mizuyama, T. and Kobashi, O. G. (1992) *Prediction of debris flow peak discharge, Intrapraevent 1992*. Bern.
- Mukherjee, Sandip *et al.* (2013) 'Evaluation of vertical accuracy of open source Digital Elevation Model (DEM)', *International Journal of Applied Earth Observation and Geoinformation*. Elsevier, 21, pp. 205–217. doi: 10.1016/j.jag.2012.09.004.
- O'Brien, J. S., Julien, P. Y. and Fullerton, W. T. (1993) 'Two-dimensional water flood and mudflow simulation', *Journal of hydraulic engineering*. American Society of Civil Engineers, 119(2), pp. 244–261.
- Oggier, N. (2011) *Simulierung von Murgängen mit RAMMS am Beispiel des Meretschibachs*. ETH Zürich.
- Pierson, T. (1986) 'Flow behaviour of channelized debris flows, Mount St. Helens, Washington', *Hillslope Processes*.
- PLANAT (no date) *Plattform Naturgefahren PLANAT - Informationsplattform zum Umgang mit Naturgefahren in der Schweiz [Murgang]*. Available at: <http://www.planat.ch/de/wissen/hochwasser/murgang/> (Accessed: 23 May 2019).
- Quan Luna, B. (2012) *Dynamic numerical run-out modelling for quantitative landslide risk assessment*. University of Twente, Enschede.
- Raetzo, H. *et al.* (2002) 'Hazard assessment in Switzerland - Codes of Practice for mass movements', *Bulletin of Engineering Geology and the Environment*. Springer-Verlag, 61(3), pp. 263–268. doi: 10.1007/s10064-002-0163-4.
- Raymond Pralong, M., Rickenmann, D. and Schneider, T. (2018) 'Vergleich dreier numerischer Simulationsmodelle für Murgänge: Anwendung auf Wildbachkegel im Kanton Wallis', *Wasser, Energie, Luft*, pp. 43–52. Available at: <https://www.dora.lib4ri.ch/wsl/islandora/object/wsl:16522> (Accessed: 12 July

2019).

Rhinoceros (no date). Available at: <https://www.rhino3d.com/> (Accessed: 10 April 2019).

Rickenmann, D. (1999) 'Empirical relationships for Debris Flow', *Natural hazards*, 19(47), pp. 47–77. Available at: ftp://ftp.wsl.ch/pub/rickenmann/Rickenmann-pdf/1999/Rickenmann-1999_NH.pdf.

Rickenmann, D. *et al.* (2006) 'Comparison of 2D debris-flow simulation models with field events', *Computational Geosciences*, 10(2), pp. 241–264. doi: 10.1007/s10596-005-9021-3.

Rickenmann, D. (2014) 'Methoden zur quantitativen Beurteilung von Gerinneprozessen in Wildbächen', *WSL Berichte*, 9, p. 105 S.

Rickenmann, D. and Zimmermann, M. (1993) 'The 1987 debris flows in Switzerland: documentation and analysis', *Geomorphology*, 8, pp. 175–189.

River Bathymetry Toolkit (RBT) - ESSA (no date). Available at: <https://essa.com/explore-essa/tools/river-bathymetry-toolkit-rbt/> (Accessed: 10 July 2019).

Ryter, U. (2017) *Forstliches Verbauungs- und Aufforstungsprojekt Briener Wildbäche 1883-2017*. Interlaken.

Sattler, K. *et al.* (2011) 'On the Connection between Debris Flow Activity and Permafrost Degradation: A Case Study from the Schnalstal, South Tyrolean Alps, Italy', *Permafrost and Periglacial Processes*, 22(3), pp. 254–265. doi: 10.1002/ppp.730.

Scheidl, C., Rickenmann, D. and McArdell, B. W. (2013) 'Runout Prediction of Debris Flows and Similar Mass Movements', *Landslide Science and Practice*, 3, pp. 221–229. doi: 10.1007/978-3-642-31310-3.

Schraml, K. *et al.* (2015) 'Modeling debris-flow runout pattern on a forested alpine fan with different dynamic simulation models', *Engineering Geology for Society and Territory - Volume 2: Landslide Processes*, pp. 1673–1676. doi: 10.1007/978-3-319-09057-3_297.

Schumm, S. A. (1960) 'The shape of Alluvial channels in relation to sediment type', *U.S. Geol. Survey Prof Paper*, 352, pp. 17–30. Available at: <https://ci.nii.ac.jp/naid/10030009629/> (Accessed: 5 July 2019).

Schürch, P. *et al.* (2011) 'Detection of surface change in complex topography using terrestrial laser scanning: application to the Illgraben debris-flow channel', *Earth Surface Processes and Landforms*. John Wiley & Sons, Ltd, 36(14), pp. 1847–1859. doi: 10.1002/esp.2206.

Sodnik, J. *et al.* (2013) 'Topographic Data and Numerical Debris-Flow Modeling', in *Landslide Science and Practice*. Berlin, Heidelberg: Springer Berlin Heidelberg, pp. 573–578. doi: 10.1007/978-3-642-31325-7_75.

Stevens, N. ., Manville, V. and Heron, D. . (2003) 'The sensitivity of a volcanic flow model to digital elevation model accuracy: experiments with digitised map contours and interferometric SAR at Ruapehu and Taranaki volcanoes, New Zealand', *Journal of Volcanology and Geothermal Research*. Elsevier, 119(1–4), pp. 89–105. doi: 10.1016/S0377-0273(02)00307-4.

Stolz, A. and Huggel, C. (2008) 'Debris flows in the Swiss National Park: The influence of different flow models and varying DEM grid size on modeling results', *Landslides*, 5(3), pp. 311–319. doi: 10.1007/s10346-008-0125-4.

Stricker, B. (2010) *Murgänge im Torrente Riascio (TI): Ereignisanalyse, Auslösefaktoren und Simulationen von Ereignissen mit RAMMS*. University of Zurich.

Su, J. and Bork, E. (2006) 'Influence of vegetation, slope, and lidar sampling angle on DEM accuracy', *Photogrammetric Engineering & Remote Sensing*. American Society for Photogrammetry and Remote Sensing, 72(11), pp. 1265–1274.

Swisstopo, B. für L. (2018) *swissALTI3D. Das hoch aufgelöste Terrainmodell der Schweiz*.

Takei, K. (1980) 'Interdependence of sediment budget between individual torrents and a river-system', in *Proc. Int. Symp. Interpraevent*. 2nd edn. Villach, Austria, pp. 35–48.

Tobler, D. and Krummenacher, B. (2013) 'Risk Concept Switzerland Hazard Analysis, Risk Evaluation and Protection Measures', *Landslide Science and Practice*, 7, pp. 9–16. doi: 10.1007/978-3-642-31310-3.

- Tognacca, C. (1999) *Beitrag zur Untersuchung der Entstehungsmechanismen von Murgängen*. ETH Zürich.
- Turnbull, B., Bowman, E. T. and McElwaine, J. N. (2015) 'Debris flows: Experiments and modelling', *Comptes Rendus Physique*. Elsevier Masson SAS, 16(1), pp. 86–96. doi: 10.1016/j.crhy.2014.11.006.
- Varnes, D. J. (1978) 'Slope Movement Types and Processes', *In Special report 176: Landslides: Analysis and Control, Transportation Research Board, Washington, D.C.* doi: In Special report 176: Landslides: Analysis and Control, Transportation Research Board, Washington, D.C.
- Weber, D. (2004) *Untersuchungen zum Fliess- und Erosionsverhalten granularer Murgänge*. Birmensdorf. Available at: https://www.dora.lib4ri.ch/wsl/islandora/object/wsl%3A10330/datastream/PDF/Weber-2004-Untersuchungen_zum_Fliess-_und_Erosionsverhalten-%28published_version%29.pdf (Accessed: 8 August 2019).
- Westoby, M. J. *et al.* (2012) "'Structure-from-Motion" photogrammetry: A low-cost, effective tool for geoscience applications', *Geomorphology*. Elsevier, 179, pp. 300–314. doi: 10.1016/j.geomorph.2012.08.021.
- Willi, C. *et al.* (2015) 'Methods for detecting channel bed surface changes in a mountain torrent - experiences from the dorfbach torrent', *Geographica Helvetica*, 70(4), pp. 265–279. doi: 10.5194/gh-70-265-2015.
- Williams, G. P. (1978) 'Bank-full discharge of rivers', *Water Resources Research*. John Wiley & Sons, Ltd, 14(6), pp. 1141–1154. doi: 10.1029/WR014i006p01141.
- Zeller, J. (1985) 'Feststoffmessung in kleinen Gebirgseinzugsgebieten', *Wasser, Energie, Luft*, 77(7/8), pp. 246–251.
- Zimmermann, M. (2006) 'Prognose von Murganggefahren: Wie Sicher ist Sie?', *Bulletin fuer Angewandte Geologie*, 11(2), pp. 65–73.
- Zimmermann, M., Pozzi, A. and Stoessel, F. (2005) *VADEMECUM HAZARD MAPS AND RELATED INSTRUMENTS THE SWISS SYSTEM AND ITS APPLICATION ABROAD CAPITALISATION OF EXPERIENCE*. Available at: www.natural-hazards.ch (Accessed: 5 April 2019).

10 Appendix

10.1 Digital elevation models

R-Script for the cross-section illustration and area calculation

```
### presettings / working directory / load and activate packages

# clean up
rm(list=ls())

# cross section name
csn <- "Val Mela - A" # adapt in "setwd" !!!

#set working directory
setwd("C:/Users/stefw/OneDrive/Persoenliche_Dokumente/Masterarbeit/030_R/field-
work/valmela/cross_sections/A")

# install.packages("packagename") / library(packagename)
library(RColorBrewer)
library(ggplot2)
library(reshape2)
library(ggthemes)
library(sf)
library(gridExtra)

##load data (csv-files of with cross-section data generated GIS for the different
DEMs)
extra <- read.table("extra.csv", header=T, sep=";")
X2m <- read.table("2m.csv", header=T, sep=";")
X5m <- read.table("5m.csv", header=T, sep=";")
X10m <- read.table("10m.csv", header=T, sep=";")
X25m <- read.table("25m.csv", header=T, sep=";")
dGPS <- read.table("dGPS.csv", header=T, sep=";")

##combine tables
profil1 <- merge(extra, X2m, by = "distance", all.x = T)
profil2 <- merge(profil1, X5m, by = "distance", all.x = T)
profil3 <- merge(profil2, X10m, by = "distance", all.x = T)
profil4 <- merge(profil3, X25m, by = "distance", all.x = T)
profil <- merge(profil4, dGPS, by = "distance", all.x = T)

#change column names
colnames(profil) <- c("distance", "extra", "X2m", "X5m", "X10m", "X25m", "dGPS")

### Plot transect -----
#ggplot
```

```

profile_long <- melt(profil, id="distance")

profileplot <-
  ggplot(profile_long, aes(x=distance, y=value, color=variable)) +
  geom_line(data = profile_long[!is.na(profile_long$value), ], size = 1) +
  xlab("horizontal profile axis [m]") +
  ylab("surface elevation [m asl.]") +
  theme(plot.title = element_text(hjust = 0.5)) +
  coord_fixed(ratio = 1/1) +
  theme(legend.position = "right") +
  scale_color_manual(labels = c("Yves Bhler (0.1 m) / University of Utrecht (0.05 m)",
"swissALTI3D (2 m)", "swissALTI3D (5 m)", "swissALTI3D (10 m)",
"DHM25 (25 m)", "dGPS measurements"),
values = c("#1b9e77", "#d95f02", "#7570b3", "#e7298a", "#66a61e",
"#e6ab02")) +
  guides(color=guide_legend("data origin (spatial resolution)")) +
  theme(plot.margin = unit(c(1, 1, 1, 1), "cm")) +
  ggtitle(csn)

profileplot

#### Cross sectional area: dGPS-cross-section -----

## Select data
profile <- dGPS

## read out axis data
# X-profile
x_profile_all <- c(profile$distance)
# Y-profile
y_profile_all <- c(profile$height)

## Calculation of max fill level
# minimum height
minheight <- min(y_profile_all)
# minimum position
minpos <- which.min(y_profile_all)
# left part
left <- profile[1:minpos, ]
# right part
indexmax <- which.max(profile$distance)
right <- profile[minpos:indexmax, ]
# highest points
maxleft <- max(left$height)
maxright <- max(right$height)
# fill up (print fill level)
fillup <- if (maxleft < maxright) {
  print(maxleft - minheight)
} else {
  print(maxright - minheight)
}

fillup <- fillup-0.0000000001 #no overflow if the bank is flat

## Prepare data to create channel polygon

# adapt data to exclude gullies outside of the main channel

# adapt X-profile
# max left positon
maxleftpos <- which.max(left$height)
# max right positon
maxrightpos <- which.max(right$height)
# indexmaxleft
indexmaxleft <- which.max(left$distance)

```

```

# max right position y-profile
maxrightpos <- indexmaxleft + maxrightpos - 1
# new X-profile
x_profile <- x_profile_all[maxleftpos:maxrightpos]

# adapt Y-profile
y_profile <- y_profile_all[maxleftpos:maxrightpos]
y_profile <- c(max(y_profile) - y_profile + 5) #add a number (e.g. 5) to have a border
for the filler function

# create matrix
m <- matrix(c(0, x_profile, max(x_profile), 0, 0, -y_profile, 0, 0),
            byrow = FALSE, ncol = 2)

## create polygon
poly <- st_polygon(list(m))
plot(poly)

## fill (function)
filler <- function(depth, profile, xprof, yprof, xdelta=100, ydelta=100){
  d = -(max(yprof))+depth
  xr = range(xprof)
  yr = range(-yprof)
  xdelta = 100
  xc = xr[c(1,2,2,1,1)] + c(-xdelta, xdelta, xdelta, -xdelta, -xdelta)
  yc = c(d, d, min(yr)-ydelta, min(yr)-ydelta, d)
  water = st_polygon(list(cbind(xc,yc)))
  st_intersection(profile, water)
}

## filled polygon
plot(filler(fillup, poly, x_profile, y_profile), add=TRUE, col="blue")

## Area [m2] of filled polygon
st_area(filler(fillup, poly, x_profile, y_profile))

## Save area
area <- st_area(filler(fillup, poly, x_profile, y_profile))

## Save fill level
fill_level <- fillup

## Save water polygon
water <- filler(fillup, poly, x_profile, y_profile)

## Extract channel width of water polygon
waterlist <- list(st_collection_extract(water))
listpoints <- unlist(waterlist)
listpointspositive <- listpoints[which(listpoints>=0)]
width <- max(listpointspositive)-min(listpointspositive)

### Saves/Values for dGPS
#Area
dGPS_area <- area
#Fill level
dGPS_fill_level <- fill_level
#Channel width
dGPS_width <- width

```

Values of cross-sectional area, channel width, channel depth (filling level)

Table 8: Resulting values of cross-sectional area computation: Area [m²], depth [m], width [m] of the different transects (see lettercode, ordered downstream)

Place	Letter	dGPS_Area	dGPS_Depth	dGPS_Width	UAV_Area	UAV_Depth	UAV_Width	2m_Area	2m_Depth	2m_Width
Val_Mela	A	43.88791	5.1156	12.96539	41.61373	5.227905	12.71992	16.83669	2.184082	11.74968
	B	25.39593	2.4107	14.55566	21.67499	1.985474	14.00465	14.23333	1.696655	14.12608
Forbesch	A	33.92815	4.7159	12.91735	29.29693	4.815063	12.26957	15.6321	2.534668	13.48776
	B	16.11635	1.7439	12.47612	15.61007	1.927002	12.61441	5.238772	1.15979	8.549659
Illgraben	A	82.97484	4.3203	30.74538	100.9128	5.709045	30.14603	81.38086	4.751648	30.37189
	B	67.8806	5.2165	20.77175	70.50275	5.536011	19.8989	56.0251	4.274841	20.49059
	C	897.6114	14.6099	109.4171	892.2933	14.73303	109.1825	864.1836	14.21405	109.5468
	D	77.21472	5.3242	25.15313	128.9545	8.823059	25.05988	64.8163	3.944336	24.44312
	E	73.50702	5.1164	23.40833	113.2047	7.955017	24.0603	73.88587	5.233887	22.79382
	F	99.61257	5.2285	31.92121	104.0849	5.546997	33.2208	111.0008	5.427063	34.23865
	G	226.9236	10.7837	33.83169	256.0952	13.49298	35.79691	157.7181	7.75946	31.47144
	H	75.84732	4.6245	31.97553	179.4866	8.140991	34.74357	108.5859	5.504211	38.77417
Fraschmardin	A	30.38242	4.5765	11.99665	31.61765	5.091674	11.79326	20.80282	2.248291	13.26698
	B	23.06709	3.7017	12.42075	22.84348	3.825318	12.50437	10.04923	2.249756	10.0732
	C	3.308836	0.4931	11.56409	2.47761	0.437744	12.28009	0.8927797	0.11914	12.10832
	D	21.72914	3.9341	9.98161	19.40015	3.900024	8.064683	9.335599	1.816162	8.31505
	E	13.22658	2.7215	8.485954	25.87285	4.672729	11.00405	7.94716	1.670044	9.144197
	F	12.77714	1.4854	15.56382	13.54094	1.566162	16.16131	13.27299	2.074463	22.46875
	G	23.8603	3.0175	11.23244	22.89789	3.748902	8.476944	1.274124	0.658814	6.00121
	H	13.98219	2.7414	7.832169	15.04334	3.884766	6.296933	0.7566678	0.374633	4.039515
	I	20.43482	2.9694	12.10097	20.53683	3.070801	11.08089	4.047081	1.044312	8.701278
	K	8.950286	2.3176	7.494015	7.330368	2.283692	7.401369	7.065468	1.776123	7.044247
Place	Letter	5m_Area	5m_Depth	5m_Width	10m_Area	10m_Depth	10m_Width	25m_Area	25m_Depth	25m_Width
Val_Mela	A	0	0	0	12.10935	2.670655	7.41904	0	0	0
	B	5.070045	1.237793	7.75657	4.190766	1.790283	4.68168	0	0	0
Forbesch	A	17.45522	2.333618	13.51211	0	0	0	0	0	0
	B	4.404614	1.183716	8.87356	0	0	0	0	0	0
Illgraben	A	84.40225	4.726623	31.86032	83.60523	4.684326	31.03031	0	0	0
	B	49.5797	3.376648	17.64483	40.90555	3.44751	22.80792	0	0	0
	C	880.3467	16.56384	109.2976	833.3175	14.53918	103.0674	522.1811	9.403992	79.28345
	D	32.11521	2.662414	20.92308	42.1789	2.714416	21.07242	0	0	0
	E	49.75151	3.700989	17.47092	23.35722	3.107117	11.20651	0	0	0
	F	87.30137	4.699829	32.19344	80.0868	4.306091	22.03477	0.492729	0.2030029	18.13988
	G	153.1484	7.326538	31.86813	112.7592	6.8078	32.2918	0	0	0
	H	114.7511	6.429687	35.56356	140.1744	6.277466	34.12605	54.70154	2.890015	28.04643
Fraschmardin	A	13.09751	2.39209	10.42784	0	0	0	0	0	0
	B	14.87279	3.18811	6.645221	0	0	0	0	0	0
	C	0	0	0	2.083063	0.373779	8.88746	0	0	0
	D	0	0	0	0	0	0	0	0	0
	E	7.170325	0.939453	11.37142	0	0	0	0	0	0
	F	9.560211	1.271729	12.2019	33.59937	3.404297	20.18879	6.916441	1.596924	5.435544
	G	0	0	0	18.72247	3.217407	7.244913	0	0	0
	H	0	0	0	5.832377	2.060669	5.660663	0	0	0
	I	7.728381	1.141235	8.318476	0.4080526	0.53772	1.517714	7.579504	1.692993	0.389354
	K	0	0	0	0.194514	0.391235	0.9943587	0	0	0

10.2 Debris flow runout modelling

R-Script for the visualisation of the real-world cases modelling results

```
### Settings / Working Directory / Packages

#working directory
setwd("E:/Dateien/Masterarbeit/cases/10_real")

# install.packages("packagename") / library(packagename)
library(raster)
library(RColorBrewer)
library(ggplot2)
library(ggthemes)
library(tidyverse)
library(rgdal)

#clean up
rm(list=ls())

## load data
mfh <- raster("forbesch/output/calibrated_cases/max_flowheight/3200cm.asc")
#map <- raster("alp_da_stugl/basic/map_forbesch.tif")
ortho <- raster("forbesch/basic/ortho_1m.tif")

## Title (spatial resolution)
spatres <- "32 m"

## order
max_flow_height <- mfh

## Set lower boundary
lb <- 0.1 #lower boundary
max_flow_height[max_flow_height<=lb]<-NA

#Number of cells with values (Area)
flowarea <- length(which(!is.na(values(max_flow_height))))

### Plot

## Set upper data boundary (for representation)
ub <- 2 #upper boundary
max_flow_height[max_flow_height>ub]<-ub

# create df
r_points = rasterToPoints(max_flow_height)
r_df = data.frame(r_points)
#map_df <- as.data.frame(map, xy = TRUE)
ortho_df <- as.data.frame(ortho, xy = TRUE)

# CRS transformation for map
r_df$x <- r_df$x - 2000000.1
r_df$y <- r_df$y - 1000000.3

## Plot

mapplot <- ggplot() +
  geom_raster(data = ortho_df, aes(x=x, y=y, fill=ortho_df[, 3])) +
  scale_fill_gradient(low = "black", high = "white", guide = FALSE) +
  coord_fixed(ratio = 1/1) +
```

```

xlim(min(r_df[, 1]) - 100, max(r_df[, 1] + 100)) +
ylim(min(r_df[, 2]) - 100, max(r_df[, 2] + 100)) +
theme_bw() +
theme(axis.title.x = element_blank(), axis.title.y = element_blank(),
      panel.grid.major = element_line(colour = "black", size = 0.3),
      panel.grid.minor = element_line(colour = "black", size = 0.3),
      panel.background = element_rect(fill = NA), panel.border = element_blank()) +
ggtitle(spatres) +
theme(plot.title = element_text(hjust = 0.5))

mapplot +
  geom_tile(data = r_df, aes(x=x, y=y, color=r_df[, 3])) +
  scale_color_gradientn(colours = rainbow(100, start = 2/6)) +
  guides(color = guide_colourbar(title = "maximum flow height [m]", barwidth = 10,
barheight = 0.5,
                                ticks = TRUE, direction = "horizontal", title.position =
"top")) +
  theme(legend.position = "bottom")

```

10.3 Sensitivity of the model to DEMs

Values for the affected area with a maximum flow height of at least 0.1 m

Table 9: Resulting values of the affected areas [m²] with a maximum flow height of at least 0.1 m according to the simulations at the different study sites for scenario A (extreme event) and B (borderline scenario).

Place	Scenario	10cm_Area	25cm_Area	50cm_Area	100cm_Area	200cm_Area	400cm_Area	800cm_Area	1600cm_Area	3200cm_Area
Forbesch	A	45240	45135	44822	45257	44922	47147	47880	46373	45049
Fraschmardin	A	51018			47729		44031		53447	
Val_Mela	A	29694			28070	31136	32553	36072	34618	48857
Illgraben	A				505137				508428	689016
East_Alpin_Stugl	A	21418			21341	21225	20534	19489	20259	
West_Alpin_Stugl	A	11675			11697			12085		
Forbesch	B				10508	10584	11257	14538	17332	20887
Fraschmardin	B				10172	10155	6362			
Val_Mela	B				8358	8051	7913	11359	14731	21438
Illgraben	B				130459			135229	158971	180984
East_Alpin_Stugl	B	3795			3767	3791	3486	3996	4285	
West_Alpin_Stugl	B				1822	1918	2505	3046		

Values for the affected area with a maximum flow height of at least 1 m

Table 10: Resulting values of the affected areas [m²] with a maximum flow height of at least 1 m according to the simulations at the different study sites for scenario A (extreme event) and B (borderline scenario).

Place	Scenario	10cm_Area	25cm_Area	50cm_Area	100cm_Area	200cm_Area	400cm_Area	800cm_Area	1600cm_Area	3200cm_Area
Forbesch	A	22492	22408	22280	22469	22904	23712	24800	26173	25653
Fraschmardin	A	17949			16027		17089		30852	
Val_Mela	A	12377			12645	13296	14123	15666	16234	15046
Illgraben	A				348361				366829	378563
East_Alpin_Stugl	A	10371			10439	10546	10087	10813	11609	
West_Alpin_Stugl	A	4526			4565			11321		
Forbesch	B				2364	2351	2335	1984	1686	1399
Fraschmardin	B				2084	2075	1664			
Val_Mela	B				2743	2881	2757	1773	1505	924
Illgraben	B				81461			84130	87692	84536
East_Alpin_Stugl	B	96			104	102	148	40	62	
West_Alpin_Stugl	B				31	9	21	0		

Values for the affected area with a maximum velocity of at least 1 m/s

Table 11: Resulting values of the affected areas [m²] with a maximum velocity of at least 1 m/s according to the simulations at the different study sites for scenario A (extreme event) and B (borderline scenario).

Place	Scenario	10cm_Area	25cm_Area	50cm_Area	100cm_Area	200cm_Area	400cm_Area	800cm_Area	1600cm_Area	3200cm_Area
Forbesch	A	32452	32441	32367	32504	33165	35955	37766	37482	36126
Fraschmardin	A	35919			32801		33936		43586	
Val_Mela	A	18427			17052	19408	21799	25874	26587	40473
Illgraben	A				404258				424939	576545
East_Alpin_Stugl	A	13126			13118	13191	12857	12894	13813	
West_Alpin_Stugl	A	10755			10810			11321		
Forbesch	B				5335	5386	5587	6747	11505	
Fraschmardin	B				7548	7691	5343			
Val_Mela	B				6378	6151	6087	9275	13085	20286
Illgraben	B				94620			99193	119397	137212
East_Alpin_Stugl	B	2358			2395	2431	2281	2701	2895	
West_Alpin_Stugl	B				1551	1646	2336	2805	6747	

Acknowledgements

First, I would like to thank my main supervisor Dr. Brian McArdell. Thank you for your constant input and support. Thanks for the great opportunity to work beside you in the office or even once in the field.

Thanks to Ilmar Hurkkens for introducing me into Rhino-CAD. You made a big contribution to use another approach in my work.

A big thanks to Prof. Dr. Christian Huggel for several inputs and suggestions on my thesis work.

I appreciate all the support I received from several researchers and employees at WSL and the department of geography at UZH. Especially I want to mention from the SLF in Davos Yves Bühler who provided me high resolution DEMs and Marc Christen who helped me in technical questions. Thanks to Dieter Rickenmann for introducing me into the case in Val de Nendaz.

Last but not least there are my family and all my friends. I want to express my great gratitude for their help. Thanks to Marco Zapatta for assisting me one day during fieldwork, to David Meier and Andreas Gantner for going through the text.

Personal Declaration

I hereby declare that the submitted thesis is the result of my own, independent work. All external sources are explicitly acknowledged in the thesis.

Zurich, 16.08.2019

A handwritten signature in black ink, appearing to read 'Stefan Wehrli', written in a cursive style.

Stefan Wehrli